金属シリサイド／シリコン界面に於ける電子構造の理論的研究

—First-principle calculations on the electronic structure at metal silicide/Si interfaces—

藤谷秀章

(1)

金属シリサイド / シリコン界面に於ける電子構造の理論的研究

– First-principle calculations on the electronic structure
at metal silicide/Si interfaces –

藤　谷　秀　章

Contents

Abstract

By means of first-principle calculations based on the density functional theory, we studied the electronic structure of the Si interface with different materials: metal silicides ($NiSi_2$, $CoSi_2$, YSi_2) and an insulator (CaF_2). Using the linear muffin-tin orbitals in the atomic sphere approximation (LMTO–ASA) with the local density approximation (LDA), we carried out heavy calculations with large supercells containing 9 – 12 Si_2 layers and 8 – 11 metal silicide or CaF_2 layers.

With large supercells, the calculated difference of Schottky barrier heights (SBH's) between the two types of $NiSi_2$/Si(111) interface well agreed with the experimental one. However, SBH's depend on the supercell size, although larger supercells have enough layers to screen the interface disturbance. We clarified that the cell size dependence of SBH's is caused by the recovery of bulk-like band structures on both silicide and Si layers. Together with calculations on the $CoSi_2$/Si(111) and YSi_2/Si(111) interfaces, we showed that LMTO–ASA calculations with a large supercell give an adequate SBH difference for the real silicide/Si interfaces although the LDA depresses the band gap of bulk Si to almost half of the experimental value.

1 Introduction

Silicon (Si) is one of the most important material in the modern industry. It is used for Large Scale Integrated Circuit (LSI), Power Devices, and Charge Coupled Devices, etc. The interface with Si is widely used in microelectronic devices. But its electronic structure has not been clarified. Since an interface is buried by an overlayer and its structure depends on materials and conditions during formation, the atomic structure of the interface is difficult to clarify. This kept the electronic structure of the real interface from being clarified for a long time.

In the last two decades, there was much progress in the *ab initio* self-consistent method for electronic band structures of solids, which is based on the density functional theory [1]. This method has had remarkable successes within the local density approximation (LDA) [2] in computing structural, vibrational, and other ground-state properties for a wide range of materials. But it was rarely applied for real interfaces. To examine the electronic structure of the interface by the LDA calculation, the interface atomic structure must be known. However, the atomic structure of ordinary interfaces are so much complicated to study microscopic characters by the theoretical method.

To understand the interface character from the view points of the interface electronic structure, well-defined interfaces are needed and *ab initio* calculations must be employed. Model theories or empirical calculations always have some assumptions, because they apply parameters derived only from the bulk properties of the two constituents forming the interface. Since the experiments about the interface cannot give unequivocal information about the interface electronic states, the validity of the adopted assumptions cannot be evaluated.

There has been a lot of intensive studies about the semiconductor interfaces during a long time and we know lots of the properties of the semiconductor interfaces. However, since the microscopic electronic state of the real interface did not be clarified, there have been much debates about the microscopic origin of the interface properties. One of the outstanding problems is how Schottky barrier (SB) is formed at the metal-semiconductor interface.

With LDA calculations we examined the electronic structures at *epitaxial* Si interfaces with four different materials: metal silicides ($NiSi_2$, $CoSi_2$, YSi_2) and an insulator (CaF_2).

These interfaces show simple atomic structures under the some formation condition, so that these offer a golden opportunity to examine the electronic structure of the real interfaces by *ab initio* calculations.

2 Outline of the method

2.1 Density functional theory

According to the Hohenberg and Kohn theorem [1], the ground state energy $E_v[\rho]$ in an external potential $v(\mathbf{r})$ of an interacting electron system is a functional of the electron density $\rho(\mathbf{r})$. In the atomic unit, the ground state energy $E_v[\rho]$ is written by

$$E_v[\rho] = T_s[\rho] + \int v(\mathbf{r})\rho(\mathbf{r})d\mathbf{r} + \int \frac{\rho(\mathbf{r})\rho(\mathbf{r}')}{|\mathbf{r}-\mathbf{r}'|}d\mathbf{r}d\mathbf{r}' + E_{xc}[\rho], \tag{1}$$

where $T_s[\rho]$ is the kinetic energy and $E_{xc}[\rho]$ is the exchange-correlation energy.

The electron density $\rho(\mathbf{r})$ is the sum of the N lowest occupied eigenstates

$$\rho(\mathbf{r}) = \sum_{i=1}^{N} |\psi_i(\mathbf{r})|^2. \tag{2}$$

From the minimal property of $E_v[\rho]$, $\psi_i(\mathbf{r})$ satisfies the Kohn–Sham equation [2]

$$\left[-\nabla^2 + v_{eff}(\mathbf{r})\right]\psi_i(\mathbf{r}) = \epsilon_i\psi_i(\mathbf{r}) \tag{3}$$

where

$$v_{eff}(\mathbf{r}) = v(\mathbf{r}) + 2\int \frac{\rho(\mathbf{r}')}{|\mathbf{r}-\mathbf{r}'|}d\mathbf{r}' + v_{xc}(\mathbf{r}). \tag{4}$$

The exchange and correlation contribution $v_{xc}(\mathbf{r})$ is defined by functional derivative,

$$v_{xc}(\mathbf{r}) = \frac{\delta E_{xc}[\rho]}{\delta\rho(\mathbf{r})}. \tag{5}$$

In the local density approximation (LDA), we put

$$E_{xc}[\rho] \simeq \int \epsilon_{xc}(\rho(\mathbf{r}))\rho(\mathbf{r})d\mathbf{r}, \tag{6}$$

where $\epsilon_{xc}(\rho(\mathbf{r}))$ is the exchange and correlation energy per particle of a uniform electron gas of density ρ. In LDA,

$$v_{xc}(\mathbf{r}) = \frac{d}{d\rho}\{\epsilon_{xc}(\rho(\mathbf{r}))\rho(\mathbf{r})\} \equiv \mu_{xc}(\rho(\mathbf{r})) \tag{7}$$

where $\mu_{xc}(\rho(\mathbf{r}))$ is exchange and correlation contribution to the chemical potential of a uniform system. Several analytic fits to $\epsilon_{xc}(\rho)$ have been devised which are of comparable accuracy. We adopted the parameters of Janak, Moruzzi, and Williams [3].

2.2 FLAPW

Of the energy band calculation methods in solids, the most accurate, but also most heavy, is the full potential linear augmented plane wave (FLAPW) method in which linearized APW are used as the basis-functions and no shape approximation in the effective potential $v_{eff}(\mathbf{r})$ is included [4, 5]. The region of space is separated into the (muffin-tin) spheres surrounding the nuclei and the interstitial region lying in between the spheres. In the interstitial region $\psi_i(\mathbf{r})$ is expanded as plane waves. Inside the spheres each plane wave is augmented by a function which is constructed from solutions of the radial Schrödinger equation. One augmented plane wave is written as

$$\chi_\mu(\mathbf{r}) = 4\pi \sum_{R,lm} i^l Y^*_{lm}(\widehat{\mathbf{k}_\mu}) Y_{lm}(\widehat{\mathbf{r}_R}) \begin{cases} j_l(k_\mu r_R) & for \quad r > s_R \\ \varphi_{Rl\mu}(r_R) & \quad\quad r \le s_R \end{cases} . \tag{8}$$

Here, R indicates the atom positions, s_R is sphere radius, and

$$\mathbf{k}_\mu = \mathbf{k} + \mathbf{K}_\mu \tag{9}$$

where $\mathbf{k}$ is a wave vector in the first Brillouin zone and $\mathbf{K}_\mu$ is a reciprocal lattice vector. The $\varphi_{Rl\mu}(r)$ is written by two solutions $\phi_{Rl\alpha}(r)$ of radial Schrödinger equation with energies $E_{Rl\alpha}$ ($\alpha = 1, 2$), which are determined by electron distribution in each sphere [6].

In each sphere, the effective one-electron potential $v_{eff}(\mathbf{r})$ is strong and is described as an expansion by spherical harmonics $Y_{lm}(\widehat{\mathbf{r}_R})$. In the interstitial region, the effective potential is week and is represented by Fourier series.

2.3 LMTO–ASA

The linear muffin-tin orbital (LMTO) method is the linearized version of the Korringa-Kohn-Rostoker (KKR) method [7]. It provides almost the same accuracy as FLAPW for some kinds of materials, and computationally it is the fastest of the band calculation methods. In the LMTO calculations, the atomic sphere approximation (ASA) is commonly used. In ASA, the region of space is divided into overlapping Wigner–Seitz spheres which contain the nuclei or sometime do not contain nuclei; so-called "empty sphere".

There are some kinds of representations of the LMTO basis. We used the nearly orthogonal representation, and did not include the combined correction. LMTO basis are

$$\chi^{\mathbf{k}}_{Rlm}(\mathbf{r}) = \phi_{Rl}(r_R) Y_{lm}(\widehat{\mathbf{r}_R}) + \sum_{R'l'm'} \dot{\phi}_{R'l'}(r_{R'}) Y_{l'm'}(\widehat{\mathbf{r}_{R'}}) \mathcal{S}^{\mathbf{k}}_{R'l'm',Rlm}. \tag{10}$$

In matrix notation,

$$\mathcal{S}^{\mathbf{k}} = -\dot{P}^{-\frac{1}{2}} (P - S^{\mathbf{k}}) \dot{P}^{-\frac{1}{2}} \tag{11}$$

where $S^{\mathbf{k}}$ is screened structure matrix. The $\phi_{Rl}(r_R)$ is radial wave function at an energy E_{Rl} which is normalized to unity in the sphere. The energy derivative is denoted by the dots. P is a diagonal matrix whose elements are potential functions P_{Rlm} written by

$$P_{Rlm} = \frac{W\{\phi_{Rl}, K_l\}}{W\{\phi_{Rl}, J_l\}} \tag{12}$$

$$K_l(r_R) = i \frac{(\kappa s_R)^{(l+1)}}{(2l-1)!!} h^{(1)}_l(\kappa r_R), \qquad J_l(r_R) = \frac{(2l-1)!!}{2(\kappa s_r)^l} j_l(\kappa r_R). \tag{13}$$

The Wronskian is defined as $W\{f, g\} \equiv (s_R)^2 [f(r)g'(r) - f'(r)g(r)]_{r=s_R}$, and $h^{(1)}_l(\kappa r_R)$, $j_l(\kappa r_R)$ are the first kind spherical Hankel and Bessel functions, respectively. The two times of κ is the kinetic energy in an interstitial region. In ASA, the region of space consists of overlapping atomic or empty spheres. Since there are no interstitial region, the κ is usually set to be zero.

3 Historical background

3.1 Schottky barrier

Metal-semiconductor interfaces play very important roles in modern electronics and microelectronic devices. Their properties have been studied by many groups for years, but the basic question of how Schottky barriers (SBs) form remains unsolved [8]. In 1942, Schottky proposed his model relating the Schottky barrier height (SBH) to the difference between the metal work function (ϕ_m) and the electron affinity (χ_s) in the semiconductor [9];

$$\Phi_{Bn} = \phi_m - \chi_s \tag{14}$$

However, experimentally observed SBH's are less dependent on the metal work function than predicted by the equation (14). Bardeen proposed a model that the Fermi level is pinned by intrinsic semiconductor surface states [10]. In 1965, Heine pointed out that the intrinsic surface states cannot exist at a metal-semiconductor interface and insisted that the pinning of the Fermi level was due to metal-induced gap states (MIGS), which are composed of the tails of metal wave functions decaying into the semiconductor [11].

In 1976, using local density formalism to calculate the Al/Si(111) interface, Louie and Cohen showed for the first time that a high density of MIGS is formed in the band gap of the semiconductor [12]. They examined different Al/semiconductor interfaces and discovered that electrons were a little transferred from the metal layer to the semiconductor layer so that the interface dipole was negatively charged on the semiconductor side and positively charged on the metal side [13]. However, since the atomic structure of the real metal-semiconductor interface was not known, they used a jellium model to represent the Al layer although the semiconductor layer was formed of layered atoms.

At the end of 1970's, new experimental evidences found for III-V semiconductors changed perspective on the metal-semiconductor interface [14]. New information showed a high reactivity and interdiffusion between the metal and the semiconductor. Moreover it showed that the SB is practically formed by sub-monolayer metal deposited on the semiconductor. This prompted Spicer and collaborators to propose the defect model, which says that the Fermi level is pinned by electronic states of interface defects [15].

Since the interface gap states in the semiconductor take their weight primarily from the valence and conduction bands, it was supposed the Fermi level must fall at or near the energy where the MIGS cross over from valence to conduction band character [16]. In 1984, Tersoff calculated *canonical* SBH's only from the semiconductor bulk band structure [17]. He also derived a simple equation [18];

$$\Phi_{Bp} = \frac{1}{2}\left\{E_g^i - \frac{\Delta}{3}\right\} + \delta_m \tag{15}$$

where Φ_{Bp} is the p-type SBH, E_g^i is minimum *indirect* band gap, Δ is spin-orbit splitting, and δ_m is a fitting parameter which is determined for the metal. When $\delta_m = -0.2$ eV is chosen, the equation (15) well agrees with experimental SBH's at Au/semiconductor interfaces.

In parallel with the Tersoff's work, Tung reported that the SBH depends on the atomic structure at a $NiSi_2$/Si(111) interface [19]. His discovery conflicts the conventional understanding that the metal-semiconductor interface has a unique and uniform SBH, at least, when the interface is flat and has no contamination. So, there has been much dispute about the $NiSi_2$/Si(111) interface, and state of the art microscopic and spectroscopic techniques have been used to examine this interface.

3.2 $NiSi_2$/Si interface

The chief obstacle to determining how SB is formed is the obscurity of the atomic structure of the metal-semiconductor interface. A well-defined interface is needed to clarify the relationship between SBH and other physical parameters. Metal silicide/silicon interfaces are good for this.

$NiSi_2$ has a fluorite (CaF_2) structure with a lattice constant 5.406 Å, which is close to Si lattice constant 5.429 Å. $NiSi_2$ is epitaxially grown on a Si(111) surface and forms an atomically abrupt, structurally perfect interface. This interface has two types of structure (Fig. 1). Type-A $NiSi_2$ has the same orientation as the Si substrate, and type-B $NiSi_2$ is rotated 180° about the Si⟨111⟩ axis. From lattice image by transmission electron microscopy (TEM) and image simulation, Cherns *et al.* proposed a model in which the interface Ni atoms are sevenfold coordinated [20]. Tung *et al.* showed that both types of epitaxial layer can be grown on a Si(111) surface by carefully controlling the deposited Ni templates [21].

A thin template (1 Å to 7 Å) forms a type-B interface and a thick one (16 Å to 20 Å) forms a type-A interface after annealing at about 500°C. In 1984, Tung discovered that the SBH's differ by 0.14 eV between the two types of interface [19]. The n-type SBH's are 0.65 eV for the type-A and 0.79 eV for the type-B interfaces. But, Liehr *et al.* argued that the two types of perfect interface yield the same SBH 0.78 eV, and that imperfections, being incorporated during interface formation as a result of silicide growth or by absorption of impurities, can lower the SBH to 0.66 eV [22, 23].

Many theoretical studies have also been performed about the structure dependence of the SBH. Using the jellium/semiconductor interface model, Zhang *et al.* showed that the SBH could be shifted substantially by changing the interfacial atomic layer, or introducing a high-density local defects [24]. Hamann and Mattheiss examined energetics of the two types of $NiSi_2$/Si(111) interface with full-potential LAPW method [25]. They found the formation energy of the two types differs only by 0.03 to 0.06 eV including calculation error. The difference is so small that two types of interface can be switchable by "template technique". Using empirical tight-binding method, Yongnian *et al.* examined general trends of the chemical bonding and electronic structure for the interface between Si(111) and a series of metal disilicides [26]. They reported that the atomic structure difference between the two types does not affect the position of the Fermi energy. Bisi and Ossicini reported LMTO–ASA calculations about the two types of $NiSi_2$/Si(111) interface [27]. They used small supercells and obtained that n-type SBH's are 1.1 eV for type-A and 0.8 eV for type-B interfaces. It was contrary to the Tung's discovery.

Tung *et al.* examined details of the interface formation condition and insisted that under the experimental condition of Liehr *et al.* a doping-compensation phenomenon occurring was capable of dominating the electrical environment near the interface and bringing the apparent SBH's of type-A and type-B close together [28]. Other groups reported the SBH's of the $NiSi_2$/Si(111) interfaces [29]-[31]. Among them, Ospelt *et al.* got the same SBH as Tung's original value for the type-B interface [30]. The difference in the SBH's has been experimentally confirmed to some extent, but some still doubt the perfection of the interfaces and hypothesize that the difference in the SBH's is due to defects or other disorders at the interfaces [32, 33].

To explain the observed SBH difference, the detailed electronic structure must be examined with the first-principle calculations. Model theories or empirical calculations cannot accurately describe the small difference between the two structure types, because they apply parameters derived only from the bulk properties of the two constituents forming the interface.

We studied the electronic structures of the $NiSi_2$/Si(111) interfaces with LMTO–ASA and obtained different SBH's for the two structure types, which is consistent with Tung's discovery [34]. Shortly after our work, Das, Blöchl, Christensen, and Andersen reported similar results [35]. Their results agreed qualitatively with ours, but showed some discrepancy [36]. To resolve the differences, we performed calculations with different conditions [37].

The observed n-type SBH at the $NiSi_2$/Si(001) interface is 0.65 eV, which is the same as the SBH of the (111) type-A interface. From lattice images of TEM the $NiSi_2$/Si(001) interface is considered to have a sixfold structure in which the interface Ni atoms are sixfold-coordinated (Fig. 2) [38]. However, there are many dislocations and (111) facets at the $NiSi_2$/Si(001) interface formed by the conventional template technique. Thus, the observed SBH at the $NiSi_2$/Si(001) interface was attributed to the (111) facets.

In 1991, Tung *et al.* reported a new SBH measurement on the single-crystal, uniform, planar $NiSi_2$/Si(001) interface formed by a novel technique in which stoichiometric $NiSi_2$ is codeposited on a Si(001) at low temperatures and annealed at high temperatures (> 700°C) [39]. This interface exhibits a low n-type SBH of about 0.4 eV. They say that together with the two types of (111) interface, the SBH at the $NiSi_2$/Si interface changes by about 0.4 eV depending on the interface atomic structure. To clarify this, we examined the $NiSi_2$/Si(001) interface [40].

3.3 $CoSi_2$/Si interface

$CoSi_2$ is one of the prime candidates for contact materials of deep submicron ULSI applications. $CoSi_2$ has a fluorite (CaF_2) structure with a lattice constant 5.356 Å, which is 1.3 % smaller than that of Si. Epitaxial $CoSi_2$ film can be grown by deposition and annealing of Co on a Si(111) surface. This primarily forms a type-B interface, but often substantial fraction of the $CoSi_2$ film possesses a type-A orientation. From a TEM lattice image [20, 41],

x-ray standing wave (XSW) measurements [42], and Rutherford backscattering (RBS) [43], it was believed that the interfacial Co atom was fivefold coordinated (Fig. 3). But, Hamann showed that by full-potential LAPW calculations the structure with eightfold coordinated interfacial Co atoms has the lowest energy and that fivefold structure is extremely unfavorable [44]. He pointed out that none of experiments can rule out the eightfold structure at the $CoSi_2$/Si(111) interface.

Rees and Matthai performed calculations on the type-B $CoSi_2$/Si(111) interface using a tight-binding method in the extended Hückel approximation [45]. They reported that the n-type SBH is 0.55 eV for the fivefold interface and 0.13 eV for the eightfold interface. However, we obtained different SBH's at the $CoSi_2$/Si(111) interface by LMTO–ASA calculations. We showed that the fivefold $CoSi_2$/Si(111) interface gives an unreasonable negative p-type SBH: the Fermi level (E_f) is lower than the valence band maximum of Si (E_v), while the eightfold interface gives a positive and reasonable SBH [46]. Since the density of states (DOS) of bulk Si and $CoSi_2$ obtained by Rees and Matthai much deviates from the DOS obtained by more accurate methods (pseudopotential [47] and full-potential LAPW [48]), it seems to us that the extended Hückel approximation cannot accurately describe the electronic structure at the silicide/Si interface.

Although the buried interface may be hardly accessible for most structure probes, a surface structure often gives a clue to the interface atomic structure. Hellman and Tung discovered that the two distinctly different surface structures can be formed on a $CoSi_2$(111) surface [49]. One has bulk-Si-like double layers on the $CoSi_2$(111) surface. This gives eightfold coordination to the surface Co atom. Thereafter, many experimental methods were employed to distinguish the fivefold or eightfold coordination of the interfacial Co atom: medium-energy ion scattering (MEIS) [50, 51], surface extended x-ray absorption fine-structure analysis (SEXAFS) [52], and angle-resolved photoemission [53]. These supported the eightfold coordination of the interfacial Co atom.

Compared with the $NiSi_2$/Si(111) interface, the $CoSi_2$/Si(111) interface has a more complicated structure depending on the formation condition, partly because of a little larger lattice mismatch with Si. Although the type-B eightfold structure is energetically more favorable than the type-A interface [44], a type-A structure can be formed at the $CoSi_2$/Si(111)

interface [54, 55]. Moreover, for the type-B $CoSi_2$/Si(111) interface, evidences for more than one quasi-stable atomic structure were observed, including high-resolution electron microscopy (HREM) images which agree with the sevenfold structure [56, 57]. Fully annealed $CoSi_2$ films with a high density of misfit dislocations usually show an SBH in the range 0.65–0.70 eV on n-type Si(111) [58, 59]. At a type-B interface with a low density of dislocations formed by using repeated deposition and annealing over thin templates, the n-type SBH varied from ~0.7 to below ~0.5 eV [57].

In 1993, by careful control of molecular beam epitaxy (MBE) processing, Sullivan *et al.* succeeded to grow single crystal type-B $CoSi_2$/Si(111) interfaces which exhibit a giant variation in SBH [60]. One interface, probably with the eightfold structure, had a n-type SBH of 0.69 eV. But, other interface had a n-type SBH of 0.27 eV, which was fabricated with a sandwich structure prepared by deposition of 7 Å Co followed by 25 Å Si at room temperature and annealed at 500°C for 10 minutes. Slight deviation in this recipe, either film stoichiometry or annealing temperature, led to interfaces which have an intermediate SBH. Since MBE growth can be dominated by kinetics, it is probable that the atomic structure of the interface formed by MBE depends on the formation condition. To clarify the interface structure with the low n-type SBH, we performed LMTO–ASA calculations for the $CoSi_2$/Si(111) interface with five different atomic structures [61].

It is well known that the Si(001) surface consists of dimerized pairs of atoms with 2×1 symmetry. Similar reconstructions are also observed at buried interfaces [62, 63]. Loretto *et al.* found separate 2×1 and 1×2 domains at the $CoSi_2$/Si(001) interface which was formed by depositing a few monolayers of either pure Co or Co and Si at room temperature and then annealed to ~500°C [64]. Since the local interface structure in the reconstructed domain is different from that in an unreconstructed domain, it is probable that this difference produces an inhomogeneous SBH at the interface. We examined an unreconstructed $CoSi_2$/Si(001) interface by LMTO–ASA calculations.

3.4 YSi_2/Si(111) interface

Rare-earth silicides are unique in that they have a higher p-type SBH (0.7–0.73 eV) than half of the Si band gap [65], while many kinds of metal silicides usually shows a lower SBH than

half of the Si band gap. With respect to the SB issue, it is important to clarify what character of rare-earth silicides brings out the higher SBH. The LDA throws another problem. Since the LDA depresses the band gap of bulk Si to almost half of the experimental value, there is a question about what SBH can be obtained by LDA calculations.

YSi_2 is one of layered rare-earth silicides. Bulk YSi_2 has C32 crystal structure (AlB_2 type) with a hexagonal primitive cell. Within each Si layer and Y layer, atoms are arranged in a planar mesh with sixfold symmetry. $YSi_{1.7}$ has defected AlB_2 structure where one Si atom of six is missing. Since YSi_{2-x} ($x = 0$ and $x = 0.3$) has an ideal 0.0 % lattice mismatch relative to the Si(111) surface lattice, it is possible to grow large perfect YSi_{2-x} silicide films on Si(111) [66, 67]. The stoichiometry of the film depends on the formation condition.

Since the atomic structure at the YSi_2/Si(111) interface is yet to be clarified, we conjectured it from a surface structure of YSi_{2-x} [61, 68]. Baptist *et al.* observed that the YSi_2 surface is Si terminated with displacement upward (0.8 Å) of one Si atom out of two so that it exhibits the same geometry as a 1×1 Si(111) surface [69]. So, it is natural to assume that the top Si layer of YSi_2 continues to the Si substrate at the interface. The interfacial Y atom resides at the H_3 site (Fig. 4). In this structure the interface bonds are only slightly bent so that there will not exist a dangling bond at the interface. It seems natural that the YSi_2/Si(111) interface takes the H_3 structure.

3.5 CaF_2/Si(111) interface

CaF_2 is an insulator with an experimental band gap of 12.1 eV. It grows on Si(111) and forms an epitaxial insulator-semiconductor interface [70]. This system has many potential applications and offers a good opportunity to study the relationship between the atomic structure and bonding configurations at the ionic-covalent interface. CaF_2 has a lattice constant of 5.463 Å which is close to that of Si (5.429 Å). The CaF_2 epitaxial film on Si(111) has type-B orientation where the film is rotated 180° about the Si(111) axis [71]-[73]. $NiSi_2$ and $CoSi_2$ have the same crystal structure as CaF_2 and grow on Si(111) to form epitaxial metal-semiconductor interfaces. It may be possible to fabricate three-dimensional, fully epitaxial devices on Si with these materials. Since the atomic structure of these interfaces is fairly well understood, it is now possible to clarify the cause of many of the physical

phenomena that occur at these interfaces.

Batstone, Phillips, and Hunke related electrical properties of CaF_2/Si(111) to the atomic structure at the interface, with the aid of high-resolution TEM [74]. They grew a thick epitaxial film on Si(111) at 700°C, and treated it by rapid thermal annealing (RTA) in a flash-lamp annealing system. They found that RTA greatly improves the electrical properties of the interface. They postulated that the as-grown interface has an eightfold structure, and that F atoms migrate from the interface during RTA, which leaves fivefold coordinated Ca atoms (Fig. 5). Shortly after the Batstone's work, Tromp and Reuter reported MEIS measurements from monolayer films of CaF_2 grown at 770° C on Si(111) [75]. They discovered that interfacial Ca atoms are located on the top of second Si atoms (T_4 site).

Zegenhagen and Patel reported XSW measurements on CaF_2 films deposited on Si(111) held at 450°C to 770°C [76]. They found that F atoms are easily dissociated when deposited at higher temperatures and that the CaF_2/Si(111) interface consists mainly of Ca–Si bonds with Ca atoms at both the H_3 and T_4 sites. They also found that at lower temperatures, fewer F atoms are desorbed and interface Ca atoms are sevenfold coordinated. Many experimental methods have been used to study the electronic structure at the CaF_2/Si(111) interface, including core-level and Auger-electron spectroscopy [77]-[80], scanning tunneling spectroscopy (STS) [81], and others. McLean and Himpsel [82] measured the energy dispersion of an interface state at the CaF_2/Si(111) with angle-resolved photoelectron spectroscopy, using monolayer CaF_2 films grown at 700°C and annealed at 800°C for 4 minutes.

Using linear muffin-tin orbitals (LMTO), Satpathy and Martin calculated the total energy and band offset of the CaF_2/Si(111) interface [83]. They used supercells with 3 (Si_2) layers and 3 Ca layers with an appropriate number of F layers, and showed that the interface without an F atom layer is stable. Using larger supercells than those of Satpathy and Martin, we also performed LMTO calculations and obtained interface state energy dispersion that can be quantitatively compared with experiments. We first studied three interface models: the eightfold, fivefold, and T_4 models [84]. We found that the Fermi level is pinned by interface states for the model with eightfold coordinated Ca atoms at the interface, but Fermi level pinning does not occur in models in which F atoms are dissociated from interface CaF_2 (fivefold and T_4 models). We also examined the calculated electronic structure of the

sevenfold and H_3 models in comparison with available experimental data [85].

4 Calculations

4.1 Atomic sphere radii

In LMTO–ASA calculations, the choice of sphere radii is more important than in FLAPW calculations where the sphere radii only specify a detail of the linear basis set. In LMTO–ASA, the sphere radii affect both band dispersion and total energy. Since there is no definite principle to determine the sphere radii, we compared the band structure between the LMTO–ASA and FLAPW calculations. The atomic sphere radii used in the LMTO–ASA calculations were determined for the band dispersion of bulk occupied states to agree with that obtained by the FLAPW calculations.

In the LMTO–ASA calculations for bulk Si in the diamond structure, two spheres are at atomic sites and two empty spheres are at tetrahedral interstitial sites. When the radii are almost equal between the Si and empty spheres, the LMTO calculations for the Si band structure, especially for the occupied states, well agreed with the FLAPW result [86].

$NiSi_2$, $CoSi_2$, and CaF_2 all have a fluorite structure which has three atomic spheres and one empty sphere in a unit cell. The $NiSi_2$ band dispersion was somewhat different between LMTO–ASA and FLAPW when equal atomic sphere radii were used for Si, Ni, and the empty sphere. With nonrelativistic LMTO, the Γ_2^- point was 0.3 eV higher than the Fermi energy [87], but with FLAPW the Γ_2^- point was 0.2 eV lower [88, 89]. To resolve the discrepancy we determined sphere radii to agree with the FLAPW result. With these radii and *s*-, *p*-, and *d*-orbitals, the Γ_2^- point became 0.05 eV lower than the Fermi energy. The highest discrepancy between LMTO and FLAPW was 0.3 eV for occupied bands. When the Ni sphere radius was 5 percent larger than the chosen value, the Fermi energy still remained 0.03 eV above the Γ_2^- point, and the band dispersion changed only slightly. As for the density of states, the anti-bonding peak just above the Fermi energy of $NiSi_2$ was at a slightly lower energy with the chosen radii than with the equal radii. In the semirelativistic calculation, the Γ_2^- point of bulk $NiSi_2$ was also 0.13 eV higher than the Fermi energy with equal sphere radii, and 0.23 eV lower than the Fermi energy with the chosen radii.

Co atom has one less *d*-electrons than Ni atom, and $CoSi_2$ has an electronic structure similar to that of $NiSi_2$ [48]. In order to precisely compare the electronic structure of the

interface, we used the same atomic sphere radii between $NiSi_2$ and $CoSi_2$.

YSi_2 has C32 crystal structure and does not contain the empty sphere. In LMTO–ASA, total volume of spheres must be equal to the unit cell volume. If the Si radius is chosen, the Y radius in YSi_2 is determined. When the Si radius in YSi_2 is set to that of bulk Si, the LMTO calculations well agreed with FLAPW result. So, these radii are used in calculations for the YSi_2/Si(111) interface.

In the LMTO–ASA calculations for CaF_2, to exclude the ghost bands, which sometimes appear in linearized band calculations, we expanded the muffin-tin orbitals from the resonance energy level of the atomic sphere. This was necessary for the calculations of the CaF_2 energy structure, because Ca and F atoms have shallow core levels (Ca $3p$, F $2s$).

The experimental bulk lattice constants are 5.406 Å for $NiSi_2$, 5.356 Å for $CoSi_2$, and 5.463 Å for CaF_2. YSi_2 has a hexagonal unit cell whose lattice constants are 3.842 Å for a-axis and 4.144 Å for c-axis [66]. Since bulk Si lattice constant is 5.429 Å, lattice mismatch between Si and these materials is very small. Although XSW measurements suggest that the interface Si-Si bond length is longer in the type-A $NiSi_2$/Si(111) interface than in the type-B interface [90], conflicting results are also reported [91]. Detailed atomic structures at the interfaces between Si and these materials are not yet available. We neglected lattice relaxation and used the Si lattice constant 5.429 Å to decide the atom position in the supercells.

Table 1 lists atomic sphere radii and number of electrons in bulk calculations. Nine muffin-tin orbitals of s-, p-, and d- are used except Y atom, for which additional f-orbitals are included. The bulk band gaps calculated by LMTO–ASA were 0.55 eV for Si and 6.96 eV for CaF_2, although the measured values of band gap are 1.12 eV for Si and 12.1 eV for CaF_2. Despite the discrepancy between the calculated and measured values, we obtained interface states at the CaF_2/Si(111) whose energy dispersion well agrees with experimental one. At the silicide/Si interface, we obtained adequate SBH differences depending on the interface structure and a kind of silicide.

Table 1: Atomic sphere radii and number of electrons in bulk calculations.

Material	Atomic sphere	Sphere radii (Å)	Number of electrons
Si	Si	1.337	13.212
	Emp.	1.336	0.788
$NiSi_2$	Ni	1.222	27.730
	Si	1.337	13.218
	Emp.	1.433	1.833
$CoSi_2$	Co	1.222	26.679
	Si	1.337	13.232
	Emp.	1.433	1.857
YSi_2	Y	1.991	40.324
	Si	1.337	13.338
CaF_2	Ca	1.466	18.707
	F	1.249	9.466
	Emp.	1.358	0.363

4.2 Supercell method

To examine the electronic structure at an interface, the most appealing theoretical method may be the one based on a self-consistent Green's function technique that describes the two side of the interface as semi-infinite media [92]. Another frequently used method employs the supercell technique to overcome the lack of periodicity perpendicular to the interface. In supercell method, self-consistent conventional band-structure calculations are performed for an infinite crystal that is considered to be made of supercells with a large number of atoms including the interface regions (Fig. 6). The supercell has two interfaces with the same atomic structure so that it has an inversion symmetry. The supercell must be large enough for the central region between the interface to be considered as bulk-like. Our study presents such supercell calculations.

We first examined the type-A and -B $NiSi_2$/Si(111) interfaces. Calculations were made for four cell sizes with m $NiSi_2$ layers and n Si_2 layers: m/n = 2/3, 5/6, 8/9, and 11/12. All these supercells have a space-group symmetry of $P\bar{3}m1$ (D^3_{3d}). The 11/12 supercell consisted of two thick regions: a 35.3 Å $NiSi_2$ region and a 37.6 Å Si region. As described later, we found that 8/9 supercell is almost large enough to examine the electronic structure at the interface. So, for other (111) interfaces, we used the supercells with the $P\bar{3}m1$ symmetry and 9 Si_2 layers. The number of silicide or CaF_2 layers were chosen to keep the space-group

Table 2: Supercell size for interfaces.

Interfaces	Structure	Supercell size
$NiSi_2$/Si(111)	7A	2/3, 5/6, 8/9, 11/12
	7B	2/3, 5/6, 8/9, 11/12
$NiSi_2$/Si(001)	6-fold	$5(NiSi_2)$·$2(NiSi)/7(Si_2)$
	8-fold	$11(NiSi_2)/11(Si_2)$
$CoSi_2$/Si(111)	8A	$10(CoSi_2)/9(Si_2)$
	8B	$10(CoSi_2)/9(Si_2)$
	7A	$8(CoSi_2)/9(Si_2)$
	7B	$8(CoSi_2)/9(Si_2)$
	T_4	$6(CoSi_2)$·$2(CoSi)/9(Si_2)$
$CoSi_2$/Si(001)	8-fold	$11(CoSi_2)/11(Si_2)$
YSi_2/Si(111)	H_3	$10(YSi_2)/9(Si_2)$
CaF_2/Si(111)	8B	$10(CaF_2)/9(Si_2)$
	5B	$2(CaF)$·$8(CaF_2)/9(Si_2)$
	7B	$8(CaF_2)/9(Si_2)$
	T_4	$6(CaF_2)$·$2(CaF)/9(Si_2)$
	H_3	$7(CaF_2)$·$2(CaF)/9(Si_2)$

symmetry. As for $NiSi_2$/Si(001) and $CoSi_2$/Si(001) interfaces, we used the supercells with space-group symmetry of $Cmmm$ (D_{2h}^{19}). Table 2 lists the interface structures and supercell sizes for which we carried out LMTO-ASA calculations.

When an interface is formed of two constituents of materials, an interstitial space at the interface depends on the atomic structure. We occupied it with empty spheres so that the total volume of spheres shall be the same as the supercell volume. When one empty sphere entered at the interface, the sphere radius is automatically determined. When two empty spheres enter, those radii are not uniquely determined, although the bulk atomic sphere radii are determined to agree with FLAPW. Positions and radii of the interfacial empty sphere are determined to fill the interfacial space and decrease the overlap between the neighboring spheres. This rule worked well for the supercells in Table 2 except 8B $CoSi_2$/Si(111) interface, where this rule makes the radius of the interfacial empty sphere so large, resultantly the overlap between the neighboring spheres becomes too large. Hence, we enlarged the radius of the first empty sphere on the Si side for the radius of the interfacial empty sphere to be appropriate.

To get an accurate self-consistent potential of these large supercells, we first calculated

a smaller supercell, for example, 5/6 supercell. The self-consistent potential of the small supercell was used as the initial potential of a larger supercell. First, we performed self-consistent iterations with small number of nonequivalent $\mathbf{k}$ points from 9 to 25 in the first Brillouin zone of the supercell. To get final self-consistent potential, we used from 81 to 162 nonequivalent $\mathbf{k}$ points to get the accurate self-consistent potential.

5 Type-A and -B $NiSi_2$/Si(111) interfaces

5.1 Band lineup and supercell size

From our calculations with the larger supercells, we can determine the band lineup between the Si and silicide layers by examining the wave function weights of the energy eigenvalues of the supercells in each atomic sphere of the Si and silicide layers. At the silicide/Si(111) interface the supercell has D_{3d}^3 symmetry, and the valence band bottoms (E_b) of both the Si and the silicide layers appear at the Γ_1^+ point and the valence band maximum (E_v) of the Si layer appears at the Γ_3^+ point. Since we did not include the spin-orbit interaction, E_v of bulk Si has threefold degeneracy, but with the supercells, E_v is doubly degenerate.

In the two-dimensional hexagonal Brillouin zone of the (111) interface, the conduction band minimum (E_c) of the Si layer appears at a location 0.875 of the way toward the M point along the Γ–M line, on which the Γ–X line of bulk Si is projected. Since the supercell is of finite size, there remains energy dispersion along the k_z direction (perpendicular to the interface). We searched for E_c by examining the wave functions of the eigenstates at the location 0.875 of the way along the Γ–M line, including those in the k_z direction. At the $NiSi_2$/Si(111) interface, 5/6, 8/9, and 11/12 supercells have the same dispersion along the k_z direction at the 0.875 point. E_c of type-A was at the $k_z = 0$ point and E_c of type-B was at the point whose k_z is the Brillouin zone boundary. As k_z increases from zero to the Brillouin zone boundary, the lowest energy levels of the Si conduction band rise 0.005 eV for type-A, and fall 0.007 eV for type-B in 11/12 supercells. This energy dispersion amounted to about 0.01 eV to 0.03 eV in 5/6 and 8/9 supercells.

Using E_b, E_v, E_c, and the Fermi energy of the supercell (E_f), we obtained the p-type SBH's, the Si thermal gaps (E_g), the Si valence bandwidths (E_w equals E_v minus E_b of the Si layer), and the $NiSi_2$ valence bandwidths (E_w equals E_f minus E_b of the $NiSi_2$ layer) listed in Table 3. From these values, we can obtain the entire band lineup of the valence bands of the Si and $NiSi_2$ layers (Fig. 7).

Bulk calculations indicate that the valence bandwidth of $NiSi_2$ is 14.08 eV, and that of bulk Si is 11.94 eV. The Si thermal gap is depressed to 0.55 eV by the local density approximation (LDA) although the experimental value is 1.12 eV. As the supercells are

Table 3: Calculated Schottky barrier height ($E_f - E_v$), thermal gap of Si layer (E_g), valence bandwidth of Si layer (E_w of Si) and valence bandwidth of $NiSi_2$ layer (E_w of $NiSi_2$) obtained from energy eigenvalues of supercells. (in eV)

	$NiSi_2$/Si_2	5/6	8/9	11/12	Expt.[a]
$E_f - E_v$	Type-A	0.48	0.34	0.38	0.47
	Type-B	0.36	0.19	0.23	0.32
E_g	Type-A	0.78	0.65	0.62	
	Type-B	0.90	0.70	0.65	
E_w of Si	Type-A	11.76	11.90	11.91	
	Type-B	11.71	11.87	11.89	
E_w of $NiSi_2$	Type-A	13.38	13.98	14.01	
	Type-B	13.38	13.96	14.01	

[a] Reference [19]

larger, E_g and E_w of both Si and $NiSi_2$ layers in Table 3 converge monotonically toward the calculated bulk values. However, the SBH's show different cell size dependence. SBH's oscillate with supercell sizes, although the oscillation becomes small as the supercell becomes larger. The difference between the SBH's of the two types is 0.15 eV in 8/9 and 11/12 supercells. This value is close to Tung's value of 0.14 eV.

In Table 3, SBH's, E_g, and E_w of both layers differ by more than 0.14 eV depending on the supercell size. However, the energy widths between E_f and E_b of the Si layer differ by only 0.06 eV with the supercell sizes (Fig. 7). The energy width between E_f and E_b of the Si layer little differs between 5/6 and 8/9 supercells and the SBH's change by about 0.15 eV, because the valence bandwidth of the Si layer recovers to the bulk value. Between 8/9 and 11/12 supercells, the energy width between E_v and E_b of the $NiSi_2$ layer little differs, so the SBH difference of 0.04 eV comes mainly from the change in the Fermi energy caused by the recovery of the valence bandwidth of the $NiSi_2$ layer.

The oscillation of the calculated SBH's with supercell size is caused by the valence band width of both Si and $NiSi_2$ layers. The calculated SBH's depend on the valence band structures of both the Si and the $NiSi_2$ layers, especially in the neighborhood of the Fermi energy and Si band gap, but they do not depend so much on the valence band bottom structures.

Table 4: Atomic sphere radii and number of electrons of the empty spheres located at the $NiSi_2$/Si(111) interfaces

	Type-A		Type-B	
Sphere radius (Å)	1.389	1.334	0.971	1.612
Number of electrons	1.102	0.780	0.315	1.630

5.2 Electron distribution

Figure 8 shows the difference in total number of electrons from the bulk values (Table 1) obtained with 11/12 supercells. In the Si layer, Si spheres close to the interface have much fewer electrons than bulk Si, and the next empty spheres have more electrons. In the $NiSi_2$ layer, Si and Ni spheres close to the interface have much fewer electrons bulk $NiSi_2$. Two empty spheres at the interface are not included in Figure 8. Their sphere radii and numbers of electrons are listed in Table 4. The interface empty spheres have smaller electron densities than the empty sphere in $NiSi_2$. In the Si layer two Si spheres are located between empty spheres (Fig. 8). In the $NiSi_2$ layer, the layer composed of one Ni and two Si spheres has empty spheres on both sides. There is additional space at the interface which is equal to about one half the diameter of an empty sphere. To fill up the additional space at the interface, electron transfer occurs. Consequently, there are fewer electrons in the interface spheres in both Si and $NiSi_2$ layers than bulk, and next spheres have more electrons to screen out the positively charged interface atom spheres. So, the electron distribution at the interface is caused primarily by the additional interface space at the sevenfold structures.

The electron distribution of other supercells resembles that of the 11/12 supercell, but the number of electrons in each sphere depends slightly on the supercell size. In 5/6 and 8/9 supercells, the difference in the number of electrons compared with the 11/12 supercell is no more than 0.002 for each sphere, but in 2/3 supercells this difference amounts to 0.01 to 0.02. The 2/3 supercell does not have enough layers to screen out the interface disturbance produced by joining of the two different materials. The difference from the 11/12 supercell is less in the 8/9 supercell than in the 5/6 supercell, and is greater in the $NiSi_2$ layer than in the Si layer for both types of interface.

5.3 Local density of states

In the LMTO-ASA calculation, local density of states (LDOS) in the i atomic or empty sphere is given by

$$N_i(E) = \sum_{\mathbf{k}_{||},n} \int_{\Omega_i} |\psi_{\mathbf{k}_{||},n}(\mathbf{r})|^2 d^3r \delta(E - E_n(\mathbf{k}_{||})), \tag{16}$$

where $\mathbf{k}_{||}$ is the wave vector parallel to the interface, n is the band index, $\psi_{\mathbf{k}_{||},n}$ is the wave function, and Ω_i is the volume of the i sphere.

Figures 9 and 10 show LDOS obtained by summing up $N_i(E)$ of the spheres in each layer of the 11/12 supercells. In the $NiSi_2$ layer farthest from the interface, LDOS agrees well with the bulk density of states (DOS). Near the interface in the $NiSi_2$ layers the large d-electron peak is shifted to a higher energy. In the farthest Si layer, the Si thermal gap almost appears, and the LDOS also agrees well with the bulk Si DOS. In the Si layers near the interface, the sharp peak at -7 eV and the small dip at 3 eV disappear. The arrows in the figures indicate interface states, which are formed mainly by d-orbitals of the interface Ni atoms, and by Si p-orbitals in the Si layers.

Figure 11 shows the LDOS of the interface Si_2 layer of type-A obtained with 2/3, 5/6, and 8/9 supercells. In the 2/3 supercell, the LDOS is rough in comparison with those of other supercell and the interface states are not easily distinguishable. The Si valence band bottom of the 2/3 supercell is at an energy about 0.3 eV higher than that of other supercells. The 2/3 supercells are too small for the interface electronic structure to be examined.

Since there are two interfaces in a unit cell with supercell geometry (Fig. 6), the tails of the interface states interact in the Si layer, so that the interface states of the 5/6 supercell are slightly different from those of the 8/9 supercell. The LDOS of the 8/9 supercell's interface Si_2 layer is almost the same as that in the 11/12 supercell in Figure 9. Type-B showed almost the same cell size dependence of LDOS.

At the $NiSi_2$/Si(111) interface, the interface Ni atoms have sevenfold coordinations in contrast to the eightfold coordinations in bulk $NiSi_2$ [93]. These imperfect bonds cause the interface states near the Si thermal gap. The interface states of $NiSi_2$/Si(111) are below the Fermi energy and are occupied by electrons.

In bulk $NiSi_2$, the quasi-gap separating the bonding and anti-bonding states is slightly

below the Fermi energy [48]. In the $NiSi_2$ layers near the interface, the anti-bonding peak just above the Fermi energy has a lower density than bulk $NiSi_2$. Since the interface states appear just below the Fermi energy, the quasi-gap seems to be shifted up in energy.

Figure 12 shows the two-dimensional band structure near the Si band gap of the type-A interface. The zero energy point corresponds to the Fermi energy of the supercell. Each dot represents the energy eigenvalue of the 11/12 supercell at the k point whose k_z element equals zero. The larger dots are eigenvalues whose wave functions exist in the Si layer more than 40 percent. The Si band is clearly distinguishable. The partial band gap of $NiSi_2$ can be seen near the M–K line in the Si band gap. The interface states appear in the partial band gap of $NiSi_2$.

In the figures of LDOS, the interface state of type-B is at a lower energy than that of type-A. In the two-dimensional band structure, its energy dispersion in the partial gap of $NiSi_2$ was a little different from that of type-A. Since the interface states are caused mainly by interface bonding configurations, this difference probably comes from the local atomic structures at the interface. The main structural difference between the two types is that the distance between the interface Ni atom and the second Si atom on the Si side is smaller in type-B than in type-A. Bonding interaction exists between these atoms in type-B, so that the interface states of the two types of interface have different energy dispersions.

5.4 Metal-induced gap states

The Si thermal gap is occupied by extra states called metal-induced gap states (MIGS). The MIGS are important for studying the metal-semiconductor interface. Figure 13 shows MIGS density (D_s) in the Si thermal gap. It was obtained from the 11/12 supercells by summing up the LDOS between E_v and E_c of all the spheres in the Si layer except the two interfacial empty spheres. Although the MIGS in the Si thermal gap depends slightly on the supercell size, their density is more than 10^{14}/eV cm^2 in every supercell.

Figure 14 shows the space distribution of the total MIGS in the Si layer. This was obtained by

$$Q_i = \int_{E_v}^{E_c} N_i(E) dE, \tag{17}$$

where N_i is the LDOS given by the equation (16). Thus, the perpendicular axis in Figure 14

indicates the number of electrons which stay in each sphere if they occupy all MIGS between E_v and E_c. Since the Fermi level is above E_v, more than half of the MIGS are occupied by electrons. The MIGS are mainly formed by Si p-orbitals and are concentrated in the Si spheres rather than in the interstitial spheres, in contrast with the total valence electron distribution in the Si layer (Fig. 8). The MIGS are formed of the states which are taken from the valence and conduction band states of the Si layer. This is why metal wave functions can penetrate deep into the Si layer even in the Si band gap, and a high density of MIGS is formed.

5.5 Frozen potential method

Two other groups performed calculations on the two types of $NiSi_2$/Si(111) interface using LMTO–ASA. Bisi and Ossicini obtained p-type SBH's which are 0 eV for type-A and 0.3 eV for type-B in 5/3 supercells [27]. The SBH difference between the two types is contrary to the Tung's experiment. Their supercells are too small to study the interface.

Das, Blöchl, Christensen, and Andersen reported on 8/6 supercell calculations [35]. Their p-type SBH's were 0.16 eV for type-A and 0 eV for type-B, using equal atomic sphere radii in the $NiSi_2$ layers with LMTO–ASA. Their SBH's are smaller than ours. To resolve this discrepancy, we performed calculations for the type-A structure using equal radii for all atomic spheres as they did, and got a smaller SBH like theirs. The difference between our SBH's and theirs comes mainly from the choice of atomic sphere radii.

We used supercell eigenvalues to calculate SBH's by examining wave function weights in the Si and $NiSi_2$ layers. However, different method for obtaining SBH's from supercell calculations gives different values. Das *et al.* used self-consistent one-electron potentials obtained by supercell calculations. Their method yields the same SBH's as those obtained by the so-called frozen potential method [94]. By the frozen potential method, one-electron potentials of the $NiSi_2$ and Si layers farthest from the interface are cut from the self-consistent potential obtained by supercell calculations, and exported to bulk band calculations, which yield the $NiSi_2$ Fermi energy (E_f') and the Si valence band maximum (E_v'). We also used the frozen potential approach and got the values of E_f' minus E_v' listed in Table 5. For every supercell size, E_f' minus E_v' values are smaller than the eigenvalue SBH's, and oscillate like

Table 5: The difference $(E'_f - E'_v)$ between the $NiSi_2$ Fermi energy (E'_f) and Si valence band maximum (E'_v) obtained by frozen potential approach. (in eV)

$NiSi_2/Si_2$	5/6	8/9	11/12
Type-A	0.41	0.32	0.36
Type-B	0.23	0.14	0.19

the eigenvalue SBH's in Table 3.

In the figures of LDOS, the dotted lines are bulk DOS's, which were drawn in the $NiSi_2$ layer for the bulk Fermi energy to coincide with the supercell Fermi energy. In the Si layer the bulk valence band maximum was fitted to the eigenvalue E_v of the supercell. If the bulk Si DOS is fitted to the E'_v obtained by the frozen potential method, the bulk DOS deviates more from the LDOS at the Si layer farthest from the interface. The LDOS is related to the eigenvalue E_v, but not to the frozen potential E'_v. This holds even with 8/9 supercells. With 5/6 supercells, however, bulk Si DOS was shifted to a much lower energy by this method because the eigenvalue SBH's are too large.

Although the choice of sphere radii affects the SBH values, SBH of type-B is smaller than that of type-A in every larger supercell. As is evident in Table 3, the SBH values converge as the supercell size increases. Although the 11/12 supercells are still too small to give conclusive SBH's, we speculate that final calculated SBH values will be within 0.04 eV of those of the 11/12 supercells. The fact that the calculated SBH is lower than the experimental value is probably due to the LDA error.

5.6 Interface dipole

In LMTO-ASA, one-electron potential consists of spherical potentials at each atomic and empty sphere site. The spherical potential is composed of two different contributions. One comes from the charge distribution inside its own sphere, and the other is long range (inter-sphere) electrostatic potential produced by surrounding spheres. The charges are treated as point charges placed at the sphere centers to calculate the inter-sphere electrostatic potential, whose on-site value is calculated by summing up the products of the Madelung constants and the point charges of the other spheres.

In Figure 15, we plotted the inter-sphere electrostatic potential at each Si site in a 11/12

supercell. It changes only near the interface and is rapidly screened. Comparing it with the electron distribution in Figure 8, we recognize a large interface electric dipole layer with a positive layer on the Si side and a negative layer on the $NiSi_2$ side. On the Si side, the potential for type-B is slightly larger than that for type-A. On the $NiSi_2$ side, the potential for type-B is smaller than that for type-A. It almost reflects the SBH difference between the two types of interface, because type-A has a smaller E_v in the Si layer and a larger E_f in the $NiSi_2$ layer than type-B.

At the interface site, the potential differs by about 1 volt for the two types, but the SBH differs by only 0.15 eV. The interface disturbance depends heavily on the atomic structure, but is screened in two or three layers on both the Si side and the $NiSi_2$ side. 2/3 supercells have almost these many layers. As was stated in a previous section, the electron distribution changes only slightly among 5/6, 8/9, and 11/12 supercells, because the interface disturbance is sufficiently screened out in two or three layers. However, the SBH changes by 0.04 eV to 0.17 eV depending on the cell size. Since supercells contain more Si and $NiSi_2$ layers, both layers have more bulk-like character. This affects the calculated SBH's. The supercell must contain many layers for the SBH to converge sufficiently.

Das *et al.* reported 0.05 eV SBH lowering including the contraction of the interface Si–Si bond length [35]. Details of interface atomic positions also affect the calculated SBH's. The LDOS difference between the two types can be seen around -3 eV and $+2$ eV in the Si layers near the interface. Since the calculated SBH depends both on the interface details and on the thickness of the Si and $NiSi_2$ layers, we speculate that how the wave functions continue through the interface affects SBH, especially the wave functions of the energy states in the neighborhood of the Si band gap and the Fermi energy.

6 $CoSi_2$/Si(111) interface

6.1 Eightfold structure

6.1.1 Local density of states

Figures 16 and 17 are LDOS of the eightfold $CoSi_2$/Si(111) interfaces, which are nowadays believed as correct interface structures. LDOS of the first Si_2 layer much deviates from the bulk Si DOS (Dotted lines) because the interfacial Co atom is eightfold coordinated and an Si–Co bond is formed at the interface (Fig. 3). A peak at -4 eV in bulk $CoSi_2$ DOS is an evidence of Co–Si bond which is constituted of Si p- and Co d-orbitals. In the first Si_2 layer, the same evidence can be partly seen at -4 eV.

An interfacial Si atom has an imperfect tetrahedral structure and has one dangling bond, which is the origin of interface states (shaded areas in Figures 16 and 17). The interface states in the Si thermal gap are formed mainly of Si p-orbitals and those at the bottom of the valence band are formed of Si s-orbitals. In the first $CoSi_2$ layer, the small peaks just above the Fermi level (shaded areas) are a little different between the two types of interface. The peak of the type-B is slightly sharper and higher than that of the type-A; dangling bond character remains more strongly at the type-B interface. Since the detail of interfacial atomic structure affects the interface states, this difference comes from structural difference between the two types of interface. At the type-A interface, the distance between the interfacial Si atom and second Si atom in the Si layer is the same as bulk Si–Si distance. Bonding interaction between these atoms is stronger at the type-A interface than at the type-B interface (Fig. 3).

Hamann reported full-potential LAPW calculations at the $CoSi_2$/Si(111) interfaces with 2/2 supercells [44]. In his contour plot of the interface electron density, there are extra contours between the interfacial Si atom and the second Si atom in the first Si_2 layer at the type-A interface and there are none at the type-B interface; the interfacial Si atom of the type-A interface is overcoodinated. Since the small peak of the dangling bond is broader in the type-A interface, our LDOS is consistent with the electron density plot of Hamann.

6.1.2 Two-dimensional band

Figure 18 shows a schematic two-dimensional band along the symmetry lines of the type-A $CoSi_2$/Si(111) interface. This was obtained by examining the wave function weights of the energy eigenvalues of the 10/9 supercell in each atomic sphere of the Si and $CoSi_2$ layer. The zero energy is the Fermi level (E_f) of the supercell.

This interface band structure reveals a new band connection. The conduction band minimum (E_c) of the Si layer appears at a location 0.875 of the way toward the M point along the Γ–M line, on which the Γ–X line of bulk Si is projected. The bottom region of the Si conduction band is swallowed in the $CoSi_2$ band stomach (partial band gap). There are no energy states in the $CoSi_2$ layer that continue into the bottom region of the Si conduction band [95]. For electrons in the Si conduction band to go through into the $CoSi_2$ layer, they must either have a high energy or change their momentum at the interface by phonon or impurity scattering. Since the band offset of the type-B interface differs only by 0.12 eV from the type-A interface, the similar band connection appears at the type-B $CoSi_2$/Si(111) interface.

Bold lines in Figure 18 are interface states whose wave functions are localized more than 40 percent in the 4 atomic spheres (three Si and one Co spheres) at the interface. The interface state indicated by the upper line in the Si band gap is formed mainly of Si p-orbitals, and the lower line is formed mainly of Si p-orbitals and a little of Co d-orbitals. The upper line corresponds to the shaded area in the Si band gap in Figure 16. The interface states indicated by the lower line make a small peak in LDOS (the peak indicated by an arrow in Fig. 16). The interface states around at -5 eV in Figure 18 correspond to the interfacial Si–Co bond as previously mentioned.

6.1.3 Interfacial gap states

The energy states in the Si band gap are classified into the two categories. One is interface states whose wave functions are localized near the interface and decaying on the both sides of the interface. The other is metal-induced gap states (MIGS) whose wave functions are decaying only on the semiconductor side. Interface states originate in the interfacial bond

configuration and sometimes overlap the projected bulk band of the metal or semiconductor. MIGS are formed only in the energy region where the bulk band of the metal is projected. As seen in Figure 18, metals have their own two-dimensional energy structure depending on the interface orientation. MIGS depend on the metal band structure at the homogeneous metal-semiconductor interface.

In Figure 18, the interface states in the Si band gap disappear near the Γ point. When the interface states overlap the bulk band, their wave functions are inclined to extend into the metal or semiconductor layers depending on the k point. Since this delocalization of the wave function gradually occurs, we cannot clearly distinguish between MIGS and the interface states.

The thermal gap of the Si layer obtained from the eigenvalues of the 10/9 supercells is 0.71 eV for the type-A and 0.70 eV for the type-B $CoSi_2$/Si(111) interfaces. Figure 19 shows the surface density of the gap states (D_s). Since it was obtained by summing up the LDOS between E_v and E_c of the all spheres in the Si layer, both of MIGS and the interface states are included in Figure 19. The gap states are mainly formed by Si p-orbitals and are concentrated in the Si spheres rather than in the interstitial empty spheres, similar to the $NiSi_2$/Si(111) interfaces (Fig. 13).

The origin of the interface states in the Si band gap is the dangling bond of the interfacial Si atom at the eightfold $CoSi_2$/Si(111) interfaces and is the dangling d-orbital of the interfacial Ni atom at the sevenfold $NiSi_2$/Si(111) interfaces. Since the interfacial gap states are formed mainly of Si p-orbitals in the Si layer, the wave function of the Si dangling bond extends more easily into the Si layer than that of the dangling d-orbital. This is the reason why the D_s of the $CoSi_2$/Si(111) is higher than that of $NiSi_2$/Si(111).

6.1.4 Electron distribution

Figure 20 shows the difference in total number of electrons from the bulk values (Table 1) at the type-A eightfold $CoSi_2$/Si(111) interface. In this structure, one empty sphere enters at the interface. Its radius is 1.386 Å because the total volume of spheres must be the supercell volume. The interfacial empty sphere had 1.448 electrons in it.

Both in the Si and $CoSi_2$ layers, spheres close to the interface have more electrons than

bulk. In the Si layer, the first and second Si spheres have more electrons and the third Si sphere has less electrons than bulk. Owing to the extra bond between the interfacial Si atom and the second Si atom as previously mentioned, the second Si sphere has to contain many electrons. Since the third Si sphere has less electrons, probably, there are less electrons between the second and third Si atoms. In the $CoSi_2$ layer, the fist Si–Co–Si spheres have more electrons than bulk. From the contour plot of the interfacial electron density, Hamann found that the Co–Si bonds within the $CoSi_2$ layer was strengthened compared to the bulk and the bonds within the Si layer were weakened [44]. Figure 20 is consistent to the Hamann's result.

In contrast with the electron distribution at the eightfold $CoSi_2$/Si(111) interface, atomic spheres close to the interface had less electrons than bulk at the sevenfold $NiSi_2$/Si(111) interfaces. Two empty spheres entered at the sevenfold $NiSi_2$/Si(111) interface, while one empty sphere enters at the eightfold $CoSi_2$/Si(111) interface. Since the sevenfold structure has larger space at the interface, electron transfer occurs to fill the interfacial space. But the eightfold structure has less interfacial space: atoms are crowded at the interface. So, electrons overflow at the eightfold $CoSi_2$/Si(111) interface so that spheres close to the interface have more electrons. The interfacial space steeply changes the electron distribution at the silicide/Si interface.

At the type-B eightfold $CoSi_2$/Si(111) interface, it was difficult to determine the radius of the interfacial empty sphere. Its radius of the type-A is naturally derived for the total volume of spheres to be the supercell volume. However, at the type-B eightfold interface, this rule makes the radius of the interfacial empty sphere so large that the overlap between the neighboring spheres becomes too large. Hence, we enlarged the radius of the first empty sphere on the Si side for the radius of the interfacial empty sphere to be appropriate. In the ASA calculations, the neighboring atomic spheres overlap with each other. To compare the number of electrons in the sphere, the spheres must have the same radius. Therefore, at the type-B eightfold $CoSi_2$/Si(111) interface, the number of electrons in spheres cannot be precisely compared with bulk. Only the outline of the electron distribution can be understood in comparison with Table 1.

Table 6 lists the number of electron of the type-B eightfold $CoSi_2$/Si(111) interface. The

Table 6: Number of electrons in the spheres near the eightfold type-B $CoSi_2$/Si(111) interface. The radius of the first empty sphere in the Si layer (indicated by a) is 1.529 Å, which is larger than the radius of other empty spheres in the Si layer. See text.

	Si layer		$CoSi_2$ layer	
	Sphere	Electrons	Sphere	Electrons
1	Si	13.451	Si	13.417
2	Si	13.063	Co	26.742
3	Emp.[a]	1.414	Si	13.245
4	Emp.	0.699	Emp.	1.846
5	Si	13.065	Si	13.221
6	Si	13.155	Co	26.682
7	Emp.	0.796	Si	13.234
8	Emp.	0.802	Emp.	1.856
9	Si	13.215	Si	13.231
10	Si	13.210	Co	26.681

interfacial empty sphere is not listed in Table 6. It has a 1.137 Å radius and 1.027 electrons in it. In the $CoSi_2$ layer, the first $CoSi_2$ spheres have more electrons than bulk, just like at the type-A interface. In the Si layer, the first Si has more electrons and the sum of number of electrons in the next Si–Emp.–Emp.–Si spheres is larger than bulk. So, we can know that, just like the type-A interface case, electrons overflow on both side of the type-B interface, because atoms are crowed at the interface.

6.2 Sevenfold and T_4 structures

At a type-B $CoSi_2$/Si(111) interface with a low density of dislocations, Tung reported that the n-type SBH varies from ~0.7 to ~0.5 [57]. Sullivan *et al.* formed the type-B $CoSi_2$/Si(111) interface which has an extremely low n-type SBH of 0.27 eV, while an ordinary $CoSi_2$/Si(111) interface shows SBH of about 0.70 eV. To examine possibility of the low n-type SBH (that is high p-type SBH), we performed the LMTO–ASA calculations for the sevenfold and T_4 structures.

6.2.1 Type-A and -B sevenfold structures

Figures 21 and 22 are LDOS of $CoSi_2$/Si(111) interfaces where the interfacial Co atom is sevenfold coordinated. These interfaces have the same structure as the type-A and -B $NiSi_2$/Si(111) interfaces. Moreover, since the radii and positions of the atomic and empty

Table 7: Atomic sphere radii and number of electrons of the empty spheres located at the sevenfold $CoSi_2$/Si(111) interfaces

	Type-A		Type-B	
Sphere radius (Å)	1.389	1.334	0.971	1.612
Number of electrons	1.120	0.777	0.312	1.648

spheres are the same as those of the $NiSi_2$/Si(111) interfaces, calculations are under the same condition. Only the metal atom differs. That is, Co atom has one less d-electrons than Ni atom.

The LDOS of the sevenfold $CoSi_2$/Si(111) interfaces resembles those of the $NiSi_2$/Si(111) interfaces. In the Si layers near the interface, the sharp peak at −7 eV and the small dip at 3 eV disappear. The interface states in the Si thermal gap are formed mainly by d-orbitals of the interfacial Co atoms and by Si p-orbitals in the Si layers, and are at a little higher energy than those of the $NiSi_2$/Si(111) interfaces (Fig. 9 and 10), because the Co d-orbital has a higher energy; the large d-electron peak of $CoSi_2$ is at a higher energy than that of $NiSi_2$. The partial band gap of $CoSi_2$ which appears in the (111) projected two-dimensional Brillouin zone is also at a higher energy than that of $NiSi_2$ (Fig. 12). In the $CoSi_2$ layers near the interface, the large d-electron peak is a little bit shifted to a higher energy. It is observed at the $NiSi_2$/Si(111) interfaces, although the shift range is smaller in the $CoSi_2$/Si(111) than in the $NiSi_2$/Si(111).

Figure 23 shows the difference in total number of electrons from the bulk value (Table 1) at the two types of sevenfold $CoSi_2$/Si(111) interface. Compared with the $NiSi_2$/Si(111) interfaces (Fig. 8), the difference in number of electrons from the bulk value is almost the same at each type interface. The sphere radii and number of electrons of interfacial empty spheres (not shown in Fig. 23) are listed in Table 7. The sum of electron numbers in the two empty spheres is 0.015 larger than that of the $NiSi_2$/Si(111) interface for each type interface (Table 4). Hence, electrons decrease slightly in spheres close to the $CoSi_2$/Si(111) interface compared with the $NiSi_2$/Si(111) interface. This is reasonable because bulk $CoSi_2$ has 0.024 more electrons in the empty sphere than bulk $NiSi_2$ (Table 1).

Compared with the electron distribution at the eightfold $CoSi_2$/Si(111) interface (Fig. 20),

the sevenfold interface shows almost the same distribution between the $CoSi_2$ and $NiSi_2$ interfaces. The large part of the electron distribution at the silicide/Si interface is determined by the interfacial atomic structure, especially by volume of the interfacial space.

With the aid of calculations on cluster modeling, Hoek *et al.* found a simple picture explaining why the interface structure differs between the $CoSi_2$/Si(111) and $NiSi_2$/Si(111) interfaces [96]. They take notice of orbital overlap populations. At the eightfold interface, the metal *d*-orbital and Si p_z orbital on the Si side make a chemical bond which has a little more electrons at the $CoSi_2$/Si(111) interface than at the $NiSi_2$/Si(111) interface. At the sevenfold interface, the Si p_z orbitals on both Si and silicide sides make a chemical bond which has slightly more electron at the $NiSi_2$/Si(111) interface than at the $CoSi_2$/Si(111) interface. The major reason for this difference is that the Ni atom has one more electron than the Co atom. Hence, the $CoSi_2$/Si(111) interface prefers the eightfold structure while the $NiSi_2$/Si(111) interface prefers the sevenfold structure.

Although it is difficult to study the structural difference of the total energy by LMTO-ASA, we can compare the interface energy between the same types of sevenfold interface, because the position and radii of the atomic spheres are the same between each type of $CoSi_2$/Si(111) and $NiSi_2$/Si(111) interfaces. The interface energy is defined as half of the supercell energy minus half the sum of energy of a number of unit cells of each bulk material. The interface energy is higher at the sevenfold $CoSi_2$/Si(111) interface than at the sevenfold $NiSi_2$/Si(111) interface; 0.55 eV higher for the type-*A* and 0.64 eV higher for the type-*B* interface. From full-potential LAPW calculations, Hamann obtained that the $CoSi_2$/Si(111) interface has a 0.51 eV higher interface energy than the $NiSi_2$/Si(111) interface for the type-*A* sevenfold structure [44]. This well agrees with our result.

6.2.2 T_4 structure

Figure 24 is LDOS of the type-*B* $CoSi_2$/Si(111) interface whose interfacial Co atom is at the T_4 site (see Fig. 5). This structure was appropriated from the CaF_2/Si(111) interface to examine the possible interface structure with a low *n*-type SBH [61]. The distance between interfacial Co layer and first Si layers was 2.037 Å [84]. In Figure 24, the interface states in the Si band gap has two peaks of bonding and antibonding states, because the interface

Table 8: Atomic sphere radii and number of electrons of the empty spheres located at the T_4 $CoSi_2$/Si(111) interface

Sphere radius (Å)	1.036	1.440
Number of electrons	0.548	1.449

states originate in the bonding interaction between the interfacial Co and Si atoms. In the Si layer, the interface bonding states are formed of Si *p*-orbitals and the antibonding states are formed of Si *s*- and *p*-orbitals. In the first CoSi layer, the interface states (shaded area) are formed mainly of Co *d*-orbitals.

In either eightfold or sevenfold structure, the interfacial Si atom on the Si side is tetrahedrically bonded to four nearest neighbor atoms even though the interfacial atom on the silicide side has a dangling bond. In the T_4 structure, the interfacial Si atom on the Si side is bonded to the nearest three Si atoms (back bonds). The interfacial Co–Si bonds have the same direction in the interface plane as the back bonds of the interfacial Si atom and the interfacial Co atom has eightfold coordination like bulk $CoSi_2$.

Figure 25 shows the difference in total number of electrons from the bulk value (Table 1) at the T_4 $CoSi_2$/Si(111) interface. Table 8 lists radii and number of electrons of two empty spheres at the interface. In Figure 25, electrons decrease on both sides of the interface. At the sevenfold structure (Fig. 23), the number of decreased electrons from the sphere close to the interface amounts to no more than 0.2 electrons. At the T_4 structure, the interfacial Si sphere on the Si side has about 0.3 less electrons and the interfacial Co sphere has about 0.5 less electrons than bulk. An extremely large number of electrons decreases at the T_4 interface compared with the $NiSi_2$/Si(111) interfaces, and the eightfold and sevenfold $CoSi_2$/Si(111) interfaces (Fig. 8, 20, and 23).

In the bulk $CoSi_2$ and $NiSi_2$, a large part of electrons in the empty sphere is supplied by the Si atoms (Table 1). The T_4 structure has a Co-Si layer at the interface, while the sevenfold and eightfold structures have a Si–Co–Si layer at the interface. The T_4 structure lacks one Si layer between the interfacial empty sphere layer and the first empty sphere layer on the $CoSi_2$ side. This is the reason why electrons extremely decrease at the T_4 structure although the total volume of the two interfacial empty spheres is slightly larger in

Table 9: Calculated Schottky barrier height ($E_f - E_v$) at the $CoSi_2$/Si(111) interfaces obtained by the eigenvalue of the supercell and by the frozen potential method. (in eV)

Structure	By eigenvalue	By frozen potential
8A	0.37	0.29
8B	0.25	0.19
7A	0.29	0.24
7B	0.07	−0.01
T_4	0.49	0.42

the sevenfold structure than in the T_4 structure (Tables 7 and 8).

6.3 Schottky barrier heights

Table 9 lists the calculated SBH's ($E_f - E_v$) at the $CoSi_2$/Si(111) interfaces. We got the values by means of two methods. One is obtained from the eigenvalue of the supercell and the other is obtained from the frozen potential method (see Section 5.5). Since the supercells consist of 9 Si_2 layers and 8 or 10 $CoSi_2$ layers (Table 2), these values probably contain an approximately 0.05 eV convergence error with respect to supercell size.

The SBH obtained by the frozen potential method is determined by the spherical potentials of the Si layer and $CoSi_2$ layer farthest from the interface. The eigenvalue SBH is concerned with the all spherical potentials of the supercell because it is derived from the Fermi level and the eigenvalue of the supercell. If the supercell was extremely large, the two methods will give the same SBH. Since the frozen potential SBH in Table 9 is smaller than the eigenvalue SBH just like the $NiSi_2$/Si(111) interfaces, we use the eigenvalue SBH's in this section.

At the $NiSi_2$/Si(111) interfaces, the difference in calculated SBH's for the two types is in good agreement with the experimental value (Table 3). But, there are different opinions about why the two types have the different SBH's. The interface state at the $NiSi_2$/Si(111) originates in the dangling d-orbital of the interfacial Ni atom and its energy dispersion differs between the two types. The interface state of type-B is at a lower energy than that of type-A. Other groups attributed this to the cause of the different SBH's at the $NiSi_2$/Si(111) interfaces [35, 98].

At the eightfold $CoSi_2$/Si(111) interface, the interface states originates in the interfacial Si dangling bond. The interfacial gap states are quite different between the eightfold $CoSi_2$/Si(111) and $NiSi_2$/Si(111) interfaces. However, at the eightfold $CoSi_2$/Si(111), the type-A had a larger SBH than the type-B, similarly to the $NiSi_2$/Si(111) interfaces. This is also true with the sevenfold $CoSi_2$/Si(111) interfaces. The difference of the eigenvalue SBH's between the two types at these interfaces is in the range 1.2 – 2.2 eV. Since the energy states near the Fermi level are formed mainly of p- and d-orbitals, we suppose that the SBH difference between the two types comes from whether the silicide layer is rotated or not rotated around the Si(111) axis.

The p-type SBH at the metal-semiconductor interface can be written as

$$\Phi_{Bp} = \chi_s + E_g - \phi_m + D_0, \tag{18}$$

where ϕ_m is the metal work function. The E_g and χ_s are the band gap and electron affinity in the semiconductor, respectively. The D_0 is the electrostatic interface dipole which is determined by the electron distribution at the interface [97]. When only the structural difference of interface is concerned, the χ_s, E_g, and ϕ_m are the same. The interfacial dipole (D_0) could differ. The electron distribution tremendously differs between the type-A eightfold and sevenfold $CoSi_2$/Si(111) interfaces but the SBH differs only by 0.08 eV. Between the two types of sevenfold interfaces, the electron distribution slightly differs compared with the eightfold structure but the SBH's differ by as large as 0.22 eV.

When atoms are crowded at the interface electrons overflow as for the eightfold structure. When the interfacial space is large, the spheres close to the interface have less electrons than bulk as for the sevenfold and T_4 structures. At the silicide/Si interface, a large part of electron transfer occurs to neutralize the charge distribution caused by the atomic structure of the interface, especially by the interfacial space. A small part of the electron transfer is concerned with the interface dipole (D_0). We suppose that some character of the interfacial bonding interaction is concerned with the interface dipole which determines the SBH.

The experimental p-type SBH of 0.43 eV for the $CoSi_2$/Si(111) interface probably with the eightfold structure [60] is between the SBH's at the two types of $NiSi_2$/Si(111) interface. The calculated SBH of 0.25 eV for the type-B eightfold $CoSi_2$/Si(111) interface is also almost directly between the SBH's calculated for the $NiSi_2$/Si(111) interface by the supercell with

9 Si_2 layers. These calculated SBH's are about 0.15 eV smaller than the experimental values. Although this deviation still contains the convergence error of about 0.05 eV with respect to the supercell size, its large part is caused by the LDA for exchange and correlation interactions.

Sullivan *et al.* reported an extremely high *p*-type SBH for the type-*B* CoSi2/Si(111) interface. To examine the possible interface structure, we examined the sevenfold and T_4 interfaces. The calculated SBH for the type-*B* sevenfold interface is 0.07 eV which is smaller than that of the type-*B* eightfold interface. The interface energy of the sevenfold structure is much larger because Co atom has one less *d*-electrons than Ni atom. So, the sevenfold interface is excluded from the possible structure with a high *p*-type SBH.

Using the T_4 structure of the CaF_2/Si(111) interface, we obtained an SBH of 0.49 eV which is 0.24 eV larger than the SBH of the type-*B* eightfold interface. This demonstrates the possibility that the type-*B* $CoSi_2$/Si(111) interface has a large *p*-type SBH caused only by the interface structure. Since the twisted interface lowers the SBH at the type-*B* interface, the SBH may be raised by the interface bond bending like that at the T_4 interface. The interfacial Co–Si distance in the T_4 structure is 3 Å which is larger than the bulk Co–Si distance of 2.319 Å. Compared with eightfold and sevenfold interfaces, the electron distribution at the T_4 structure is extremely deviated from the bulk. Hence, we consider that the T_4 structure is not realized at the type-*B* $CoSi_2$/Si(111) interface. Sullivan *et al.* mentioned possibility of the existence of an interface reconstruction similar to that found for $CoSi_2$Si(001) interface [64]. We suppose that the extremely high SBH may be caused by the bond bending in the interfacial reconstructed structure.

7 Silicide/Si(001) interfaces

7.1 Schottky barrier height

The $NiSi_2$/Si(001) is considered to have the sixfold structure from the lattice image of TEM (The interface Si atoms in Fig. 2 do not exist). With a supercell containing 6(Si_2) and 7($NiSi_2$) layers, the sixfold structure had a calculated *p*-type SBH of −0.02 eV: the Fermi energy is lower than the valence band maximum of the Si layer (E_v). This is an unreasonable SBH. We previously reported that an incorrect fivefold model of the $CoSi_2$/Si(111) interface gives a negative SBH although a correct eightfold model gives a positive and reasonable SBH [46]. Hence, we conclude that the sixfold model does not represent the $NiSi_2$/Si(001) interface. Another possible structure of the $NiSi_2$/Si(001) interface is the eightfold model in which the interface Si atoms have two dangling bonds (Fig. 2). With a supercell containing 7(Si_2) and 7($NiSi_2$) layers, the eightfold model shows a SBH of 0.36 eV, which is a reasonable SBH.

Since the $CoSi_2$/Si(111) interface has an eightfold structure, the eightfold model of (001) interface may be one possible structure at the $CoSi_2$/Si(001) interface. So, we performed calculations for the eightfold $CoSi_2$/Si(001) interface, too.

The supercell size affects the calculated SBH through the valence band width of each silicide and Si layer [37]. To compare the SBH between the (001) and (111) interfaces, we used supercells with 11 Si_2 layers and 11 $NiSi_2$ or $CoSi_2$ layers for the eightfold (001) interface. We obtained an *p*-type SBH of 0.35 eV for the $NiSi_2$/Si(001) and of 0.28 eV for the $CoSi_2$/Si(001).

To obtain these SBH's at the (001) interface, we used the frozen potential method. Since the spin-orbit interaction is not included, the E_v of bulk Si has three-fold degeneracy. At the (111) interface, the E_v of the Si layer was doubly degenerate and easily distinguishable by the wave function weights of each eigenvalue at the Γ point of the supercell. At the (001) interface, all eigenstates at the Γ point are single-valued because the interface structure lowers the space symmetry of the supercell. Among the eigenstates near the Fermi level at the Γ point, we can identify the E_v of the Si layer and obtain the eigenvalue SBH. It was about 0.13 eV larger than the frozen potential SBH for each $NiSi_2$/Si(001) and $CoSi_2$/Si(001)

interface. When the bulk Si DOS is fitted to the eigenvalue E_v, it much deviates from the LDOS at the Si layer farthest from the interface. The eigenvalue SBH at the (001) interface is too large compared with the frozen potential SBH.

The SBH of the $NiSi_2$/Si(111) interface obtained from the supercells with 12(Si_2) and 11($NiSi_2$) layers is 0.36 eV for type-A and 0.19 eV for type-B by the frozen potential method (Table 5). The SBH of the eightfold $CoSi_2$/Si(111) interface is 0.29 eV for type-A and 0.19 eV for type-B (Table 9). The eightfold $NiSi_2$/Si(001) and $CoSi_2$/Si(001) interfaces have almost the same SBH as the type-A (111) interface. Since these supercells are still too small to remove the cell-size dependence from the calculated SBH, it must be noticed that these values contain convergence error probably within 0.07 eV range.

7.2 Electronic structure

Figure 26 shows the difference in total number of electrons from the bulk value (Table 1) at the eightfold $NiSi_2$/Si(001) and $CoSi_2$/Si(001) interfaces. No extra empty sphere enters at the interface. Since atoms are crowded at the eightfold (001) interface, spheres close to the interface have more electrons than bulk. Although the SBH differs by 0.07 eV between the $NiSi_2$/Si(001) and $CoSi_2$/Si(001) interfaces, there is a little difference in Figure 26.

Figure 27 is LDOS of the eightfold $NiSi_2$/Si(001) interface. Its LDOS is very different from that of type-A $NiSi_2$/Si(111) interfaces (Fig. 9). At the (111) interface, the large peak of d-electrons of the interface Ni atom is shifted to a higher energy, however, at the (001) interface, it remains at almost the same energy. At the (111) interface, the interface states originated in the interfacial Ni d-orbital, while they originate in the two dangling bonds of the interface Si atom at the (001) interface. Figure 28 is LDOS of the eightfold $CoSi_2$/Si(001) interface. It resembles the LDOS of the eightfold $CoSi_2$/Si(111) interface. At the eightfold (001) interfaces, the interface Si atom has two 'dangling bonds', which form the interface states both in the Si band gap and at the bottom of the valence band, similarly to the eightfold $CoSi_2$/Si(111) interfaces where the interface Si atom has one 'dangling bond'.

Figure 29 shows a schematic two-dimensional band along the symmetry lines of the eightfold $CoSi_2$/Si(001) interface. This was obtained by examining the wave function weights of the eigenvalue in the Si and $CoSi_2$ layer. The zero energy is the Fermi level (E_f) of the

supercell. Figure 29 reveals the lowering of the space-group symmetry of the supercell. The projected bulk band of Si and $CoSi_2$ is almost symmetric for the vertical line at the K point, while the interface states are not symmetric.

In Figure 30, we plotted the intersphere electrostatic potential on each Si site at the $NiSi_2$/Si interfaces. For the sake of comparison, we set the value of both series on the right side to be zero. Near the interface, the potential is quite different between the (001) and (111) interfaces according to the electron distribution. This large difference is dielectrically screened out in two or three layers on both the Si and $NiSi_2$ sides, and the potential difference between Si and $NiSi_2$ layers becomes the same level as between the (001) and (111) interfaces. The (001) interface has much lower potential at the interface. This is the reason why the interface states exist at the bottom of the valence band.

7.3 Interface structure

At the $NiSi_2$/Si(001) interface formed by the conventional template technique, there are many (111) facets which have the (111) type-A structure. Thus, the observed n-type SBH of 0.65 eV at the $NiSi_2$/Si(001) interface is attributed to the (111) facets. Our calculation shows that the eightfold $NiSi_2$/Si(001) interface has almost the same SBH as the (111) type-A interface. We purport that the observed SBH at the (001) interface can be attributed not only to the (111) facets with the type-A structure but also to the eightfold (001) structure.

Tung *et al.* formed the single-crystal, uniform, planar $NiSi_2$/Si(001) interface by the novel technique and got a SBH of 0.4 eV, which is 0.25 eV lower than the n-type SBH of the (111) type-A interface. They also reported that the planar $NiSi_2$/Si(001) interface may have inhomogeneous atomic structure because of an evidence of 1×2 reconstructed regions at the interface [39]. At the $CoSi_2$/Si(001) interface, Loretto *et al.* observed the evidence of separate 2×1 and 1×2 domains [64]. Since there are two 'dangling bonds' at the eightfold (001) interface, we suppose that during the formation of the interface, the 'dangling bonds' form bonding states with each other or with other atoms so that other atomic structures exist in the (001) interface.

8 YSi_2/Si(111) interface

8.1 Two-dimensional band

Since the atomic structure at the YSi_2/Si(111) interface is not yet clarified, we conjectured it from a surface structure of YSi_2 [61]. The distance between the interfacial Y and Si layers (d in Fig. 4) was assumed to be the same as the distance between the Y and Si layers of bulk YSi_2. Including additional *f*-orbitals, sixteen muffin-tin orbitals are used for Y atoms. Calculated *p*-type SBH of 0.56 eV was obtained from the Fermi energy and the eigenvalue of the supercell. It is 0.17 eV smaller than the experimental SBH.

Figure 31 is a schematic two-dimensional projected band of YSi_2/Si(111) interface, which was obtained by examining the wave function weight of the energy eigenvalues of the supercell in each atomic sphere of the Si and YSi_2 layers. In the projected band, there are many regions in which bulk YSi_2 states do not appear. This comes partly from the layered crystal structure of bulk YSi_2. For instance, the energy dispersion of bulk *s*-band at the bottom of the valence band is larger in the layered plane than in the direction perpendicular to the layers.

Bold lines in Figure 31 are interface states whose wave functions are localized near the interface. The interface states in the Si band gap are formed mainly of interface Si *p*-orbitals and Y *d*-orbitals, and they maintain a bonding and antibonding character, because atomic structure changes little at the interface. The interface state which overlaps the bulk YSi_2 states is inclined to extend from the interface. Near -8 eV there is the interface state which is formed mainly of interface Si *s*-orbitals.

8.2 Local density of states

Figure 32 is LDOS of YSi_2/Si(111) interface. Bulk Si DOS (dotted line) is adjusted to the eigenvalue E_v of the supercell. There are interface states in the Si band gap which appeared in the two-dimensional band. Since Y atoms have only one *d*-electrons, a small peak of *d*-orbitals is above the Fermi energy.

Around -9 eV in the two-dimensional band, there are bulk states of YSi_2 only near the K point. This correspond to the dip at -9 eV in LDOS of the YSi_2 layer. The energy state below the dip is formed of Si *s*-orbitals. Just above the dip the Si *s*- and *p*-orbitals are

Table 10: Sphere radii and number of electrons of the empty sphere located at the YSi_2/Si(111) interface

	Rigid	Contracted
Sphere radius (Å)	1.061	0.961
Number of electrons	0.461	0.357

hybridized. Near the interface the dip becomes smaller because the hybridized states have a lower energy. The interface affects the layered electronic structure in the YSi_2.

From preliminary calculations without *f*-orbitals for Y atom, we obtained an SBH of 0.44 eV [61], which is 0.12 eV lower than the calculation including the *f*-orbitals. Figure 33 shows density of states of bulk YSi_2 obtained with or without *f*-orbitals for Y atom. The valence band width between the Fermi energy and the bottom of valence band is 0.63 eV smaller with *f*-orbitals than without *f*-orbitals. The peak around -5 eV consists mainly of Si *p*-orbitals and the small peak around -2 eV consists mainly of Y *d*-orbitals. These two peaks are shifted to higher energies when the *f*-orbitals for Y atom are included.

8.3 Electron distribution

Since we thought of the possibility that the distance between the interface Si and Y layers (d in Fig. 4) may be smaller than bulk, we performed calculations with the interface Y–Si distance 0.1 Å smaller than bulk. In this structure SBH was 0.66 eV and the thermal gap of the Si layer was 0.64 eV. The conduction bottom of the Si layer was 0.02 eV lower than the Fermi energy of the supercell. Anyway, the 0.1 Å contraction of the interface Y–Si distance makes the SBH 0.1 eV higher. The 0.1 Å difference of the interface distance has the same importance for the SBH as the *f*-orbitals for Y atom. At the type-*A* $NiSi_2$/Si(111) interface, the contraction of the interface Si–Si bond length makes the SBH 0.05 eV lower [35]. It is contrary to the YSi_2/Si(111) interface.

Figure 34 shows the difference in number of electrons in each sphere from the bulk values (Table 1) for the supercell with or without the contraction of the interface distance. Because of the displacement of one of two Si atoms, one empty sphere enters at the YSi_2/Si(111) interface. Its radius and number of electrons in it are listed in Table 10.

In Figure 34, the interfacial Y sphere has about 0.6 less electrons. It seems that too much

electrons left the interfacial Y atom. But, the interface empty sphere has 0.46 electrons. Since the interface empty sphere overlaps the interfacial Y sphere, the substantial number of electrons stay within the region near the interfacial Y atom. In the Si layer, spheres close to the interface have more electrons than bulk. This seems reasonable because the Si sphere of bulk YSi_2 has about 0.12 more electrons than that of bulk Si (Table 1).

When the interface distance is contracted by 0.1 Å, the interface empty sphere becomes small and has about 0.36 electrons. In the Si layer, two Si spheres close to the interface have less electrons than with the rigid distance. Total electron transfer from the YSi_2 layer to the Si layer is less when the interface distance is contracted, although the p-type SBH becomes 0.1 eV higher.

At the $NiSi_2$/Si(111) interface, the interface Si atoms are tetrahedrically bonded to four nearest neighbor atoms. When the interface distance is contracted, the direction of the interface Si–Si bond does not change. At the YSi_2/Si(11) interface, the interfacial Y atom is at the H_3 site so that the interface Y–Si bonds are rotated 60° with respect to the interfacial Si back bonds. When the interface distance is contracted, interface Y–Si bonds are bent with respect to the interface plane. This structural difference causes the different changes of the SBH when the interface distance is contracted.

9 CaF_2/Si(111) interface

9.1 Eightfold and fivefold structures

9.1.1 Local density of states

Figure 36 is LDOS of the eightfold model, which Batstone *et al.* considered to be the interface structure of as-grown films (see Section 3.5). A large peak of interface state occupies the Si band gap near the interface. Although this interface state remains at the Si layer farthest from the interface, it hardly penetrates the CaF_2 layer. The LDOS of the second CaF_2 layer from the interface was very similar to bulk DOS. At the first Si layer, LDOS decreases near the lower part of the conduction band, and at about -4 eV of the valence band compared with bulk DOS of Si. This resembles LDOS of free Si(111) surface (with the lattice not relaxed). The Fermi level of the eightfold model is pinned by the interface state in the Si band gap.

Figure 35 shows LDOS of the fivefold model, which Batstone *et al.* considered to be the interface structure of RTA films. When the interface F atoms were removed, the large peak of the interface states disappeared from the Si band gap, and the highest occupied states are at the E_v of Si. The interface states are divided into occupied and unoccupied states. At the first Si layer, LDOS does not so much decrease compared with the eightfold model.

The interface F atoms of the eightfold model are three-coordinated, whereas the F atoms are four-coordinated in bulk CaF_2. But in the LDOS there are no dangling orbitals in the CaF_2 layer, since CaF_2 is an ionic crystal.

9.1.2 Two-dimensional band

Figure 37 shows the two-dimensional band structure of the eightfold and fivefold models. The band structures are obtained by examining the wave function weights of the energy eigenvalues of the supercells in each atomic sphere of the Si and CaF_2 layer. To determine the interface states, we compared the band structure of both models with the calculations by the supercell containing $9(Si_2)$ layers and 41 empty sphere layers. Since the interface states of the fivefold model are extended near the Γ point, it was difficult to distinguish the interface states from the bulk bands.

For the eightfold model, the interface states in the Si band gap have a very similar band dispersion to the surface state of Si (with the lattice not relaxed). They consist of two lines, which separate 0.13 eV at the Γ point and about 0.02 eV near the M–K line. Because the supercell has two interfaces in the unit cell, interface states have two lines in the two-dimensional Brillouin zone. With a 6(Si_2)/7(CaF_2) supercell, this separation was about 0.4 eV at the Γ point, which is larger than 0.13 eV of the 9(Si2)/10(CaF_2) supercell. These interface states are formed mainly by Si p-orbitals, and occupied by electrons near the M–K line. There are also interface states at -8 eV which appear at the Si surface.

For the fivefold model, there are unoccupied and occupied interface states in the Si band gap. They are both formed by two lines. The unoccupied interface states are strongly localized near the interface. They are formed by Si s-orbitals and interface Ca d-orbitals near the Γ point, and an amount of empty sphere s-orbitals at the interface increases near the M–K line. The two lines of the unoccupied states are located 1.12 eV and 1.14 eV above E_v at the Γ point and are about 0.01–0.02 eV apart along the whole symmetry line.

The two lines of the occupied interface states separate near the Γ point. The upper line extends into the Si layer near the Γ point. It has the same energy as E_v at the Γ point, and is 1.00 eV lower than E_v at the M point and 1.20 eV at the K point. The lower line is hidden by the Si bulk band near the Γ point. It is localized near the interface so that it can be distinguished from the bulk Si band. This line reaches the Γ point which is 0.39 eV lower than E_v (not shown in Fig. 37(b)), and is located 1.12 eV at the M point and 1.19 eV at the K point. Both occupied interface states are formed mainly by Si p-orbitals and by a small amount of the interface Ca orbitals.

From these energy structures, it is obvious that the interface Si atoms have dangling bonds in the eightfold model, and that the interface Si–Ca bonds are formed in the fivefold model.

9.1.3 Electron distribution

Figure 38 shows the difference in number of electrons in each sphere at the interfaces from the bulk values (Table 1). The two empty spheres at the interface are not shown in Figure 38. Their radii and number of electrons are listed in Table 11.

Table 11: Atomic sphere radii and number of electrons of the empty spheres located at the CaF_2/Si(111) interfaces.

	Eightfold		Fivefold	
Sphere radius (Å)	0.768	1.258	1.459	1.087
Number of electrons	0.156	0.743	0.751	0.421

The number of electrons near the interface differs from the bulk values depending on the interface structure. Although the interface F atom of the eightfold model has fewer electrons than bulk, it still takes electrons from the interface Ca atom. This prevents the formation of an interface Si–Ca bond. By removing the interface F atom, the Ca atom can give electrons to the interface Si atom, so that the interface Si–Ca bond can be formed.

9.2 Sevenfold, T_4, and H_3 structures

9.2.1 Local density of states

Figure 39 is LDOS of the sevenfold model. A large peak of an interface state occupies the Si band gap near the interface and is formed mainly of Si p-orbitals. It originates in a dangling bond of an interfacial Si atom. In the sevenfold model, an interfacial F atom are located just above the interfacial Si atom (see Fig. 5). However, the interfacial Si atom has a dangling bond and the F atom cannot terminate it. Since the zero energy denotes the Fermi energy of the supercell, the Fermi level is pinned by the interface state in the Si band gap. This agrees with a metallic CaF_2/Si(111) interface formed at lower temperatures, which allows an electric current to flow along the interface. The interface state in the Si band gap deeply penetrates the Si layer, but it hardly penetrates the CaF_2 layer, because the band gap of CaF_2 is larger than that of Si.

Figure 40 shows LDOS of the T_4 model, and Figure 41 shows LDOS of the H_3 model. In both models, the interface states in the Si band gap are split into occupied and unoccupied states, and their highest occupied states are at the valence band maximum of Si (E_v). So, the electronic structures of both models are consistent with the electrical properties of the interface after the interfacial F atoms were dissociated. The H_3 model has the interface states also at the bottom of the Si valence band.

9.2.2 Two-dimensional band

Figure 42 shows the two-dimensional band structure near the Si band gap of the T_4 and H_3 models along the selected symmetry lines. The zero energy is the E_v. Each dot represents the energy eigenvalue of the supercells at the $\mathbf{k}$ points whose k_z element equals zero. The larger dots are eigenvalues whose wave functions are much localized near the interface; more than 30 percent of their wave function are in the five spheres near the interface (two Si, one Ca, and two empty spheres at the interface). The smaller dots are eigenvalues whose wave functions are more than 40 percent in the Si layer. Since the band offsets of the T_4 and H_3 models are larger than 5 eV, the filled band of CaF_2 layer does not appear in Figure 42.

For the T_4 model, there are occupied and unoccupied interface states in the Si band gap. The occupied interface states are formed of two eigenstates near the M-K line. Their energy values from the E_v are 1.11 eV and 1.31 eV at the M point, and 1.53 eV and 1.55 eV at the K point. They are formed mainly of Si p-orbitals and of a small amount of the interfacial Ca p- and d-orbitals. Moving to the Γ point along the M-Γ and K-Γ lines, one of the occupied interface states spreads over the Si layer and only another eigenstate can be regarded as an interface state. At the Γ point, it is at 0.56 eV lower than the E_v and formed mainly of the Si p-orbitals and of a small amount of the interfacial Ca s- and d-orbitals. The unoccupied interface states in the Si band gap are formed of the interfacial Ca d-orbitals, Si s-, p-, d-orbitals, and interfacial empty sphere s-orbitals: it has an anti-bonding character.

In our previous paper, the interfacial Si–Ca distance in the T_4 model was assumed to be 0.3 nm [84]. It is 0.01 nm shorter than the present study. In the previous T_4 model, the occupied interface states in the Si band gap were about 0.05 eV higher than the present ones, and the unoccupied interface states were about 0.15 eV lower than the present ones. The bonding interaction between the interfacial Si–Ca atoms is a little stronger in the present Si–Ca distance of 0.31 nm. It better agrees with the measured distance at the CaF_2/Si(111) interface [75, 76] and with the theoretical study on the crystal structure of a $CaSi_2$ [99, 100].

The H_3 model has also occupied and unoccupied interface states in the Si band gap. The occupied interface states are 0.56 eV below the E_v at the Γ point, 0.74 eV and 0.82 eV at the M point, and 0.91 eV and 0.92 eV at the K point. Although the energy dispersion

of the interface states in the Si band gap differ between the T_4 and H_3 models, their wave functions at each $\mathbf{k}$ point are formed of the similar elements of orbitals. The H_3 model has interface states also at the bottom of the Si valence band (not shown in Fig. 42). They are formed mainly of the s-orbitals of the interfacial Si and second Si atoms.

Since the supercell has two interfaces in the unit cell, the interface states are formed primarily of two eigenstates at each $\mathbf{k}$ point in the projected Brillouin zone. The interface states separating from the bulk states are formed of the two eigenstates which are well localized at the interface and split little in energy due to the interaction between their own tails in the Si layer. The interface states overlapping the bulk states become one eigenstate near the Γ points due to the interaction with the bulk states. Since real interface states should be a single state at each $\mathbf{k}$ point, the calculated dispersion of the occupied interface state has an ambiguity of about the split energy.

In the T_4 and H_3 models, the interface states in the Si band gap originate in the bonding interaction between the interfacial Ca and Si atoms. Although an interfacial Ca–Si distance is the same between the two models, the energy dispersion of the interface states differs. Figure 45 is an plane figure of the surface structure in which the Ca atoms are at the T_4 or H_3 sites of a Si(111) surface. In the T_4 model, the Ca–Si bonds has the same direction as the back bonds of the interfacial Si atoms in the interface plane. In the H_3 model, the interfacial Ca–Si bonds are rotated 60° with respect to the interfacial Si back bonds. This structural difference produces the different interface states both in the Si band gap and at the bottom of the valence band of the H_3 model. At the $NiSi_2$/Si(111) interface, the different direction of the overlayer bring about the different Schottky barrier heights of the type-A and type-B interfaces [19]. At the interface between the different materials, the electronic structures are affected not only by the bonding interaction at the interface but also by the bond angles between the two materials.

The band dispersion of the interface state of the CaF_2/Si(111) was measured with angle-resolved photoelectron spectroscopy by Mclean and Himpsel [82], and other groups [101, 102]. The occupied states were 0.75 eV lower than the E_v at the Γ point, 1.35 eV at the M point, and 1.55 eV at the K point [82]. They also reported that at the Γ point an unoccupied interface state is at 1.65 eV above the E_v from optical second-harmonic-generation data

Table 12: Number of valence electrons in empty spheres at the interface.

	Sevenfold		T_4		H_3	
Sphere radius (Å)	1.632	0.787	1.434	0.960	1.434	0.960
Number of electrons	1.067	0.094	1.121	0.389	0.937	0.290

[103]. In comparison with our calculations, the occupied interface state well agrees with the T_4 model. However, the unoccupied interface state does not appear below the Si conduction band at the Γ point [104].

At the Γ point of the T_4 model, the bottom of the conduction band of the Si layer is at 1.75 eV above the E_v and the bottom of the empty band of the CaF_2 layer is at 1.42 eV above the E_v. In the H_3 model, the former is at 1.77 eV and the latter is at 2.11 eV above the E_v. The experimental band gap of the CaF_2 is 12.1 eV. Hence, even if the band offset is as large as 8.5 eV, the empty band of the CaF_2 layer does not appear under the Si conduction band. In the T_4 model, the band alignment between the Si conduction band and the CaF_2 empty band is unreasonable because of the LDA. This may affect the dispersion of the unoccupied interface states, about which more sophisticated calculations are needed [105].

9.2.3 Electron distribution

In the bulk CaF_2, F atoms have much electrons taken from Ca atoms as to make a closed shell and Ca atom has only a little valence electrons (see Table 1). Figure 43 and 44 show the difference in valence electrons from the bulk values in each sphere at the CaF_2/Si(111) interface. The two empty spheres at the interface are not shown in Figures 43 and 44. Their sphere radii and number of electrons are listed in Table 12. In the sevenfold model, the interfacial F atom is surrounded by three Ca and one Si atoms and takes electrons from these atoms, but it cannot terminate the Si dangling bond. In the T_4 and H_3 models, an interfacial Ca–Si distance is the same. But the interfacial Si atom of the H_3 model has more electrons than than of the T_4 model. Since the interfacial Si–Ca bond of the T_4 model has the same direction as the back bonds of the interfacial Si atom (Fig. 45), electrons spread at the interface. The empty spheres at the interface has more electrons than those of the H_3 model (Table 12).

Table 13: Calculated Fermi energy for the eightfold and sevenfold models and band offset between the Si and CaF_2 layers. (eV)

	Eightfold	Fivefold	Sevenfold	T_4	H_3
Fermi level	0.28	—	0.46	—	—
Band offset	2.41	5.31	3.88	5.69	5.01

In LMTO-ASA, one-electron potential consists of spherical potentials at each atomic and empty sphere site. The spherical potentials are composed of two different contributions. One comes from the charge distribution inside its own sphere (inner-sphere), and the other is long range electrostatic potential produced by surrounding spheres (inter-sphere). To evaluate the inter-sphere potential, the charge in the sphere is treated as a point charge placed at the sphere center , whose on-site value is a sum of Madelung constants times the point charges of the surrounding spheres. Thus, the inner-sphere potential reflects the details of the electron distribution in its own sphere, and the inter-sphere potential is determined by the electron distribution at each sphere site like Figures 43 and 44.

In the H_3 model, there is the interface state at a lower energy than the Si valence band. This does not mean a strong bonding interaction. Since the inter-sphere potential is lower at the interfacial Si site than at the Si sites farther from the interface, the interface state can be located at the bottom of valence band.

9.3 Band offset

Table 13 lists the Fermi level ($E_f - E_v$) and band offsets (the E_v minus the top of the filled band of the CaF_2 layer). Olmstead *et al.* reported that the band offset changes from 7.3 eV to 8.3 eV when thermal annealing causes the F atoms to dissociate from the interface [79]. Himpsel also reported a band offset of 8.5 eV for the interface grown at a high temperature [77]. The presence of F atoms at the interface decreases the offset value. This is valid among the calculated values although they are smaller than the measured value due to the LDA for exchange and correlation interactions.

Previously Satpathy and Martin reported an LMTO–ASA study on the band offset of the CaF_2/Si(111) interface [83]. They used the supercells which contain only 3(Si_2) and 3 Ca layers with appropriate number of F layers, and obtained 7.2 eV for the fivefold model

Table 14: Core energy level shifts of atoms near the interface. A plus sign indicates a small binding energy compared to atoms in layers farther from the interface. A minus sign indicates a larger binding energy in eV.

	Eightfold	Fivefold	Sevenfold	T_4	H_3	Expt.
First Si $2p$	+0.16	+0.18	−0.35	+0.02	+0.22	+0.4[a]
Second Si $2p$	+0.19	−0.44	−0.14	−0.50	−0.56	−0.8[a]
First Ca $3p$	+0.30	+0.51	+0.05	−0.04	−0.27	+2.3[b]
First F $2s$	−0.20	−0.02	+0.20	+0.10	−0.32	0[c]

[a] Reference [78]
[b] Reference [79]
[c] Reference [80]

and 5.3 eV for the T_4 model as band offsets. Their values differ from ours. The calculated band offset for the $NiSi_2$/Si(111) interface, that is Schottky barrier height, depends on the supercell size. The supercell must be large enough to obtain an accurate value, because the energy band structure of each layer affects the calculated band offset. The discrepancy with Satpathy comes from the difference of the supercell size.

9.4 Core level shifts

Table 14 shows the core level shifts of the Si, Ca, and F atoms near the interface. These were obtained from the comparison of the core levels near and far from the interface. In the H_3 model, the first Si atom has more electrons than bulk, and its $2p$ level shifts to a higher energy despite the lower inter-sphere potential. The $2p$ level of the second Si atom is shifted to a lower energy in the fivefold, T_4, and H_3 models, despite the small charge transfer (Fig. 38 and Fig. 44).

Figure 46 shows the radial potential of the first, second, and farthest Si atoms from the interface of the H_3 model. For the convenience of comparison, we multiply the square of radii to it: $r^2 \times V(r)$. At the sphere edges, the radial potential is higher in the order of the farthest, second, first Si atoms due to the inter-sphere potential. Near the center of the spheres, the radial potential is higher in the order of the first, farthest, and the second Si atoms (shown in the mini-window in Fig. 46). This agrees with the core level shifts in Table 14. The radial potential near the nucleus determines the core level. The first Si atom gets much electrons from the interfacial Ca atom, and it screen the nuclear charge. Thus, the core level shifts to a higher energy.

At the second Si atom in the fivefold, H_3, and T_4 models, the $2p$ level shifts to a lower energy. At these interfaces, the $3p$-orbitals of the first Si atom interacts with the Ca $3d$-orbitals, which locate at a high energy and mainly form the empty band of bulk CaF_2. The $3p$ electrons in the second Si atom have a little lower energy than the other Si atoms. It affects the radial potential near the nucleus and results in the lowering of the Si $2p$ level.

The measured Si $2p$ level shows shifts both to lower and higher energies (Table 14). This can be seen in the calculations of the fivefold and H_3 models, although the values are smaller than the measured ones. However, the experimentally observed shift of the interfacial Ca $3p$ level cannot be seen in the calculations. From XSW measurements, Zegenhagen and Patel reported the T_4 and H_3 structures at higher temperatures and the sevenfold structure at lower temperatures with emphasis on the interface stoichiometry caused by the growing conditions and by a larger lattice mismatch at higher temperatures. If there were Ca-rich regions at the interface due to an extra dissociation of F atoms, Si and Ca atoms would have more electrons than those surrounded by F atoms. This would make the core levels shift to a higher energy.

9.5 Interface structure

A metallic CaF_2/Si(111) interface is formed when the CaF_2 layer is grown at a low temperature and not sufficiently annealed. Batstone *et al.* reported that for as-grown films on a p-type Si substrate it is difficult to form an inversion layer of minority carriers (electrons). These properties are consistent with the Fermi level pinning in the eightfold and sevenfold models. When the Si dangling bonds are terminated by the Ca atoms by removing the F atoms from the interface, the Fermi level pinning disappears. This coincides with the dramatic improvement in the electrical properties measured by Batstone *et al.*

When the F atoms are dissociated from the interface by annealing, the CaF_2 layer would not slide along the interface. So, it is natural that the eightfold model is transformed to the fivefold model, or that the sevenfold model is transformed to the T_4 model. Although the paired model of the eightfold and fivefold structure was postulated from the TEM lattice images, MEIS measurement supports the T_4 model and XSW data supports the sevenfold, T_4,

and H_3 models. The calculated electronic structures of the sevenfold and T_4 are consistent with the experiments. We suppose that the paired model of the sevenfold and T_4 structures is better for the CaF_2/Si(111) interface. However, there still remains discrepancies between the calculations and experiments, especially with respect to the unoccupied interface states and the core level shifts at the interface. So, more theoretical and experimental studies are needed.

10 Concluding remarks

At the metal silicide/Si and CaF_2/Si interfaces, there are electronic states peculiar to the interface: the MIGS and interface states. In the Si layer, these interfacial gap states are formed by the states stolen from the Si valence and conduction band as shown in Figure 47. The upper panel of Figure 47 shows how we obtained the lines in the lower panel. The solid line in the upper panel is the local density of states for the whole interface Si layer obtained by the supercell with 9 Si_2 layers. The dotted line is 9 times of bulk Si DOS. The thermal gap of the bulk Si is matched to that of supercell. The difference between the two lines is integrated from the lowest energy and plotted in the lower panel. Vertical zero means that the state numbers of the interface Si layer and bulk Si are equal. Near -3 eV, the number of states in the interface decreases compared with the bulk, and increases in the Si band gap, indicating that the interfacial gap states are formed by states stolen from the Si valence and conduction band states.

In the Si band gap, the energy distribution of the interfacial gap state much depends on the interface atomic structure, that is, the interfacial bonding interaction. But, Figure 47 indicates that the interfacial gap states are formed by the states stolen from the similar energy range. From the cell size dependence of the calculated SBH's, it was clarified that the SBH depends on the valence band structure of both Si and silicide layer, especially near the Fermi level. So, the energy states just below the Fermi level are very significant to form the interfacial gap states, and are deeply concerned with the SB formation.

The type-B has a lower SBH than the type-A at the $CoSi_2$/Si(111) and $NiSi_2$/Si(111) interfaces. The T_4 $CoSi_2$/Si(111) and H_3 YSi_2/Si(111) interfaces have larger SBH's than the type-A interfaces. There are common features to aforementioned interfaces that the twisted interface lowers the SBH and that the interface bond bending raises the SBH. At the $NiSi_2$/Si(001) and $CoSi_2$/Si(111) interfaces with large p-type SBH's, there are experimental evidences that the reconstructed regions exist at the buried interface, where the bond bending probably occurs. We speculate that the reconstructed regions are concerned with the large experimental SBH's.

The YSi_2/Si(111) interface naturally takes the H_3 structure as previously explained. The

Table 15: Calculated Schottky barrier height ($E_f - E_v$) by the supercells with 9 Si_2 and 8 - 10 silicide layers and experimental values. (in eV)

Structure	Calculations	Experiments
Type-A $NiSi_2$/Si(111)	0.32	0.47
Type-B $NiSi_2$/Si(111)	0.19	0.33
Type-B eightfold $CoSi_2$/Si(111)	0.25	0.42
H_3 YSi_2/Si(111)	0.56	0.73

$CoSi_2$/Si(111) interface prefers the eightfold structure to the sevenfold structure because Co atom has d-electrons one less than Ni atom [44, 96]. The interface property is intimately connected with bulk property of silicides. Figure 48 shows bulk density of states of each silicide. The dotted lines are total density of states (DOS) and solid lines are partial DOS of d-orbitals of metal atoms. The positions of the large peak of the d-orbitals (indicated by arrows) move to a higher energy in the order of $NiSi_2$, $CoSi_2$, and YSi_2. If compared with the same types, the $NiSi_2$/Si(111) interface has a lower SBH than the $CoSi_2$/Si(111) interface. This corresponds with the position of d-orbitals, although the energy scale differs by fifty times between the d-positions and SBH's.

Table 15 summarizes the experimental SBH's ($E_f - E_v$) and the calculated SBH's for the silicide/Si interface whose atomic structure is almost clarified. Since the supercells consist of 9 Si_2 layers and 8 or 10 silicide layers, these values probably contain an approximately 0.05 eV convergence error with respect to supercell size. Although the calculated SBH's are about 0.15 eV smaller than the experimental values, calculations reproduce the difference of the SBH's depending on the interface atomic structure and a kind of metal silicide. Charlesworth *el at.* calculated the quasiparticle electronic structure of a Al/GaAs(110) using the GW self-energy operator [106]. They showed that the SBH ($E_f - E_v$) at the Al/GaAs(110) interface become about 0.1 eV larger by the GW correction. This well agrees with out result that the calculated SBH is about 0.1 eV smaller than the experimental one owing to the LDA error.

The type-A and -B $NiSi_2$/Si(111) interfaces are the first example which demonstrated that the SBH depends on the interface atomic structure. Until now, the following examples are reported: Pb/Si(111) interface [107, 108], Sb/GaAs(001) interface [109], and others [110]. The first-principle calculations about the electronic structure at the metal-semiconductor interface are also performed for the following interfaces: metal/GaAs interfaces [111], Al/Ge interface [112], and others [113]. It was shown that the abnormal electric property at metal-semiconductor interfaces can be explained by the inhomogeneity of SBH [114]. In recent years, much progress has been made on understanding about the metal-semiconductor interfaces. However, many problems still remain unresolved.

Acknowledgments

I would like to express my sincere thanks to Professor S. Asano for encouraging and guiding me at every stage of this work. I also wish to thank Dr. R. R. Tung in Bell Laboratories for valuable discussions and sending me his results prior to publication. I am grateful to Messrs. H. Ishikawa, T. Itoh, and N. Nakayama in Fujitsu Laboratories for encouraging me to accomplish this work.

References

[1] P. Hohenberg and W. Kohn, Phys. Rev. **136**, B864 (1964).

[2] W. Kohn and L. J. Sham, Phys. Rev. **140**, A1133 (1965).

[3] J. F. Janak, V. L. Moruzzi, and A. R. Williams, Phys. Rev. B **12**, 1257 (1975).

[4] E. Wimmer, H. Krakauer, M. Weinert, and A. J. Freeman, Phys. Rev. B **24**, 864 (1981).

[5] L. F. Mattheiss and D. R. Hamann, Phys. Rev. B **33**, 823 (1986).

[6] T. Takeda and J. Kübler, J. Phys. F **9**, 661 (1979).

[7] O. K. Andersen, Phys. Rev. B **12**, 3060 (1975); O. K. Andersen, O. Jepsen, and D. Glötzel, in *Highlights of Condensed Matter Theory*, edited by F. Bassani, F. Fumi, and M. P. Tosi (North-Holland, Amsterdam, 1985), 59; O. K. Andersen, O. Jepsen, and M. Sob, in *Electronic Band Structure and its Applications*, edited by M. Yussouff (Springer-Verlag, Heidelberg, 1987).

[8] For a review of the metal/semiconductor interface, refer, for example, to F. Flores and C. Tejedor, J. Phys. C **20**, 145 (1987).

[9] W. Schottky, Z. Phys. 118, 118 (1942).

[10] J. Badeen, Phys. Rev. **71**, 717 (1947).

[11] V. Heine, Phys. Rev. **138**, 138 (1965).

[12] S. G. Louie and M. L. Cohen, Phys. Rev. B **13**, 2461 (1976).

[13] S. G. Louie, J. R. Chelikowsky, and M. L. Cohen, Phys. Rev. B **15**, 2154 (1977).

[14] L. J. Brillson, Surf. Sci. Rep. **2**, 123 (1982).

[15] W. E. Spicer, I. Lindau, P. Skeath, C. Y. Su, and P. Chye, Phys. Rev. Lett. **44**, 420 (1980).

[16] C. Tejedor, F. Flores, and E. Louis, J. Phys. C **10**, 2163 (1977).

[17] J. Tersoff, Phys. Rev. Lett. **52**, 465 (1984).

[18] J. Tersoff, Phys. ReV. B **32**, 6968 (1985).

[19] R. T. Tung, Phys. Rev. Lett. **52**, 461 (1984).

[20] D. Cherns, G. R. Anstís, J. L. Hutchinson, and J. C. H. Spence, Philos. Mag. A **46**, 849 (1982).

[21] R. T. Tung, J. M. Gibson, and J. M. Poate, Phys. Rev. Lett. **50**, 429 (1983).

[22] M. Liehr, P. E. Schmidt, F. K. LeGoues, and P. S. Ho, Phys. Rev. Lett. **54**, 2139 (1985)

[23] W. Mönch, Phys. Rev. Lett. **58**, 1260 (1987).

[24] S. B. Zhang, M. L. Cohen, and S. G. Louie, Phys. Rev. B **32**, 3955 (1985).

[25] D. R. Hamann and L. F. Mattheiss, Phys. Rev. Lett. **54**, 2517 (1985).

[26] X. Yongnian, Z. Kaiming, and X. Xide, Phys. Rev. B **33**, 8602 (1986).

[27] O. Bisi and S. Ossicini, Surf. Sci. **189**, 285 (1987).

[28] R. T. Tung, K. K. Ng, J. M. Gibson, and F. J. Levi, Phys. Rev. B **33**, 7077 (1986).

[29] R. J. Hauenstein, T. E. Schlesinger, T. C. McGill, B. D. Hunt, and L. J. Schowalter, J. Vac. Sci. Technol. A **4**, 860 (1986).

[30] M. Ospelt, J. Henz, L. Flepp, and H. von Känel, Appl. Phys. Lett. **52**, 227 (1988).

[31] J. Vrijmoeth, J. F. van der Veen, D. R. Heslinga, and T. M. Klapwijk, Phys. Rev. B **42**, 9598 (1990).

[32] A. Kikuchi, T. Ohshima, and Y. Shiraki, J. Appl. Phys. **64**, 4614 (1988).

[33] A. Kikuchi, Phys. Rev. B **40**, 8024 (1989).

[34] H. Fujitani and S. Asano, J. Phys. Soc. Jpn. **57**, 2253 (1988).

[35] G. P. Das, P. Blöchl, N. E. Christensen, and O. K. Andersen, in *Metallization and Metal-Semiconductor Interfaces*, edited by I. P. Batra (Plenum, New York, 1988); G. P. Das, P. Blöchl, O. K. Andersen, N. E. Christensen, and O. Gunnarsson, Phys. Rev. Lett. **63**, 1168 (1989).

[36] M. D. Stiles and D. R. Hamann, Phys. Rev. B **40**, 1349 (1989).

[37] H. Fujitani and S. Asano, Phys. Rev. B**42**, 1696 (1990).

[38] D. Cherns, C. J. D. Hetherington, and C. J. Humphreys, Philos. Mag. A **49**, 165 (1984).

[39] R. T. Tung, A. F. J. Levi, J. P. Sullivan, and F. Schrey, Phys. Rev. Lett. **66**, 72 (1991).

[40] H. Fujitani and S. Asano, J. Phys. Soc. Jpn. **60**, 2526 (1991).

[41] J. M. Gibson, J. C. Bean, J. M. Poate, and R. T. Tung, Appl. Phys. Lett. **41**, 818 (1982).

[42] J. Zegenhagen, K. G. Huang, B. G. Hunt, and L. J. Schowalter, Appl. Phys. Lett. **51**, 1176 (1987).

[43] E. J. van Loenen, J. W. M. Frenken, J. F. van der Veen, and S. Valeri, Phys. Rev. Lett. **54**, 827 (1985).

[44] D. R. Hamann, Phys. Rev. Lett. **60**, 313 (1988).

[45] N. V. Rees and C. C. Matthai, J. Phys. C: Solid State Phys. **21**, L981 (1988).

[46] H. Fujitani and S. Asano, Appl. Surf. Sci. **41/42**, 164 (1989).

[47] M. L. Cohen and J. R. Chelikowsky, *Electronic Structure and Optical Properties of Semiconductors*, (Springer-Verlag, New York, 1988).

[48] J. Tersoff and D. R. Hamann, Phys. Rev. B **28**, 1168 (1983).

[49] F. Hellman and R. T. Tung, Phys. Rev. B **37**, 10786 (1988).

[50] J. Vrijmoeth, A. G. Schins, and J. F. van der Veen, Phys. Rev. B **40**, 3121 (1989).

[51] J. Vrijmoeth, S. Zaima, E. Vlieg, and J. W. M. Frenken, Phys. Rev. B **45**, 6700 (1992).

[52] A. Santaniello, P. DePadova, X. Jin, D. Chandesris, and G. Rossi, J. Vac. Sci. Technol. B **7**, 1017 (1989).

[53] L. Haderbache, P. Wetzel, C. Pirri, J. C. Peruchetti, D. Bolmont, and G. Gewinner, Phys. Rev. B **39**, 12704 (1989).

[54] R. T. Tung, A. F. J. Levi, and J. M. Gibson, Appl. Phys. Lett. **48**, 635 (1986).

[55] R. T. Tung and J. L. Batstone, Appl. Phys. Lett. **52**, 1611 (1988).

[56] R. T. Tung and J. L. Batstone, Appl. Phys. Lett. **52**, 648 (1988).

[57] R. T. Tung, J. Vac. Sci. Technol. **A7**, 598 (1989).

[58] R. T. Tung, J. Vac. Sci. Technol. **2**, 465 (1984).

[59] E. Rosencher, S. Delage, and F. Arnaud D'Avitaya, J. Vac. Sci. Technol. **B3**, 762 (1985).

[60] J. P. Sullivan, R. T. Tung, D. J. Eaglesham, F. Schrey, and W. R. Graham, paper presented at the Physics and Chemistry of Semiconductor Interfaces meeting (PCSI20) held in Williamsburg, Virginia, USA, 1993.

[61] H. Fujitani and S. Asano, Mat. Res. Soc. Proc. **193**, 77 (1990).

[62] J. Mizuki, K. Akimoto, I. Hirosawa, K. Hirose, T. Mizutani, and J. Matsui, J. Vac. Sci. Technol. **B6**, 31, (1988).

[63] K. Akimoto, I. Hirosawa, J. Mizuki, S. Fujieda, Y. Matsumoto, and J. Matsui, Jpn. J Appl. Phys. Pt. 2 **27**, L1401 (1988).

[64] D. Loretto, J. M. Gibson, and S. M. Yalisove, Phys. Rev. Lett. **63**, 298 (1989).

[65] K. N. Tu, R. D. Thompson, and B. Y. Tsaur, Appl. Phys. Lett. **38**, 626 (1981).

[66] J. A. Knapp and S. T. Picraux, Appl. Phys. Lett. **48**, 466 (1986).

[67] M. P. Siegal, J. J. Santiago, and W. R. Graham, Mat. Res. Soc. Proc. **198**, 589 (1990).

[68] H. Fujitani and S. Asano, Appl. Surf. Sci. **56–58**, 408 (1992).

[69] R. Baptist, S. Ferrer, G. Grenet, and H. C. Poon, Phys. Rev. Lett. **64**, 311 (1990).

[70] H. Ishiwara and T. Asano, Apple. Phys. Lett. **42**, 415 (1982).

[71] T. Asano and H. Ishiwara, Appl. Phys. Lett. **42**, 517 (1983).

[72] J. Gibson and J. M. Phyllips, Appl. Phys. Lett. **43**, 828 (1983).

[73] K. Nath and A. B. Anderson, Phys. Rev. B **38**, 8264 (1988).

[74] J. L. Batstone, J. M. Phillips, and E. C. Hunke, Phys. Rev. Lett. **60**, 1394 (1988).

[75] R. M. Tromp and M. C. Reuter, Phys. Rev. Lett. **61**, 1756 (1988).

[76] J. Zegenhagen and J. R. Patel, Phys. Rev. B **41**, 5315 (1990).

[77] F. J. Himpsel, U. O. Karlsson, J. F. Morar, D. Rieger, and J. A. Yarmoff, Phys. Rev. Lett. **56**, 1497 (1986).

[78] F. J. Himpsel, F. U. Hillebrecht, G. Hughes, J. L. Jordan, U. O. Karisson, F. R. McFeely, J. F. Morar, and D. Rieger, Appl. Phys. Lett. **48**, 596 (1986).

[79] M. A. Olmstead, R. I. G. Uhrberg, R. D. Bringans, and R. Z. Bachrach, Phys. Rev. B **35**, 7526 (1987).

[80] D. Rieger, F. J. Himpsel, U. O. Karlsson, F. R. McFeely, J. F. Morar, and J. A. Yarmoff, Phys. Rev. B **34**, 7295 (1986).

[81] Ph. Avouris and R. Wolkow, Appl. Phys. Lett. **55**, 1074 (1989).

[82] A. B. McLean and F. J. Himpsel, Phys. Rev. B **39**, 1457 (1989).

[83] S. Satpathy and R. M. Martin, Phys. Rev. B **39**, 8494 (1989).

[84] H. Fujitani and S. Asano, Phys. Rev. B **40**, 8357 (1989).

[85] H. Fujitani and S. Asano, Surf. Sci. **268**, 265 (1992).

[86] W. R. L. Lambrecht and O. K. Andersen, Phys. Rev. B **34**, 2439 (1986).

[87] W. R. L. Lambrecht, N. E. Christensen, and P. Blöchl, Phys. Rev. B **36**, 2493 (1987).

[88] Y. J. Chabal, D. R. Hamann, J. E. Rowe, and M. Schluter, Phys. Rev. B **25**, 7598 (1982).

[89] D. M. Bylander, L. Kleinman, K. Mednick, and W. R. Grise, Phys. Rev. B **26**, 6379 (1982).

[90] E. Vlieg, A. E. M. J. Fischer, J. F. van der Veen, B. N. Dev, and G. Materlik, Surf. Sci. **178**, 36 (1986).

[91] J. Zegenhagen, K. G. Huang, W. M. Gibson, B. D. Hunt, and L. J. Schowalter, Phys. Rev. B **39**, 10254 (1989).

[92] W. R. L. Lambrecht and O. K. Andersen, Surf. Sci. **178**, 256 (1986).

[93] J. M. Gibson, R. T. Tung, and J. M. Poate, in Defects in Semiconductor II, edited by S. Mahajan and James W. Corbett, Proceedings of the Materials Research Society Symposium, Boston, (North-Holland, New York, 1983), **14**, 395 (1982).

[94] C. G. van de Walle and R. M. Martin, Phys. Rev. B **35**, 8154 (1987); N. E. Christensen, Phys. Rev. B **37**, 4528 (1988).

[95] L. F. Mattheiss and D. R. Hamann, Phys. Rev. B **37**, 10623 (1988).

[96] P. J. van den Hoek, W. Ravenek, and E. J. Baerends, Phys. Rev. Lett. **60**, 1743 (1988); Surf. Sci. **205**, 549 (1988).

[97] F. Flores and J. Ortega, Appl. Surf. Sci. **56–58**, 301 (1992).

[98] S. Ossicini, O. Bisi, and C. M. Bertoni, Phys. Rev. B **42**, 5735 (1990).

[99] O. Bisi, L. Braicovich, C. Carbone, I. Lindau, A. Iandelli, G. L. Olcese, and A. Palenzona, Phys. Rev. B **40**, 10194 (1989).

[100] S. Fahy and D. R. Hamann, Phys. Rev. B **41**, 7587 (1990).

[101] S. Bouzidi, F. Coletti, J. M. Debever, J. L. Longueville, and P. A. Thiry, Appl. Surf. Sci. **56–58**, 821 (1992).

[102] H. Ohnuki, K. Higashiyama, and H. Fukutani, private communication.

[103] T. F. Heinz, F. J. Himpsel, E. Palange, and E. Burstein, Phys. Rev. Lett. **63**, 644 (1989).

[104] M. R. Salehpour, S. Satpathy, and G. P. Das, Phys. Rev. B **44**, 8880 (1991).

[105] M. Hybersten and S. G. Louie, Phys. Rev. B **34**, 5390 (1986).

[106] J. P. A. Charlesworth, R. W. Godby, and R. J. Needs, Phys. Rev. Lett. **70**, 1685 (1993).

[107] G. Le Lay, K. Hricovini, and J. E. Bonnet, Appl. Surf. Sci. **41/42**, 25 (1989).

[108] D. R. Heslinga, H. H. Weitering, D. P. van der Werf, T. M. Klapwijk, and T. Hibma, Phys. Rev. Lett. **64**, 1589 (1990).

[109] K. Hirose, K. Akimoto, I. Hirosawa, J. Mizuki, T. Mizutani, and J. Matsui, Phys. Rev. B **43**, 4538 (1991).

[110] S. Chang, L. J. Brillson, Y. J. Kime, D. S. Rioux, P. D. Kirchner, G. D. Pettit, and J. M. Woodall, Phys. Rev. Lett. **64**, 2551 (1990).

[111] M. van Schilfgaarde and N. Newman, Phys. Rev. Lett. **65**, 2728 (1990).

[112] S. Ciraci, A. Baratoff, and I. P. Batra, Phys. Rev. B **43**, 7046 (1991).

[113] W. E. Pickett and S. C. Erwin, Phys. Rev. B **41**, 9756 (1990).

[114] T. Tung, Phys. Rev. B **45**, 13509 (1992).

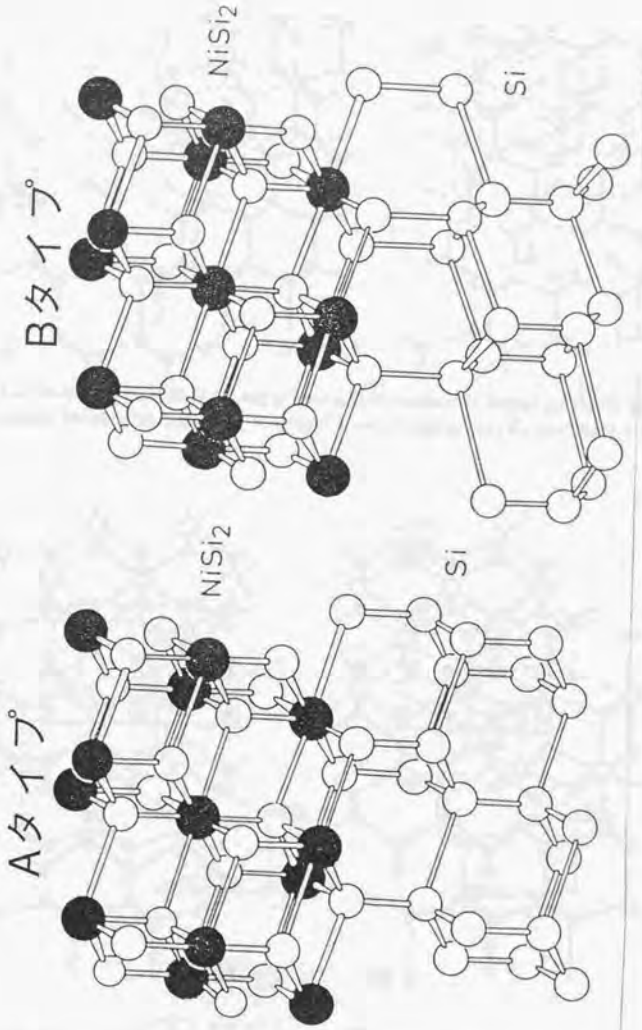

Figure 1: [A] Atomic structure of the two types of $NiSi_2$/Si(111) interface

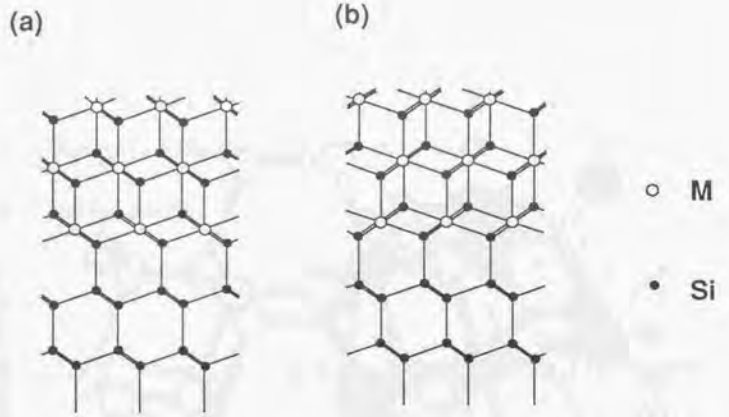

Figure 1: [B] Cross-sectional structure of the two types of $NiSi_2$/Si(111) interface: (a) sevenfold type-A interface, (b) sevenfold type-B interface. M represents metal atoms.

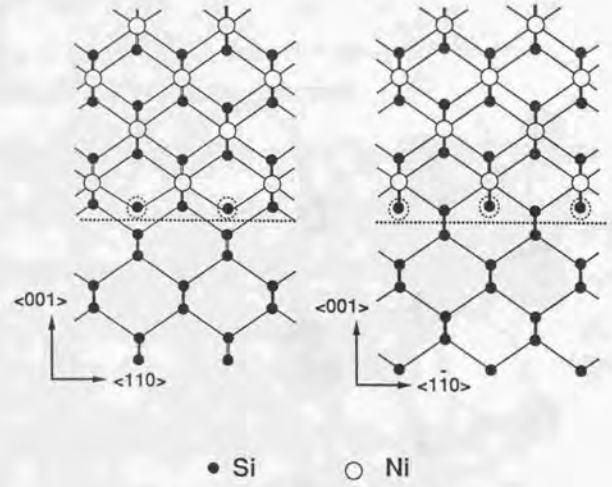

Figure 2: Atomic structure at $NiSi_2$/Si(001) interface.

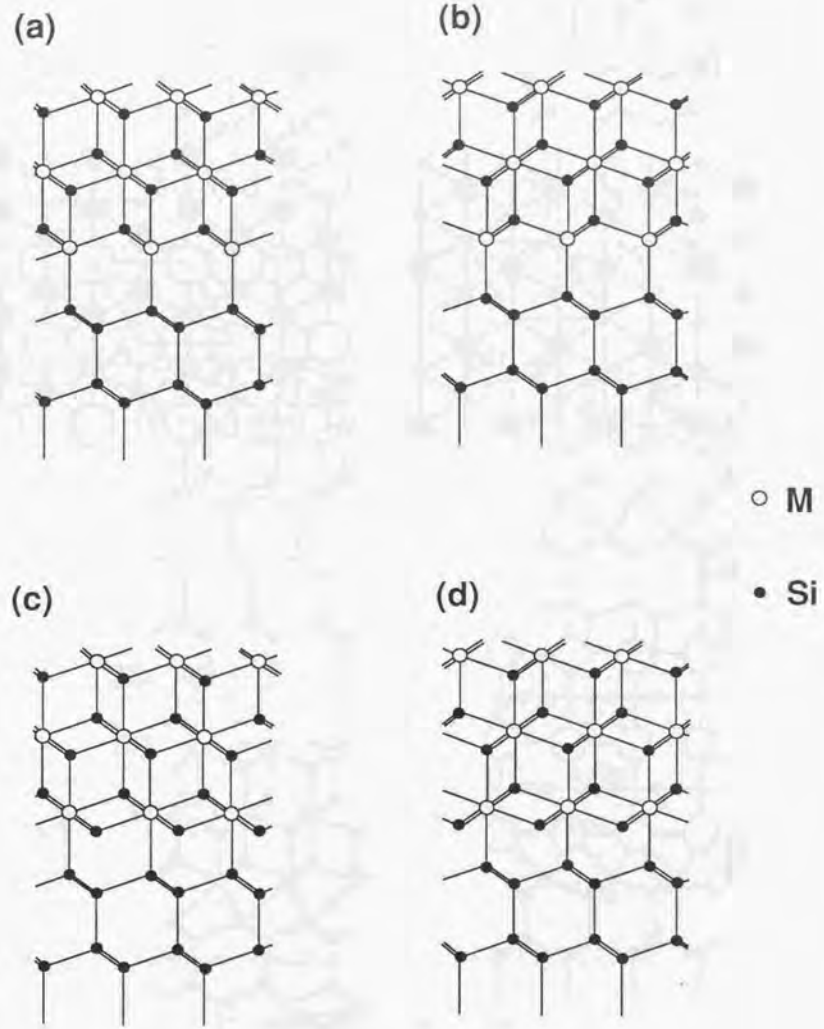

Figure 3: Atomic structure at $CoSi_2$/Si(111) interface: (a) fivefold type-A interface, (b) fivefold type-B interface, (c) eightfold type-A interface, and (d) eightfold type-B interface. M represents metal atoms.

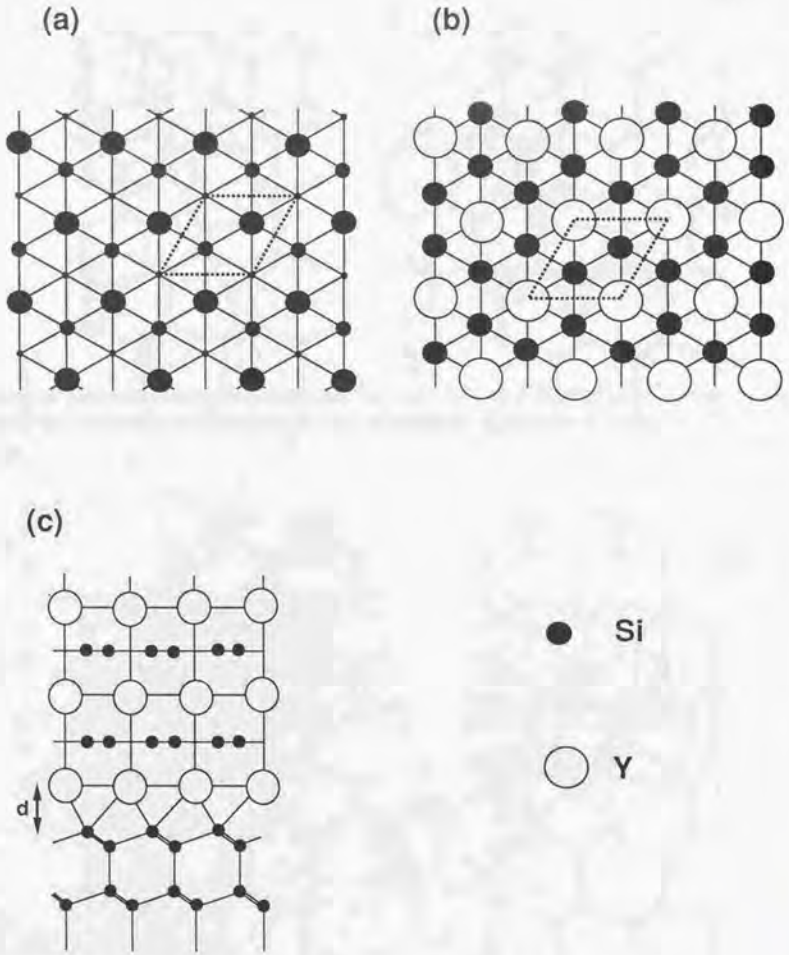

Figure 4: (a) Overview of unrelaxed Si(111) surface, (b) overview of YSi_2 surface, and (c) cross section at YSi_2/Si(111) interface.

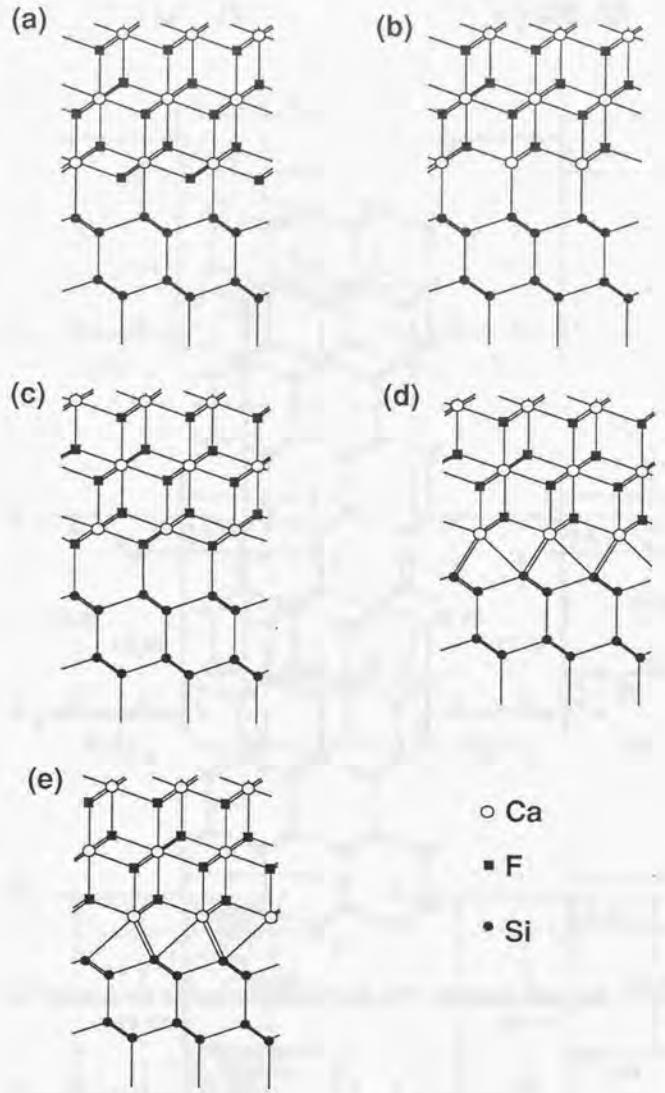

Figure 5: Atomic structure models for the CaF_2/Si(111) interface: (a) eightfold-coordinated Ca, (b) fivefold-coordinated Ca, (c) sevenfold-coordinated Ca, (d) Ca at the T_4 site, and (e) Ca at the H_3 site.

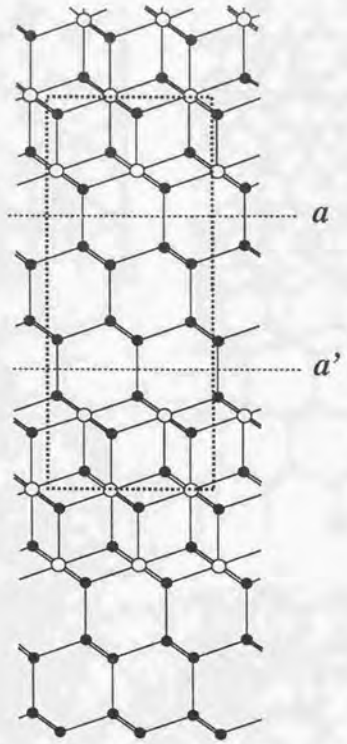

Figure 6: Supercell geometry. Two interfaces contained in the supercell are indicated by a and a'.

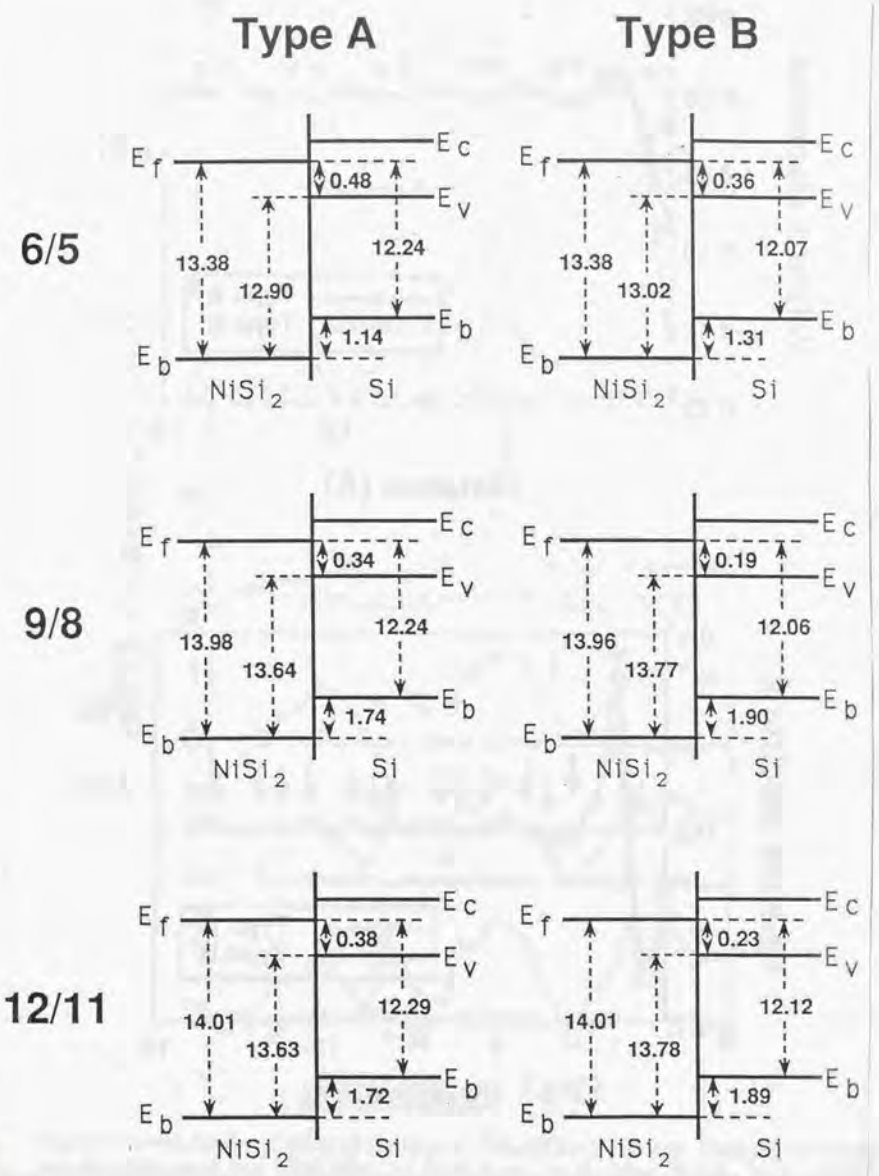

Figure 7: Band lineup between the Si and $NiSi_2$ layers obtained with different supercells. (in eV)

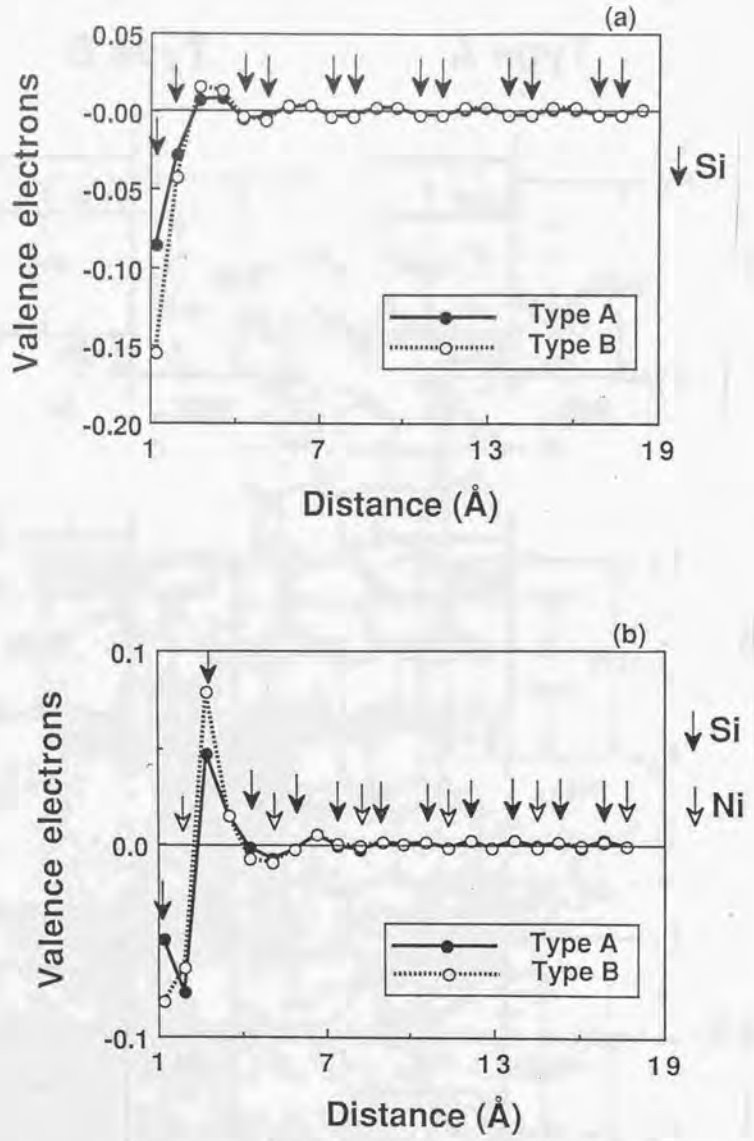

Figure 8: Difference in the number of electrons from the bulk values in Table 1: (a) in the Si layer and (b) in the $NiSi_2$ layer. The interface is on the left. Arrows indicate atomic sphere locations.

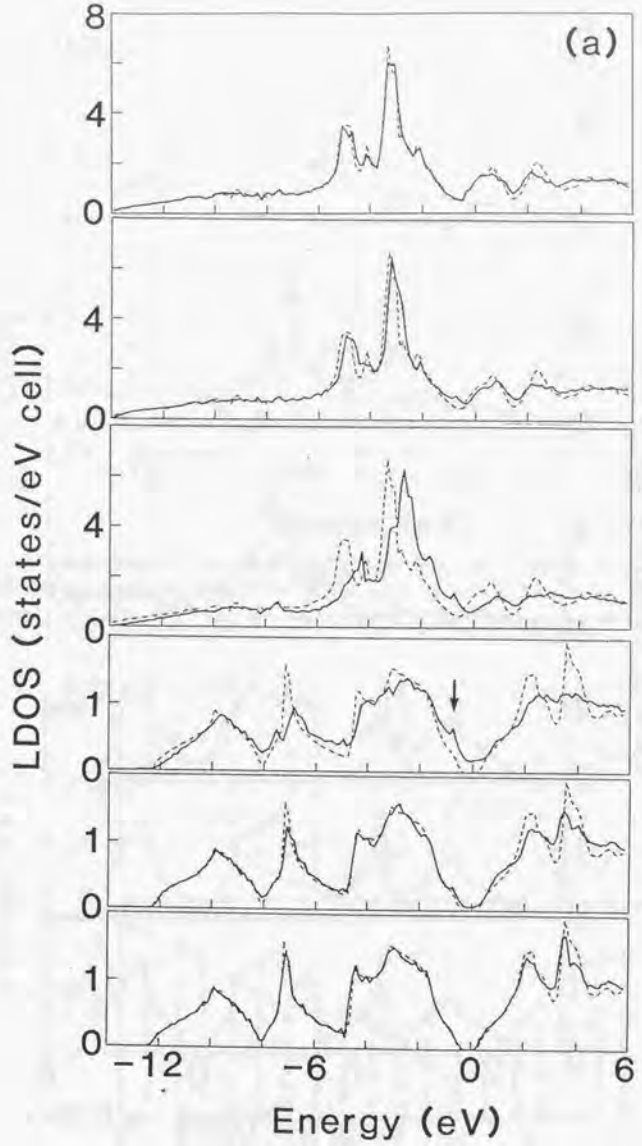

Figure 9: Local density of states of the type-*A* $NiSi_2$/Si(111) interface. From top to bottom are 6th $NiSi_2$ layer, 2nd $NiSi_2$ layer, 1st $NiSi_2$ layer, 1st Si_2 layer, 2nd Si_2 layer, and 6th Si_2 layer from the interface. Dotted lines are bulk density of states of Si and $NiSi_2$. Arrows indicate interface states. The zero energy point indicates the Fermi energy of the supercell.

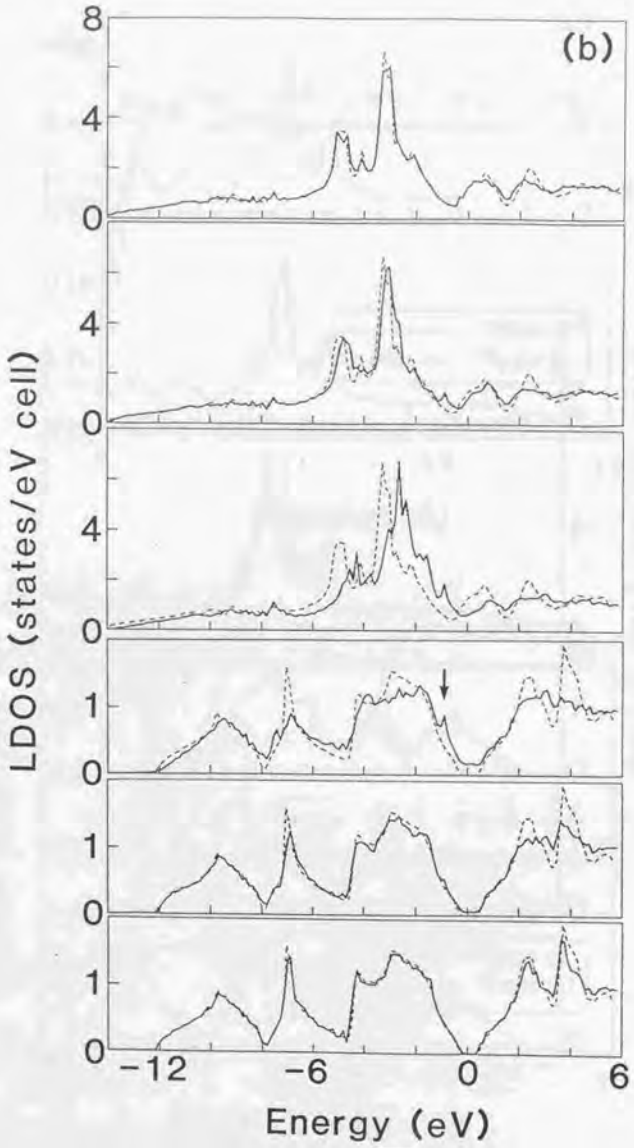

Figure 10: Local density of states of the type-B $NiSi_2$/Si(111) interface just like Fig. 9.

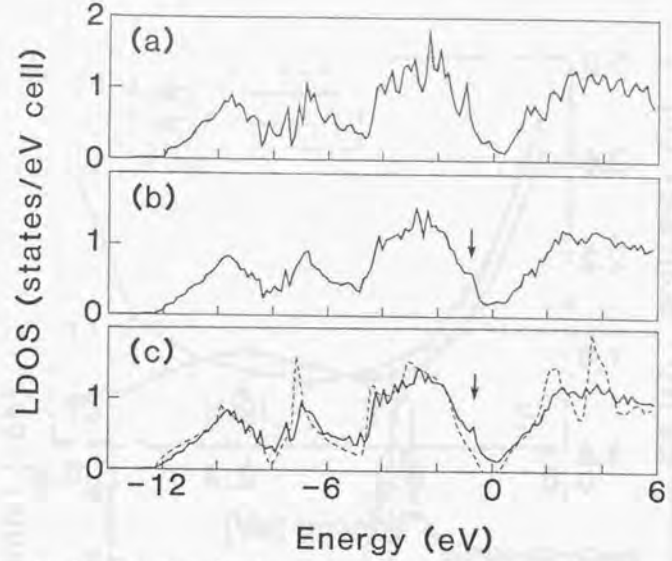

Figure 11: Local density of states of 1st Si_2 layer from the interface of type-A calculated: (a) with 2/3 supercell, (b) with 5/6 supercell, and (c) with 8/9 supercell. Dotted lines are bulk density of states of Si. The zero energy point is the Fermi energy of the supercells.

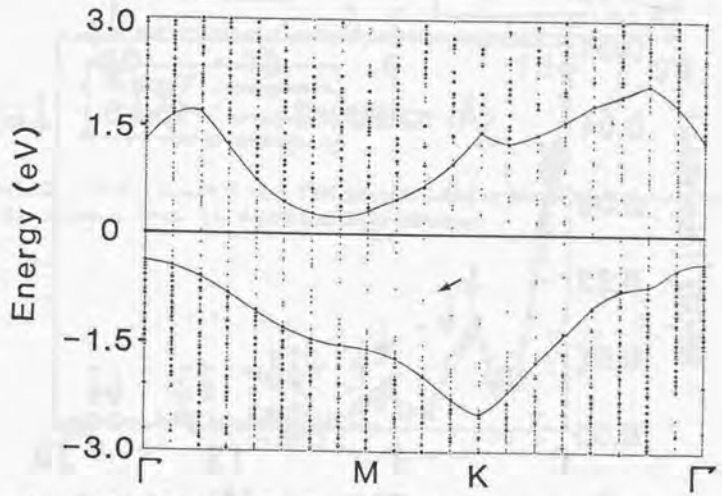

Figure 12: Two-dimensional band structure near the Si band gap of the type-A interface. The zero energy point is the Fermi energy of the supercell. Dots present an energy eigenvalue. The larger dots indicate the eigenvalues more than 40 percent of which wave functions exist in the Si layer. The interface band is indicated by an arrow.

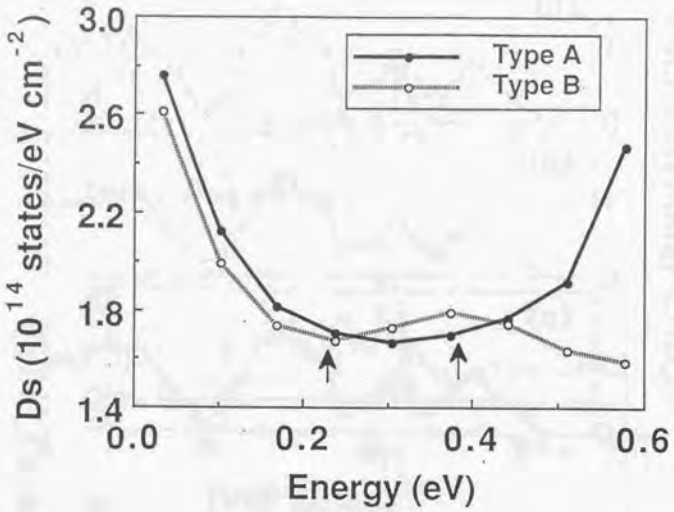

Figure 13: Surface density of metal-induced gap states in the Si thermal gap. Arrows indicate the Fermi energy of the two types of interface. Circles show calculated energy points. By LDA, the Si thermal gap is depressed to about 0.6 eV (see Table 3).

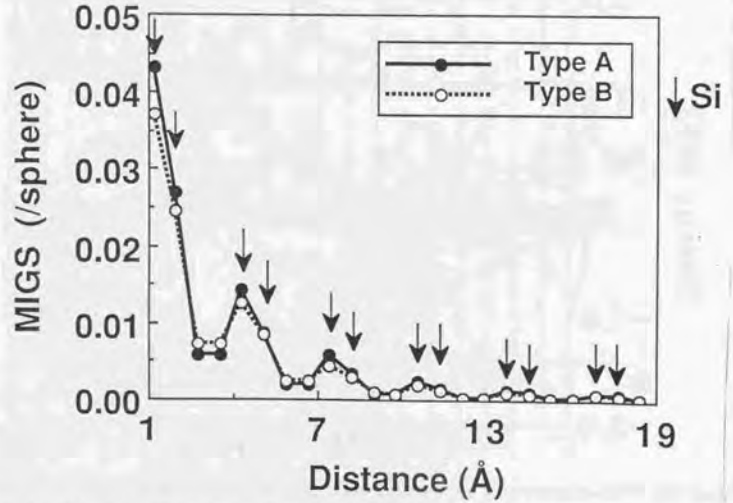

Figure 14: Number of electrons obtained by integrating the density of metal-induced gap states in the Si thermal gap at each sphere. Arrows indicate Si locations.

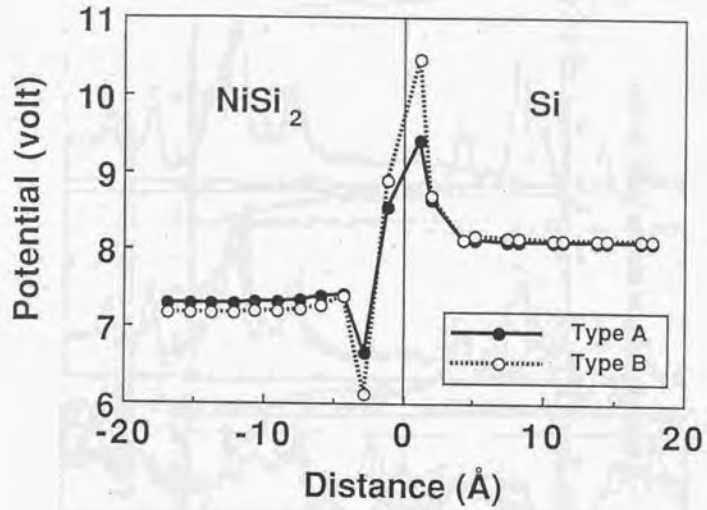

Figure 15: Potential in each Si site. This was calculated by Madelung constants and charges in other atomic spheres. The center line is the interface.

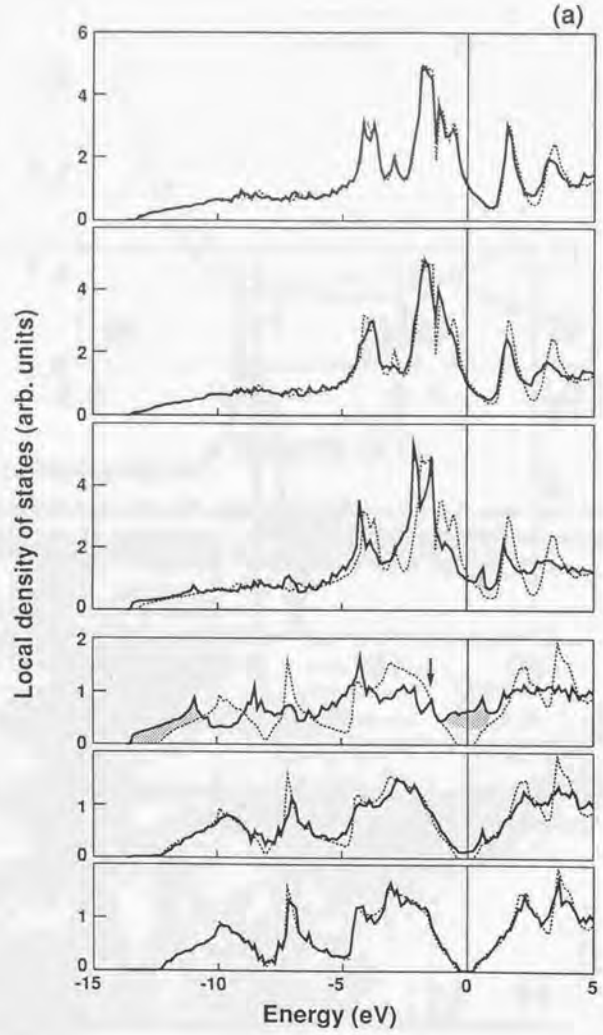

Figure 16: Local density of states of the type-A eightfold $CoSi_2$/Si(111) interface. From top to bottom are the $CoSi_2$ layer farthest from the interface, 2nd $CoSi_2$ layer, 1st $CoSi_2$, 1st Si_2 layer, 2nd Si_2 layer, and the Si_2 layer farthest from the interface. Dotted lines are bulk density of states of Si and $CoSi_2$. Shaded areas are interface states. The zero energy point is the Fermi energy of the supercell.

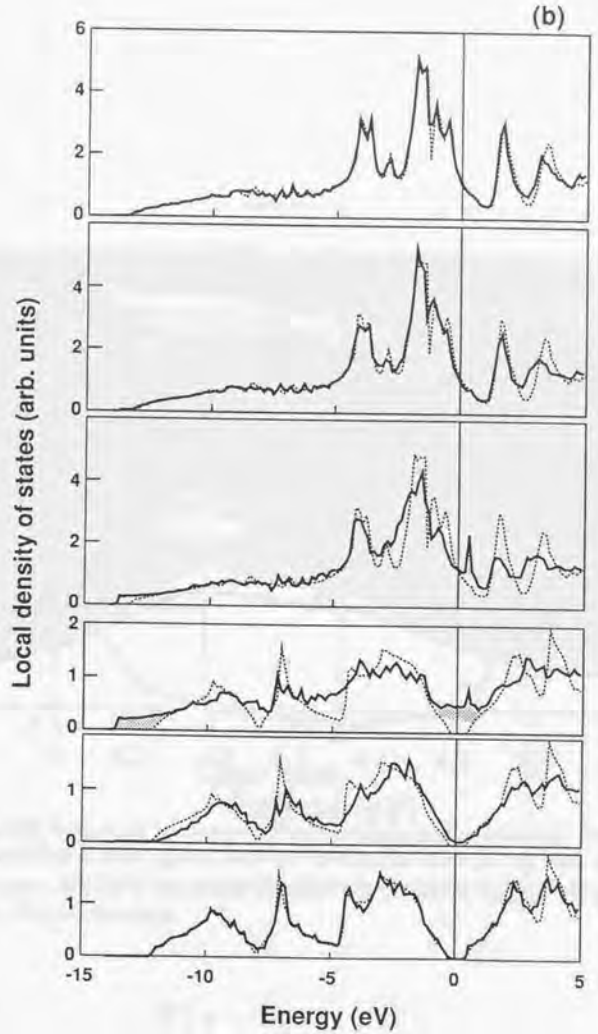

Figure 17: Local density of states of the type-B eightfold $CoSi_2$/Si(111) interface just like Fig. 16.

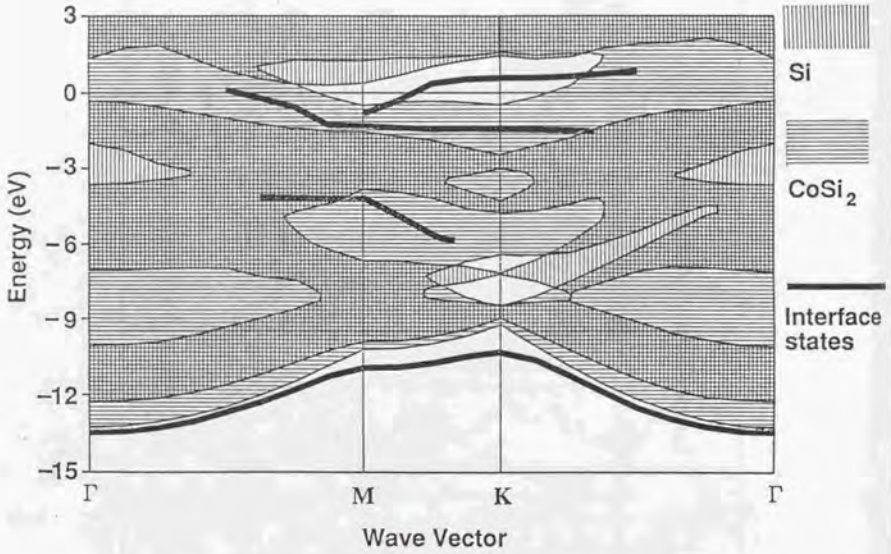

Figure 18: Two-dimensional projected band structure of the type-*A* $CoSi_2$/Si(111) interface obtained from the supercell calculation. The zero energy point is the Fermi level. Bold lines indicate the interface states which are localized near the interface.

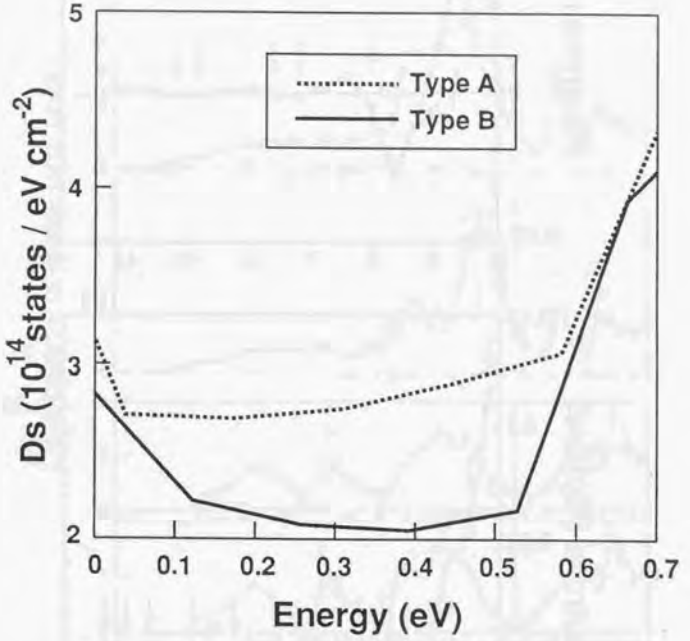

Figure 19: Surface density of interfacial states in the Si thermal gap at the two types of eightfold $CoSi_2$/Si(111) interface.

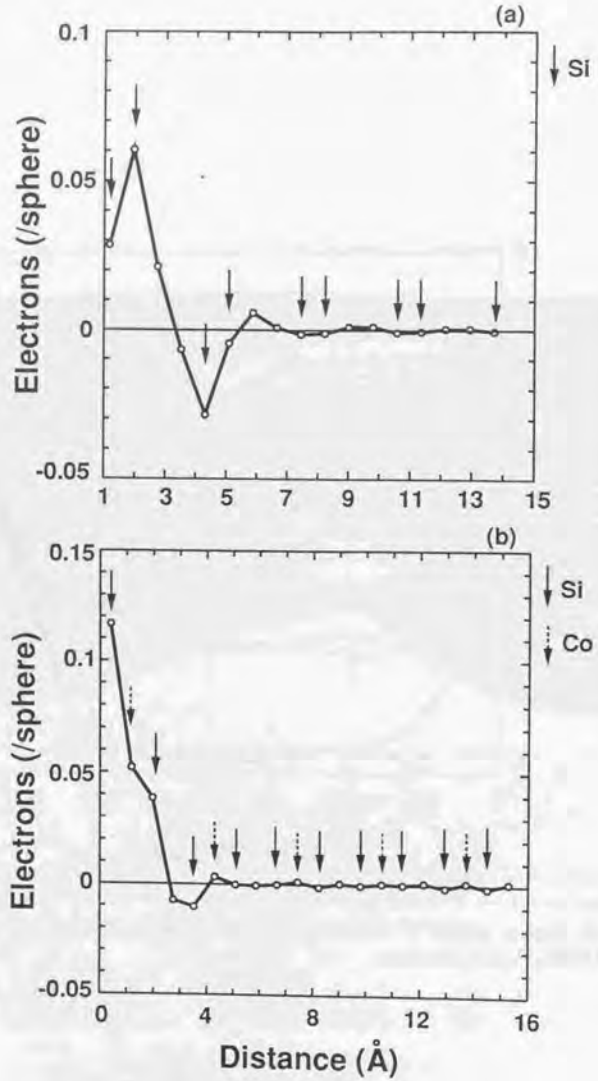

Figure 20: Difference in the number of electrons from the bulk values in Table 1 at the type-*A* eightfold $CoSi_2$/Si(111) interface: (a) in the Si layer and (b) in the $CoSi_2$ layer. The interface is on the left. Arrows indicate atomic sphere locations.

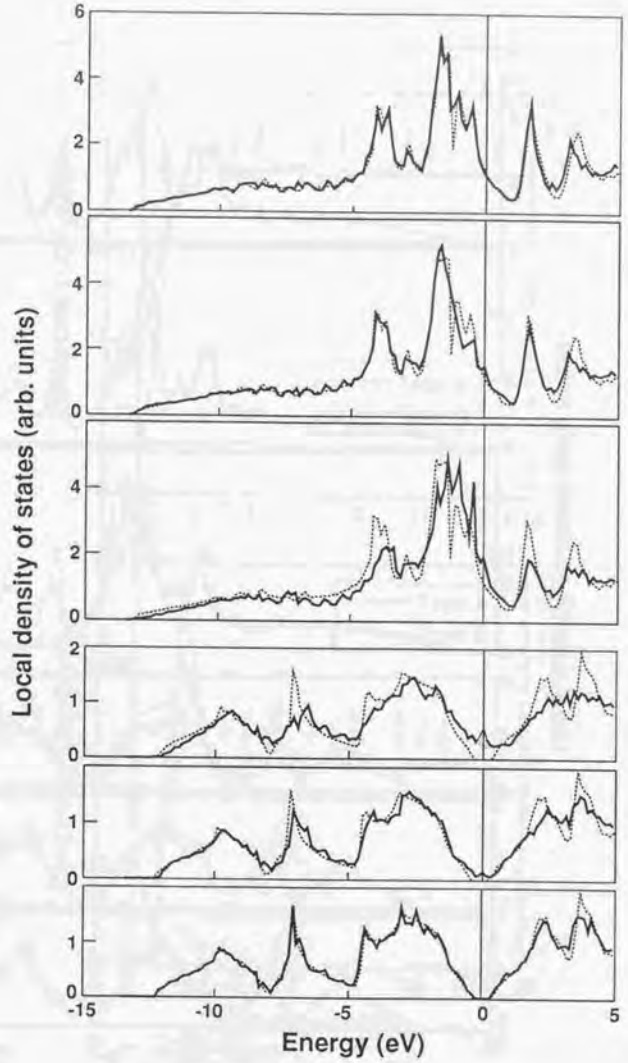

Figure 21: Local density of states of the type-*A* sevenfold $CoSi_2$/Si(111) interface. From top to bottom are the $CoSi_2$ layer farthest from the interface, 2nd $CoSi_2$ layer, 1st $CoSi_2$, 1st Si_2 layer, 2nd Si_2 layer, and the Si_2 layer farthest from the interface. Dotted lines arebulk density of states of Si and $CoSi_2$. Shaded areas are interface states. The zero energy point is the Fermi energy of the supercell.

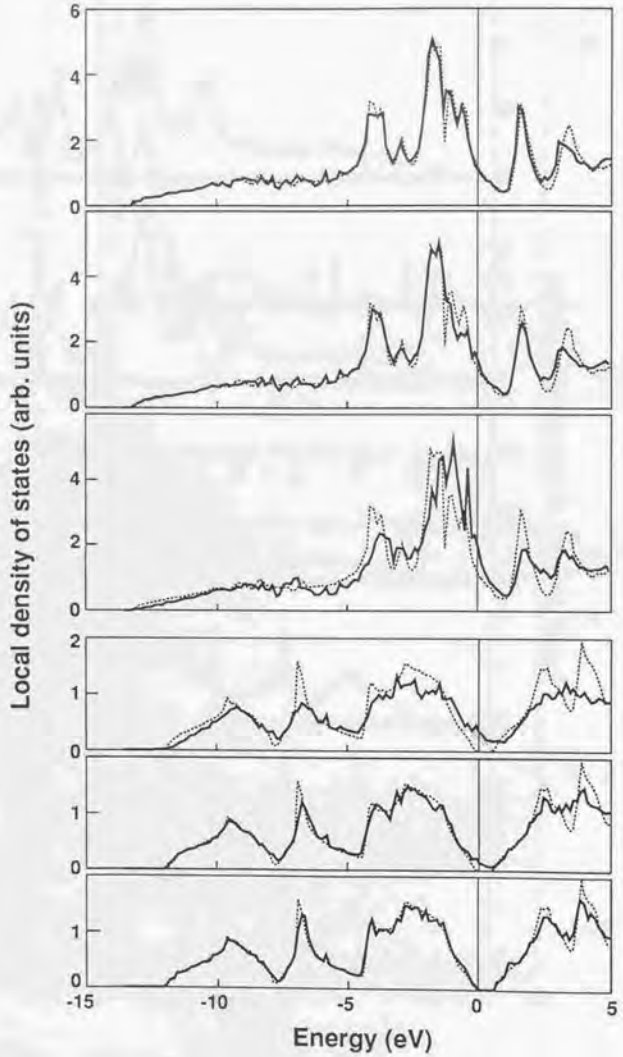

Figure 22: Local density of states of the type-B sevenfold $CoSi_2$/Si(111) interface just like Fig. 21.

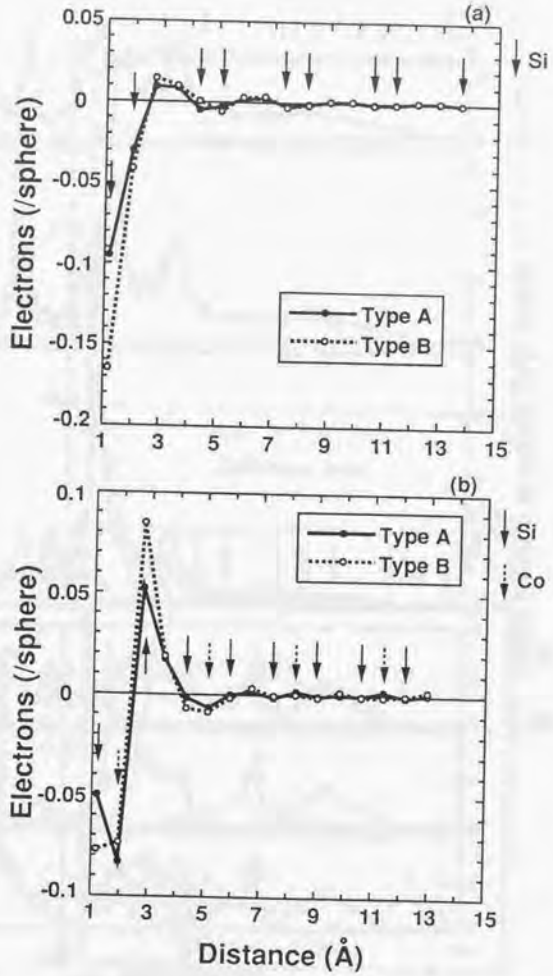

Figure 23: Difference in the number of electrons from the bulk values in Table 1 at the sevenfold $CoSi_2$/Si(111) interfaces: (a) in the Si layer and (b) in the $CoSi_2$ layer. The interface is on the left. Arrows indicate atomic sphere locations.

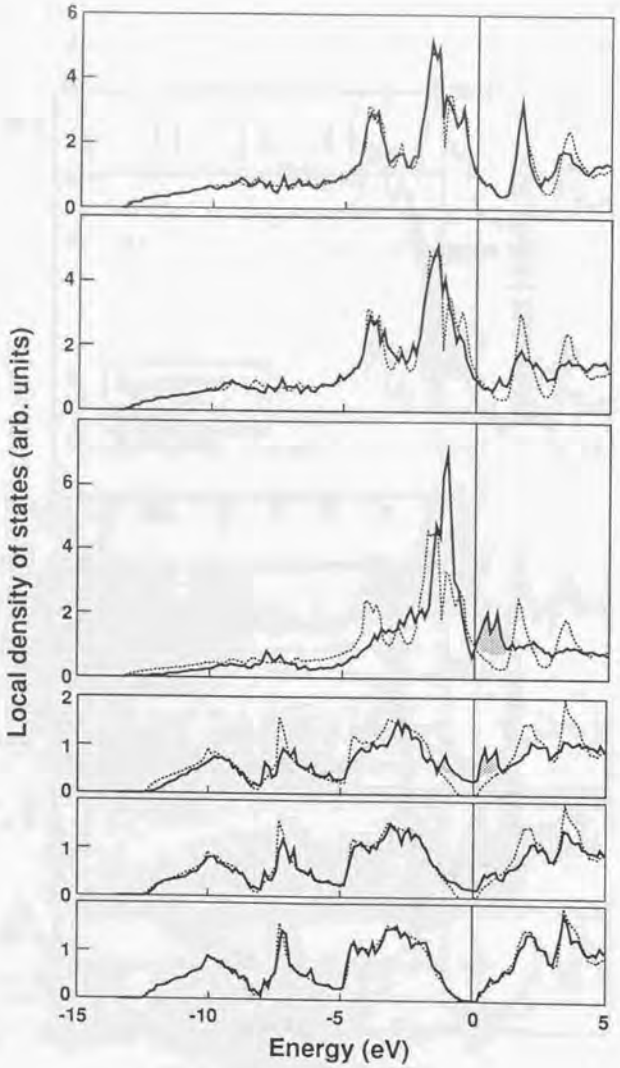

Figure 24: Local density of states of the type-B $CoSi_2$/Si(111) interface whose interfacial Co atom is at T_4 site. From top to bottom are the $CoSi_2$ layer farthest from the interface, 2nd $CoSi_2$ layer, 1st CoSi, 1st Si_2 layer, 2nd Si_2 layer, and the Si_2 layer farthest from the interface. Dotted lines are bulk density of states of Si and $CoSi_2$. Shaded areas are interface states. The zero energy point is the Fermi energy of the supercell.

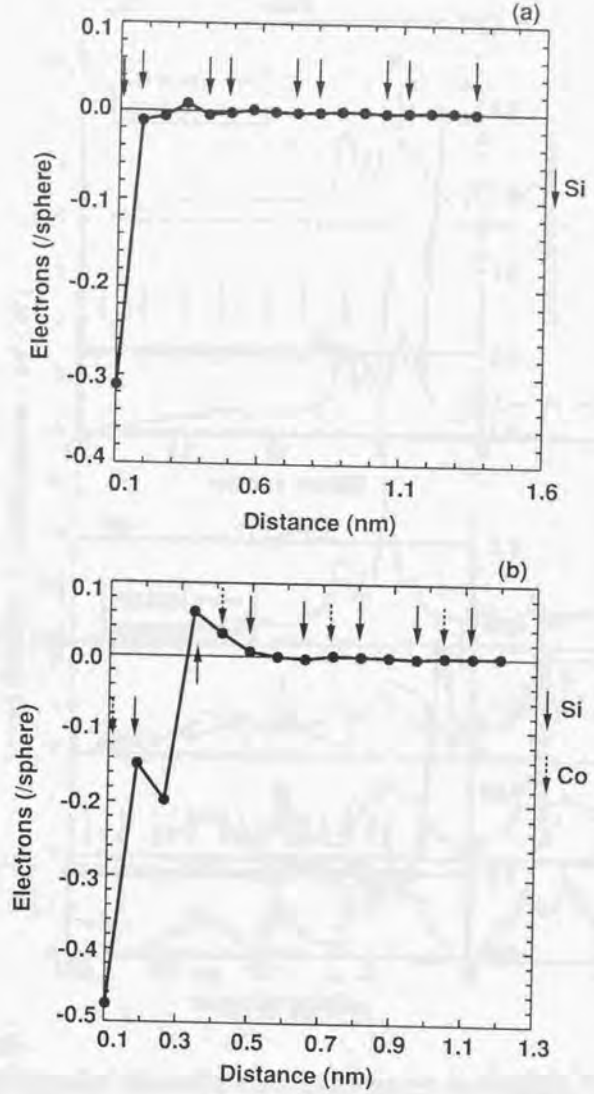

Figure 25: Difference in the number of electrons from the bulk values in Table 1 at the type-B $CoSi_2$/Si(111) interface whose interfacial Co atom is at T_4 site: (a) in the Si layer and (b) in the $CoSi_2$ layer. The interface is on the left. Arrows indicate atomic sphere locations.

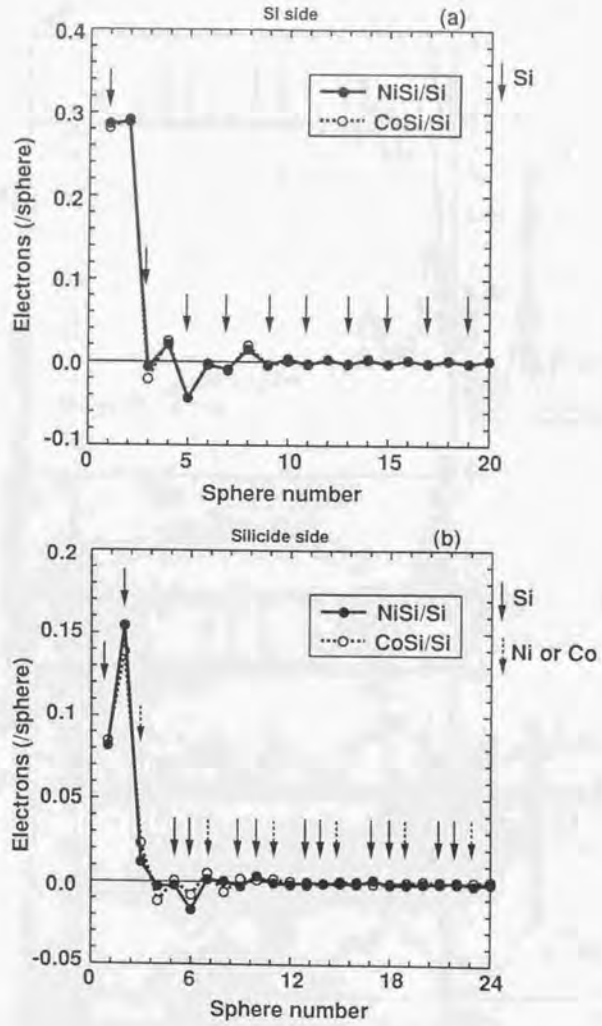

Figure 26: Difference in the number of electrons from the bulk values in Table 1 at the eightfold $NiSi_2$/Si(001) and $CoSi_2$/Si(001) interfaces: (a) in the Si layer and (b) in the silicide layer. The interface is on the left. Arrows indicate atomic sphere locations. In the Si layer, a couple of Si and empty spheres is at the same distance from the interface. In the silicide layer, a couple of two Si sphere and a couple of Ni or Co and empty spheres are at the same distance from the interface

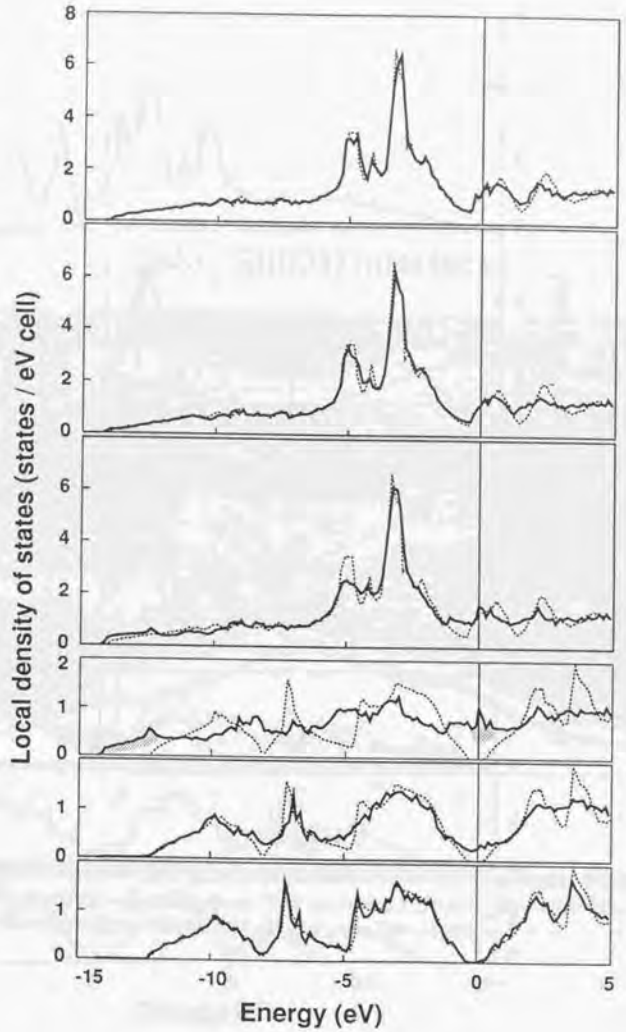

Figure 27: Local density of states of the eightfold $NiSi_2$/Si(001) interface. From top to bottom are the $NiSi_2$ layer farthest from the interface, 2nd $NiSi_2$ layer, 1st $NiSi_2$, 1st Si_2 layer, 2nd Si_2 layer, and the Si_2 layer farthest from the interface. Dotted lines are bulk density of states of Si and $NiSi_2$. Shaded areas are interface states. The zero-energy point is the Fermi energy of the supercell.

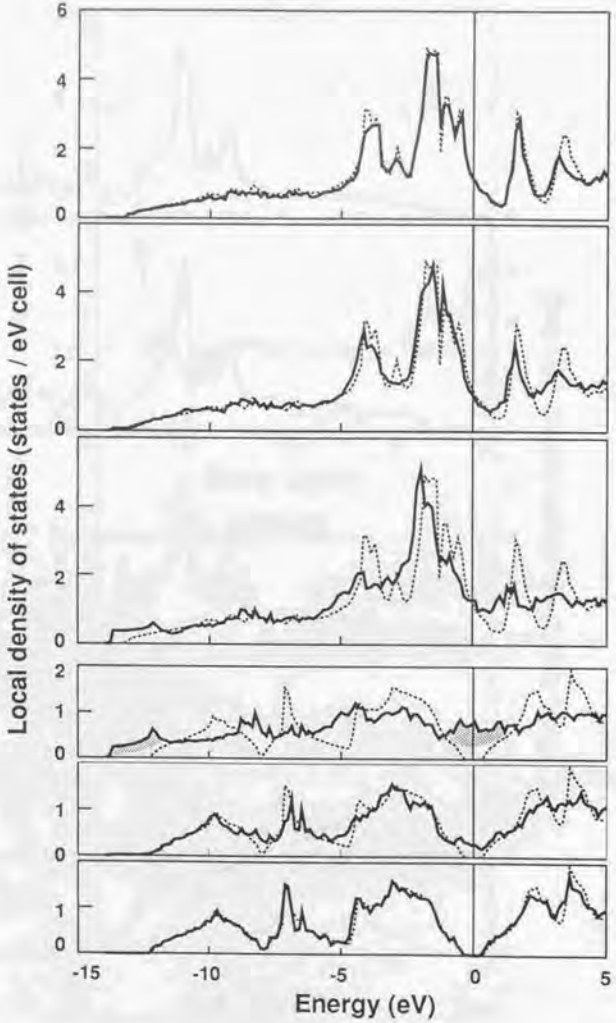

Figure 28: Local density of states of the eightfold $CoSi_2$/Si(001) interface. From top to bottom are the $CoSi_2$ layer farthest from the interface, 2nd $CoSi_2$ layer, 1st $CoSi_2$, 1st Si_2 layer, 2nd Si_2 layer, and the Si_2 layer farthest from the interface. Dotted lines are bulk density of states of Si and $CoSi_2$. Shaded areas are interface states. The zero-energy point is the Fermi energy of the supercell.

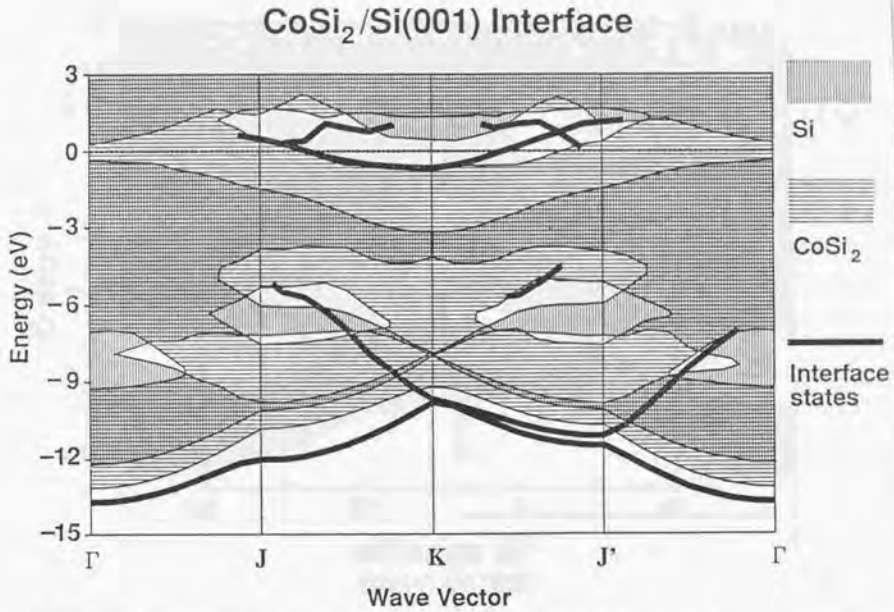

Figure 29: Two-dimensional projected band structure of the eightfold $CoSi_2$/Si(001) interface obtained from the supercell eigenvalues. The zero energy point is the Fermi level. Bold lines indicate the interface states which are localized near the interface.

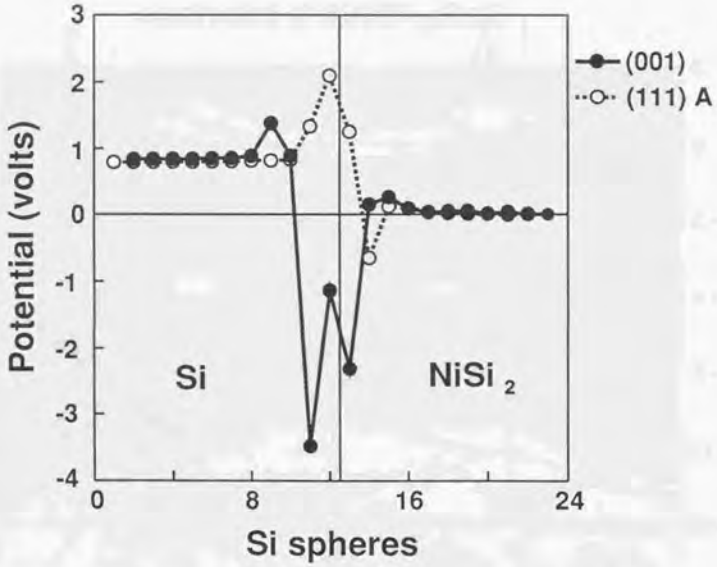

Figure 30: Potential at Si locations calculated using Madelung constants and charges in other atomic spheres. For convienience, the origin of vertical axis is set at the value of the right end. The vertical line inside the chart indicates the interface. The abscissa does not indicate real distance.

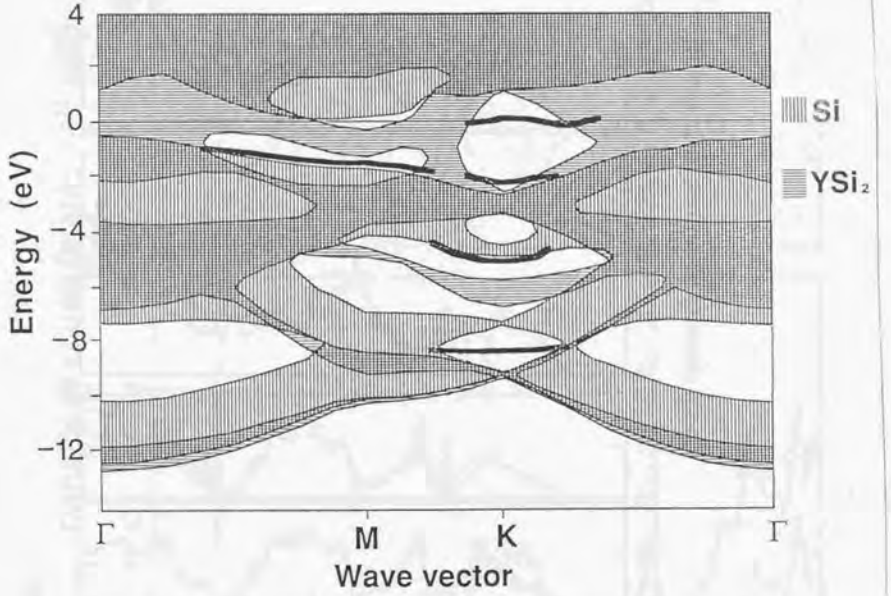

Figure 31: Two-dimensional projected band structure of the YSi_2/Si(111) interface obtained from the supercell calculation. The zero energy point is the Fermi level. Bold lines indicate the interface states which are localized near the interface.

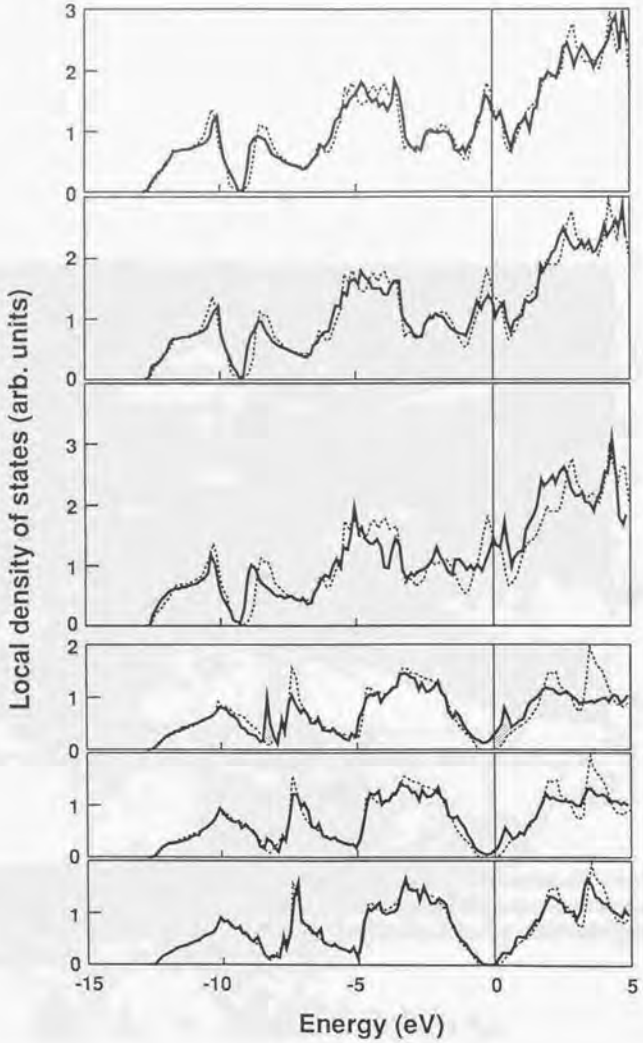

Figure 32: Local density of states of the YSi_2/Si(111). From top to bottom are the YSi_2 layer farthest from the interface, 2nd YSi_2 layer, 1st YSi_2, 1st Si_2 layer, 2nd Si_2 layer, and the Si_2 layer farthest from the interface. Dotted lines are bulk density of states of Si and YSi_2. Shaded areas are interface states. The zero energy point is the Fermi energy of the supercell.

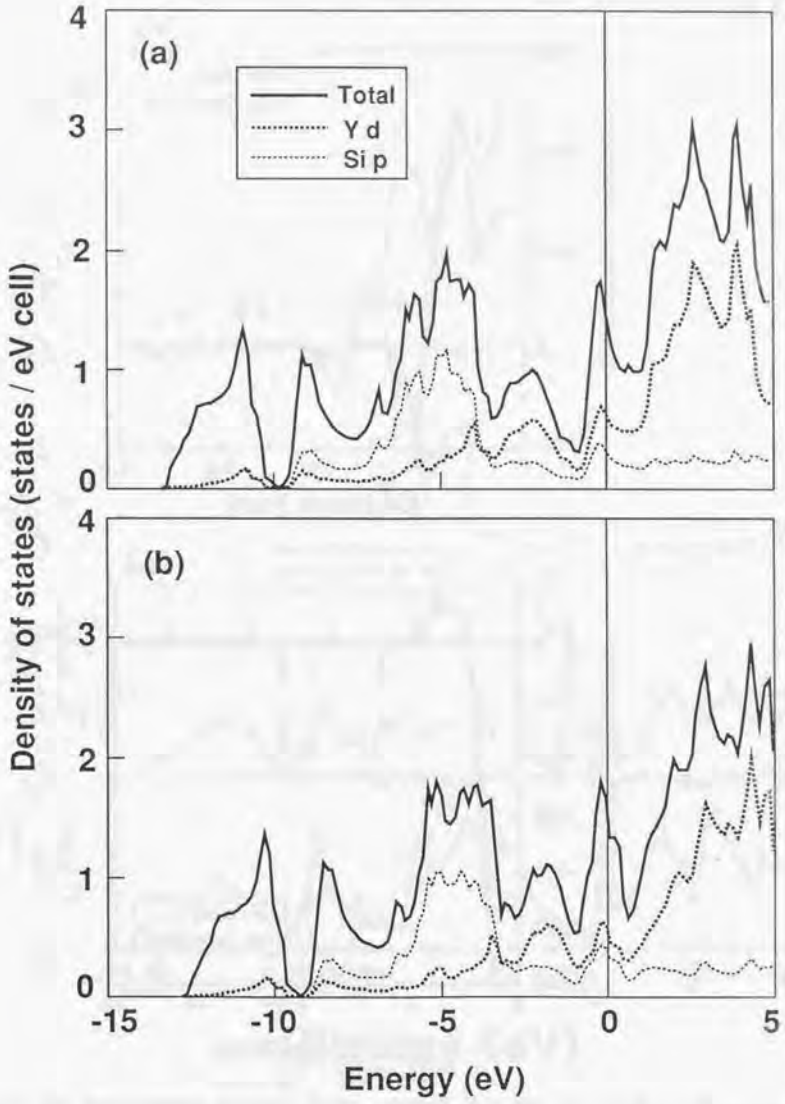

Figure 33: Density of states of bulk YSi_2. (a) without *f*-orbitals and (b) with *f*-ortibtals for Y atom. The zero energy point is the Fermi energy.

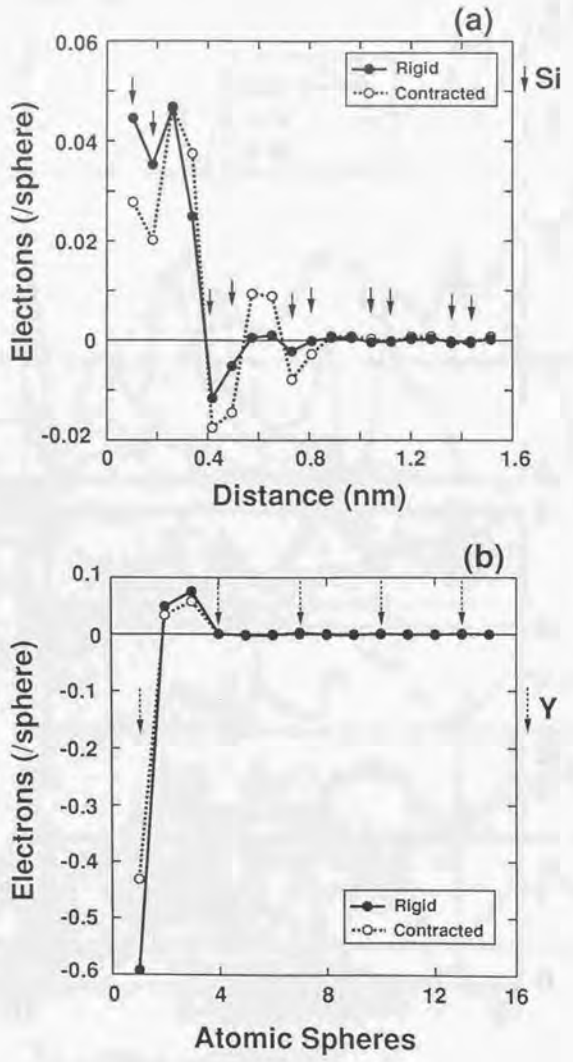

Figure 34: Difference in the number of electrons from the bulk values in Table 1: (a) in the Si layer, (b) in the YSi_2 layer. The interface is on the left. Arrows indicate atomic sphere locations.

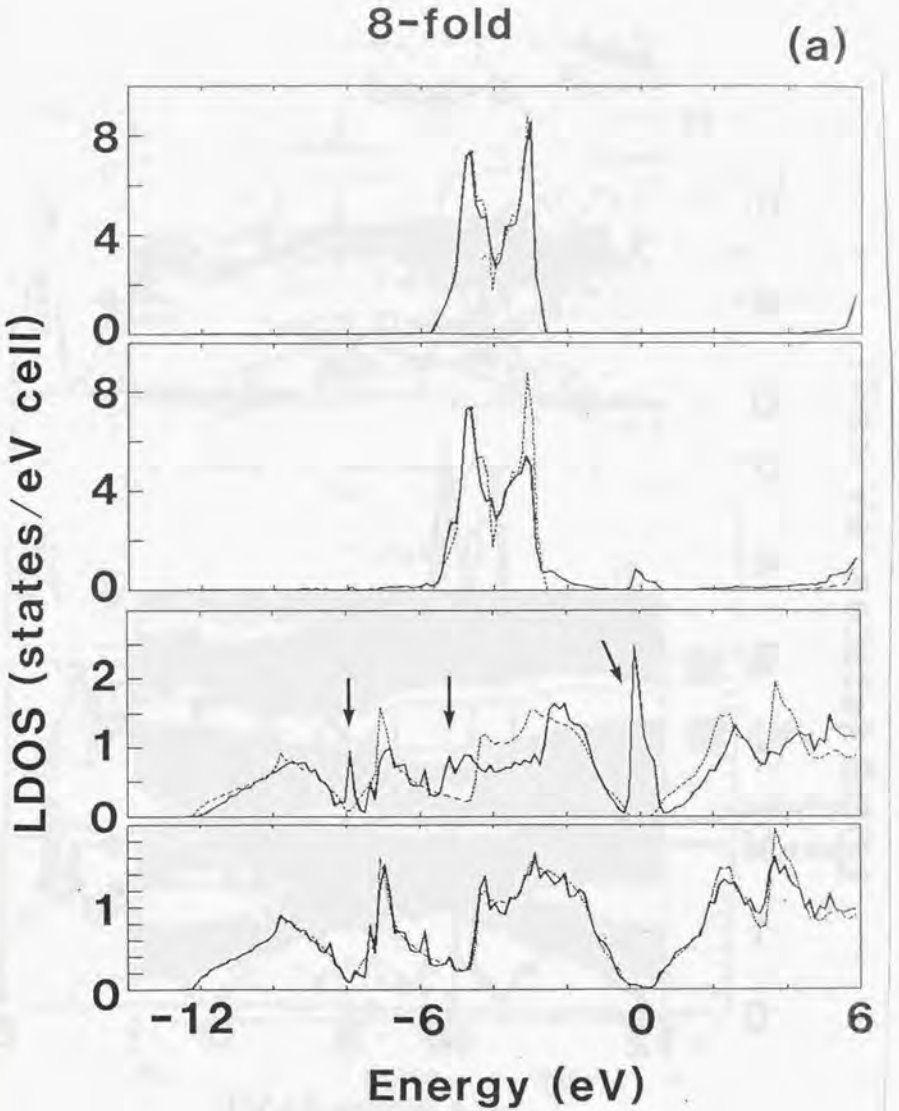

Figure 35: Local density of states of the eightfold $CaF_2/Si(111)$ interface. From top to bottom are 5th CaF_2 layer, 1st CaF_2 layer, 1st Si_2 layer, and 4th Si_2 layer from the interface. Dotted lines are bulk density of states of Si and CaF_2. Arrows show the interface states. The zero energy point is the Fermi energy of the supercell.

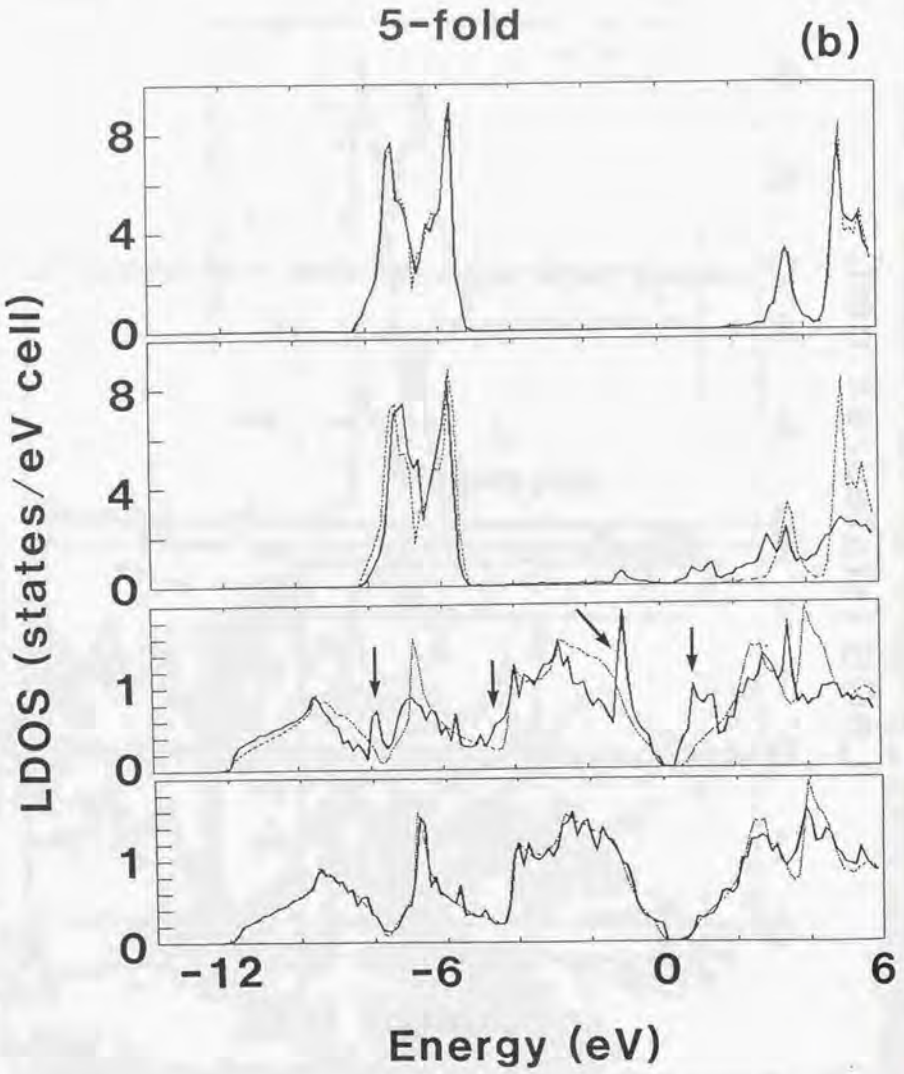

Figure 36: Local density of states of the fivefold CaF_2/Si(111) interface just like Fig. 35.

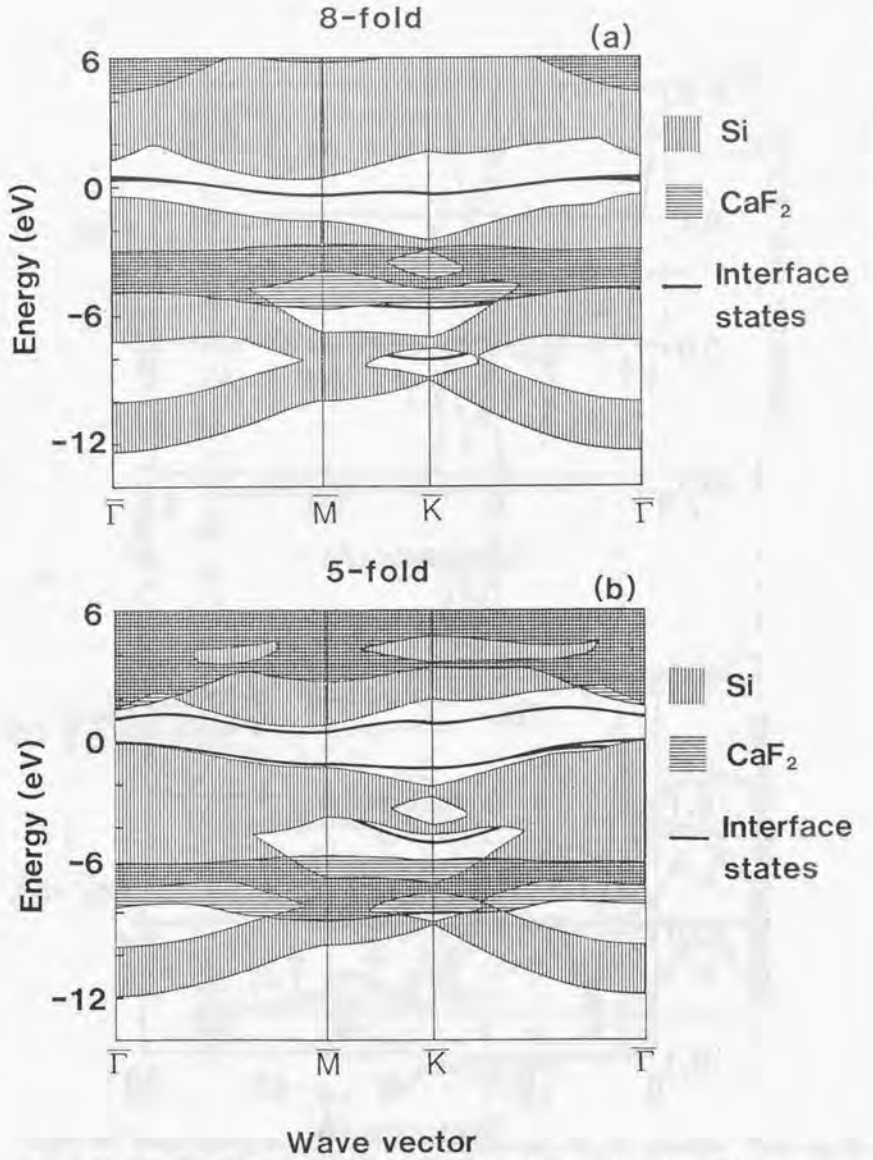

Figure 37: Two-dimensional band structure of the CaF_2/Si(111) interface: (a) the eightfold model and (b) the fivefold model. The zero energy point is the Fermi energy of the supercell. Since this was calculated by LDA, band alignments of both valence and conduction band differ from the measured values.

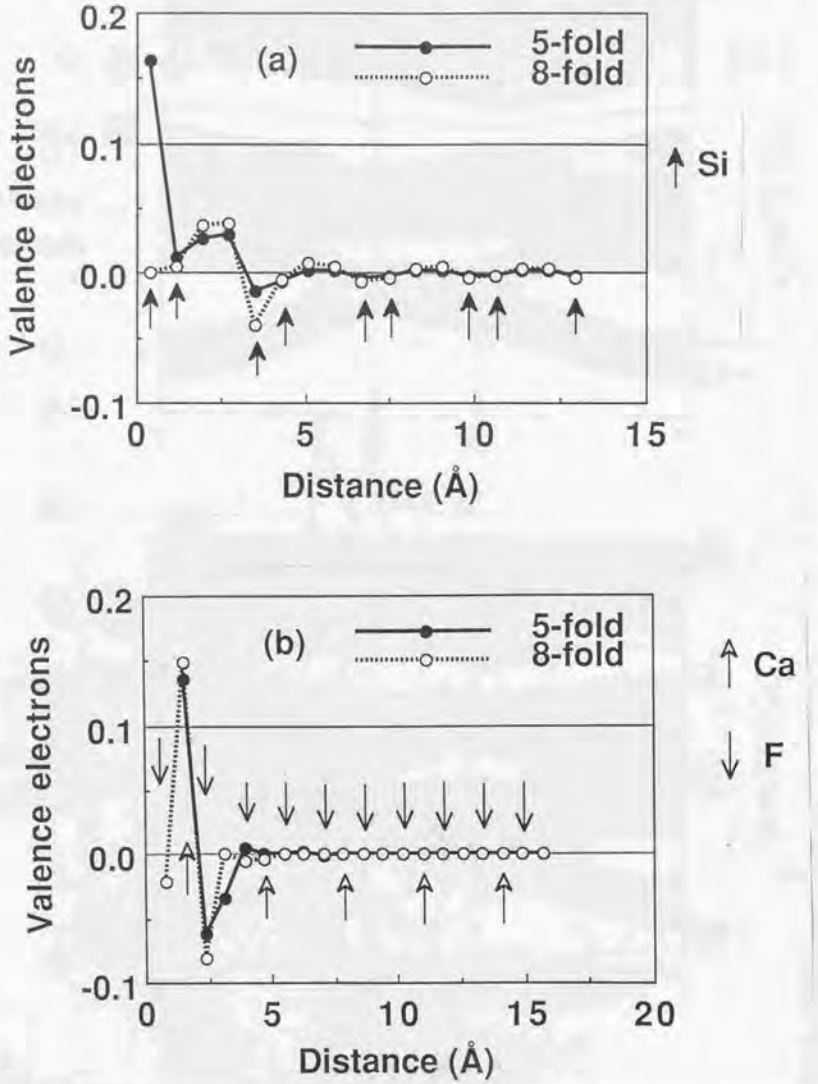

Figure 38: Difference in the number of electrons from the bulk value in Table 1: (a) in the Si layer and (b) in the CaF_2 layer. The interface is on the left. Arrows indicate atomic sphere locations.

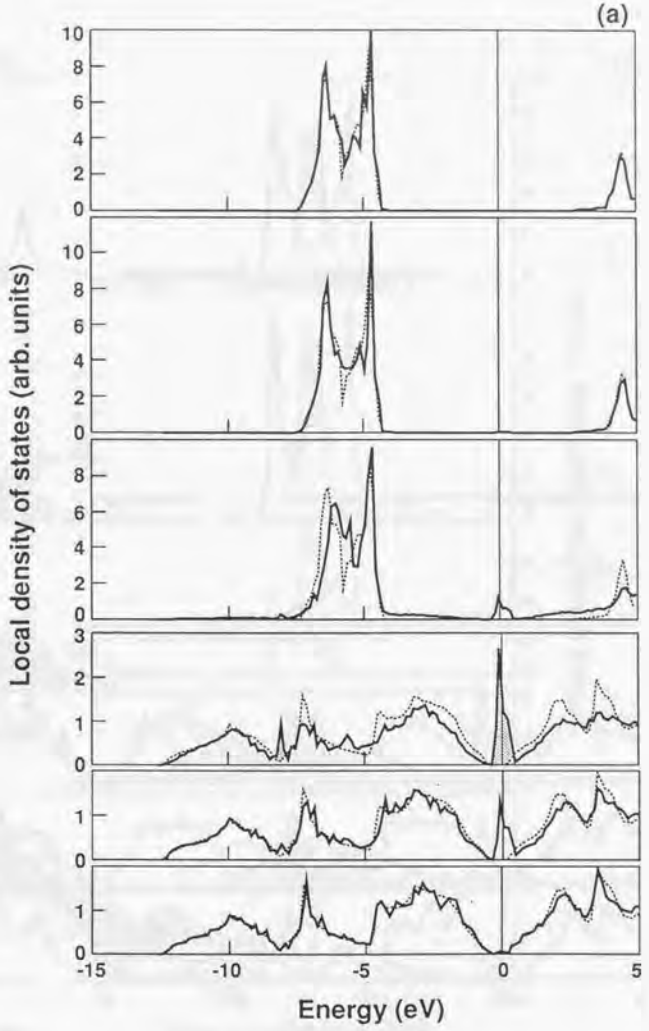

Figure 39: Local density of states of the sevenfold $CaF_2/Si(111)$ interface. From top to bottom are the CaF_2 layer farthest from the interface, 2nd CaF_2 layer, 1st CaF_2 or CaF layer, 1st Si_2 layer, 2nd Si_2 layer, and the Si_2 layer farthest from the interface. Dotted lines are bulk density of states of Si and CaF_2. Shaded areas are interface states. The zero energy point is the Fermi energy of the supercell.

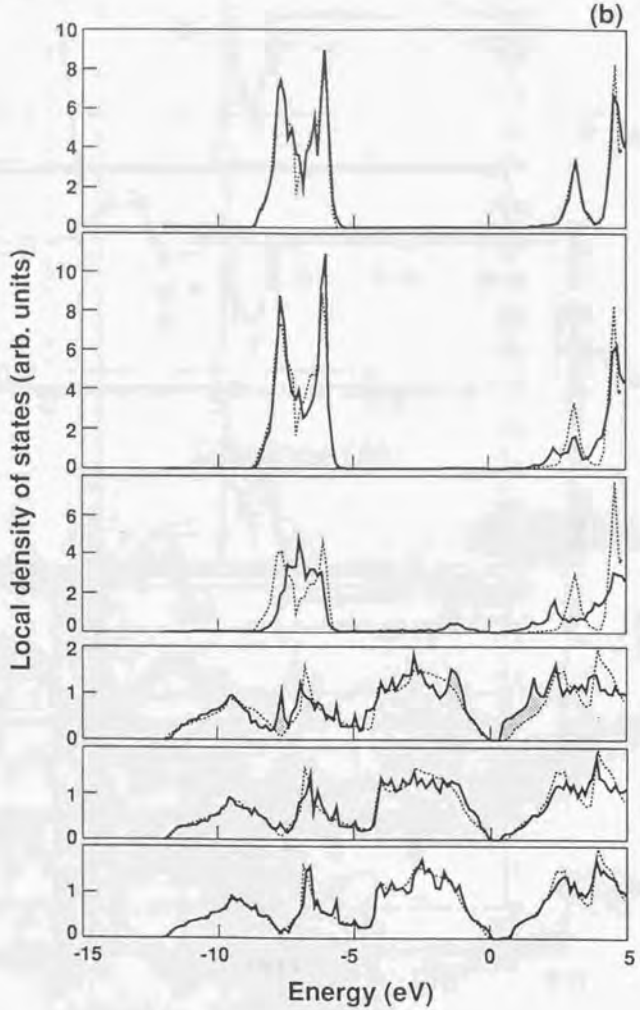

Figure 40: Local density of states of the CaF_2/Si(111) interface with the T_4 structure just like Fig. 39.

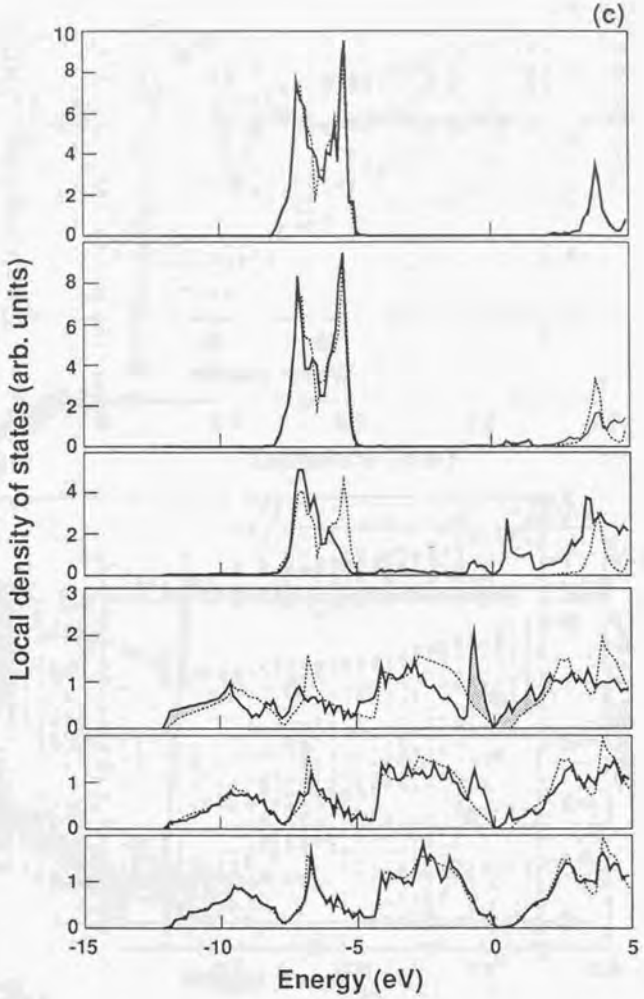

Figure 41: Local density of states of the CaF_2/Si(111) interface with the H_3 structure just like Fig. 39.

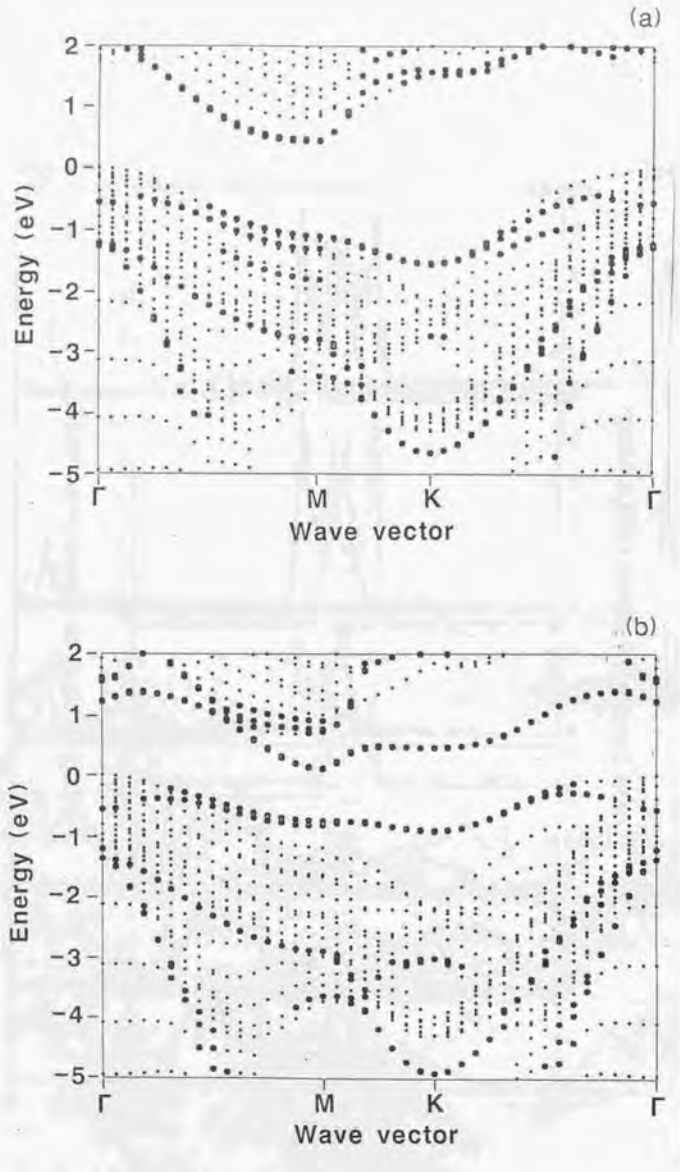

Figure 42: Two-dimensional band structure of the CaF_2/Si(111) interface: (a) the T_4 model and (b) the H_3 model. The zero energy point is the Fermi energy of the supercell. Dots represent energy eigenvalue of the supercells and the larger dots are eigenvalues whose wave functions are mostly localized in the Si layer. The filled band of the CaF_2 layer does not appear in this energy scale.

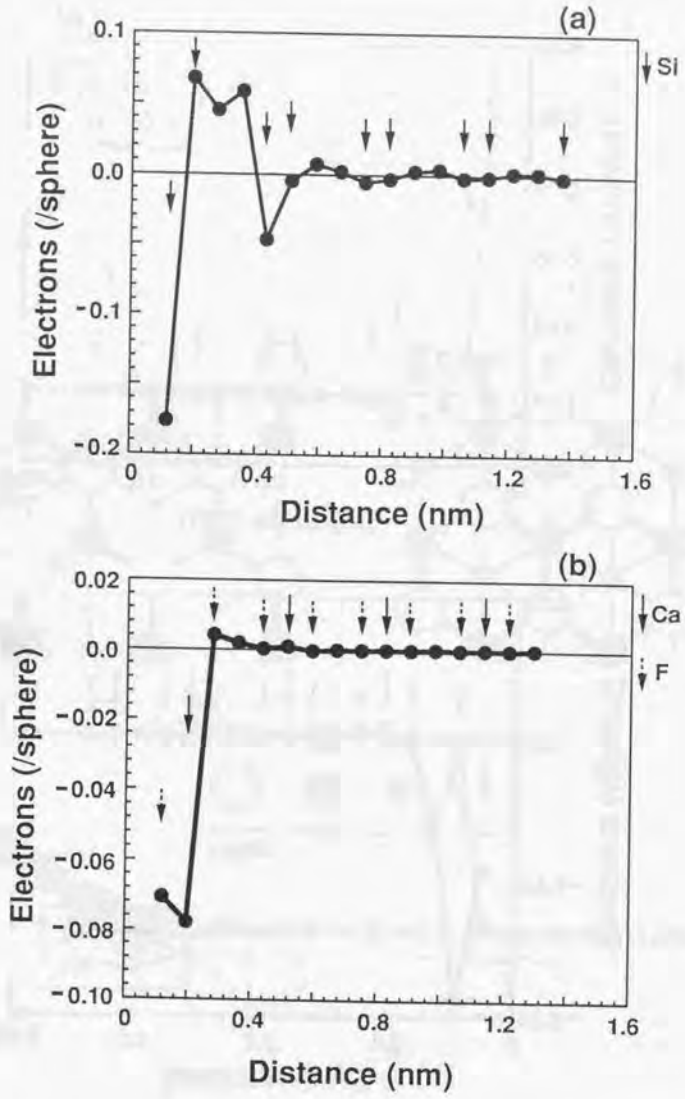

Figure 43: Difference in the number of electrons from bulk values in Table 1: (a) in the Si layer and (b) in the CaF_2 layer of the sevenfold model. The interface is on the left. Arrows indicate atomic sphere locations.

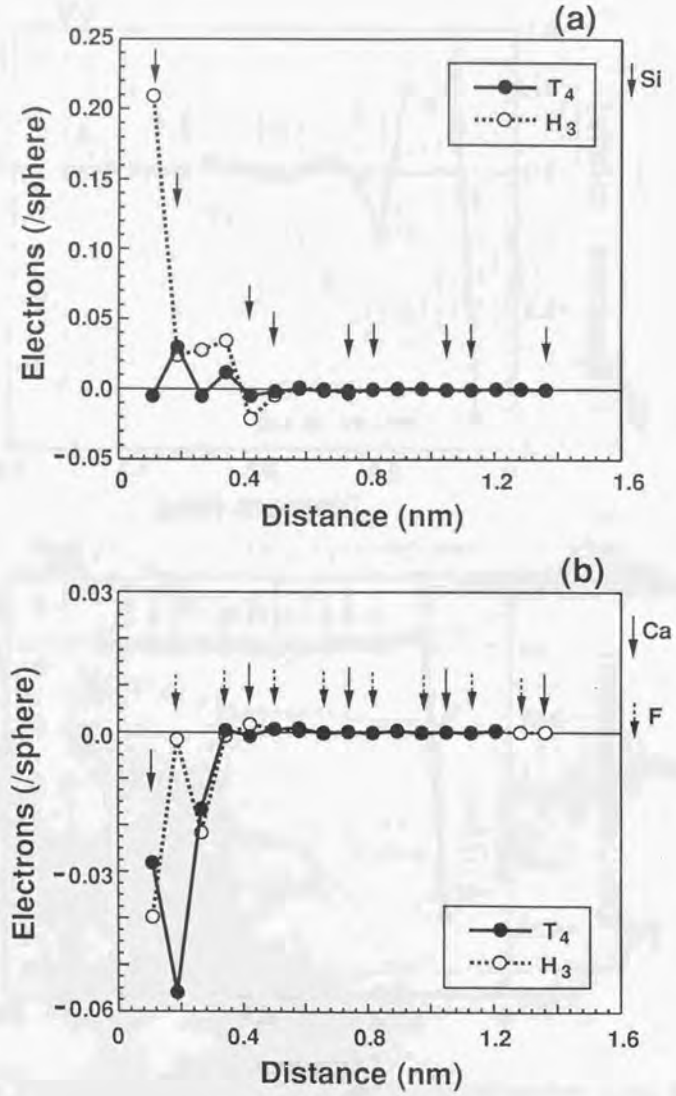

Figure 44: Difference in the number of electrons from bulk values in Table 1 of the T_4 and H_3 models just like Fig. 43.

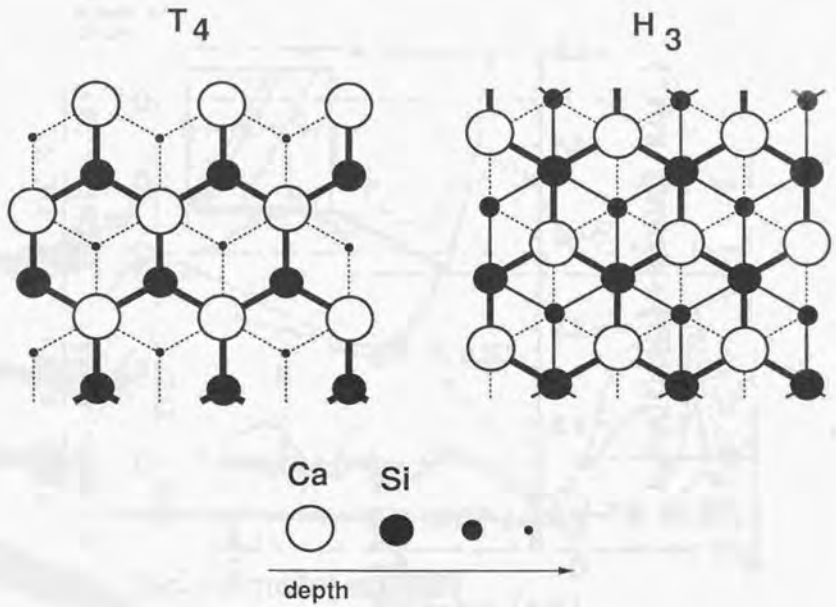

Figure 45: Overview with Ca atoms at the T_4 and H_3 sites on the Si(111) surface.

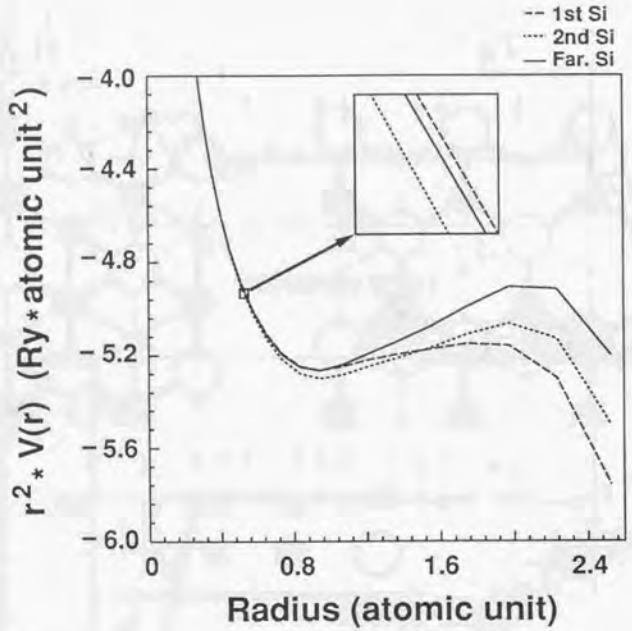

Figure 46: Spherical potential multiplied by the square of radii ($r^2 \times V(r)$) in the 1st Si, 2nd Si, and Si sphere farthest from the interface.

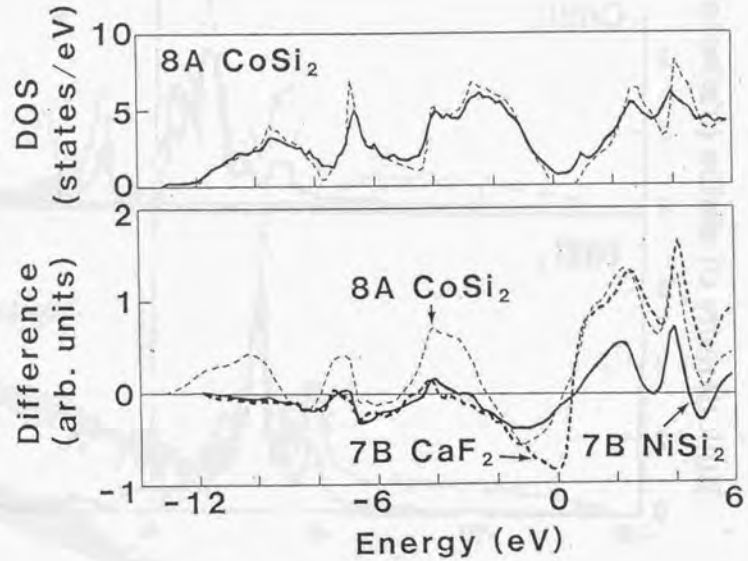

Figure 47: Difference in state number between the interface Si layer and bulk Si. The zero energy point is the top of the Si valence band.

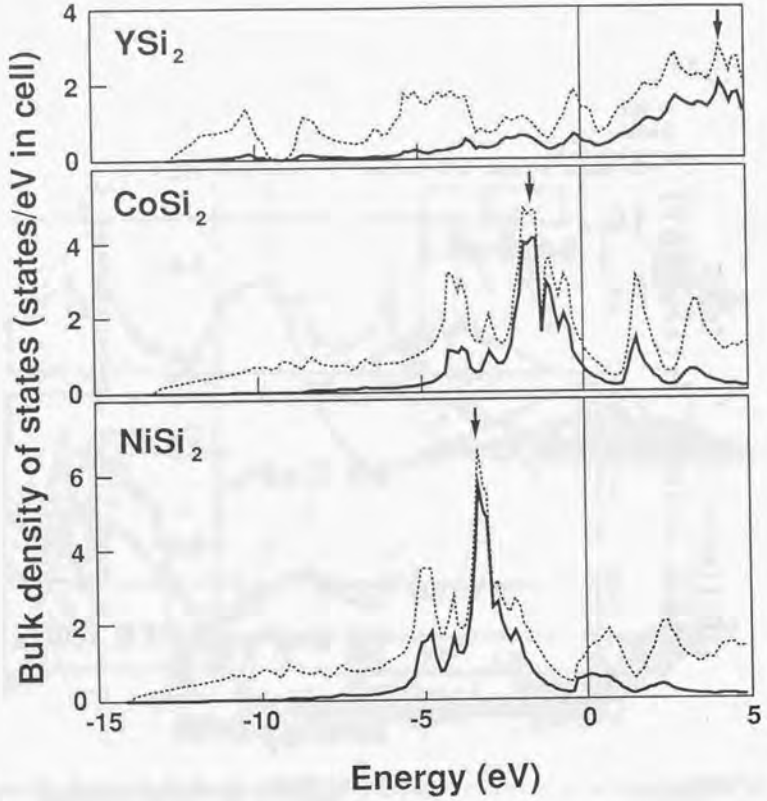

Figure 48: Density of states (DOS) of bulk $NiSi_2$, $CoSi_2$, and YSi_2. Solid lines are partial DOS of d–orbitals of metal atoms. Dotted lines are total DOS. The zero energy is the Fermi energy. Positions of the largest peaks of *d*-orbital are indicated by arrows.